NASA
Technical Memorandum 4345

AVSCOM
Technical Report 92-B-005

Effect of Blade Planform Variation on the Forward-Flight Performance of Small-Scale Rotors

Kevin W. Noonan, Susan L. Althoff,
Dhananjay K. Samak, and Michael D. Green

APRIL 1992

NASA

US ARMY
AVIATION
SYSTEMS COMMAND
AVIATION R&T ACTIVITY

NASA
Technical Memorandum 4345

AVSCOM
Technical Report 92-B-005

Effect of Blade Planform Variation on the Forward-Flight Performance of Small-Scale Rotors

Kevin W. Noonan and Susan L. Althoff
Aeroflightdynamics Directorate—AVSCOM
JRPO—Langley
Langley Research Center
Hampton, Virginia

Dhananjay K. Samak and Michael D. Green
University of Maryland
College Park, Maryland

National Aeronautics and
Space Administration

Office of Management

Scientific and Technical
Information Program

1992

Contents

Abstract

An investigation was conducted in the Glenn L. Martin Wind Tunnel to determine the effects of blade planform variation on the forward-flight performance of four small-scale rotors. The rotors were 5.417 ft in diameter and differed only in blade planform geometry. The four planforms were (1) rectangular, (2) 3:1 linear taper starting at 94 percent radius, (3) 3:1 linear taper starting at 75 percent radius, and (4) 3:1 linear taper starting at 50 percent radius. Each planform had a thrust-weighted solidity of 0.098. The investigation included forward-flight simulation at advance ratios from 0.14 to 0.43 for a range of rotor lift and drag coefficients. Among the four rotors, the rectangular rotor required the highest torque for the entire range of rotor drag coefficients attained at advance ratios greater than 0.14 for rotor lift coefficients C_L from 0.004 to 0.007. Among the rotors with tapered blades and for C_L = 0.004 to 0.007, either the 75-percent tapered rotor or the 50-percent tapered rotor required the least amount of torque for the full range of rotor drag coefficients attained at each advance ratio. The performance of the 94-percent tapered rotor was generally between that of the rectangular rotor and the 75- and 50-percent tapered rotors at each advance ratio for this range of rotor lift coefficients.

Introduction

The U.S. Army and NASA have an ongoing program to improve helicopter rotor performance and efficiency through the development of advanced airfoils and blade planform shapes. As part of this program, a parametric analytical study (ref. 1) was conducted to design a main rotor to meet selected aerodynamic performance goals for the integrated technology rotor. (See ref. 2.) Reference 1 considered linear variations in planform shapes with taper ratios from 2 to 4 and taper initiation stations from 50 to 95 percent radius. The study in reference 1 indicated unexpectedly that for a constant thrust-weighted solidity, twist, and taper ratio, the configuration that required the least amount of power to cruise at 170 knots (advance ratio μ of 0.40) had the blade taper initiation point nearest the blade tip (95 percent radius). Previous work had confirmed that alternate rotor blade designs that combined advanced airfoils, twist, and linearly tapered planforms were improvements over the baseline rectangular blades (refs. 3 to 6). However, the rotor configurations in references 3 to 6 did not permit an apportionment of the power savings to the various rotor blade design variables because more than one variable was changed between the baseline blade set and the alternate blade set in each case.

In references 3 and 4, the baseline blade set was rectangular with a twist of −10.9° and an NACA 0012 airfoil from root to tip. The alternate blade set had a planform that tapered linearly from 50 percent radius to the blade tip, a twist of −14°, and three different airfoils distributed along the blade span. The baseline blade set in reference 5 was rectangular with a nonlinear twist distribution and two Sikorsky airfoils (SC1095 and SC1095 R8) distributed along the blade span. The alternate blade set in reference 5 had a planform that tapered linearly from 80 percent radius to the blade tip, a linear twist of −16°, and three different airfoils distributed spanwise. In reference 6, the baseline blade set was rectangular with a twist of −9°, and it used the Hughes Helicopters HH-02 and NACA 64A006 airfoils. The alternate blade set in reference 6 had a planform that tapered linearly from 80 percent radius to the blade tip, a twist of −12°, and three different airfoils distributed along the span.

The work reported in references 7 and 8 indicates the effect of tip planform shape on rotor performance. Reference 7 used two sets of rotor blades to show the effect of blade taper ratio on hover performance. One set of blades had a planform with a 3:1 linear taper starting at 80 percent radius, and the second set had a planform with a 5:1 linear taper also starting at 80 percent radius. In reference 8, the rotor blade sets had different tip planform shapes (stations > 85 percent radius), but the sets were not closely related to each other.

Therefore, an experiment was initiated to quantify the effects of significant blade planform changes on the hover and forward-flight performance of small-scale rotors. The effect of large planform changes on hover performance was reported in reference 9, and

this report describes the effects of those planform changes on forward-flight performance. The hover performance investigation was conducted in the rotor test cell at the Langley 14- by 22-Foot Subsonic Tunnel with four small-scale rotors. The forward-flight investigation was conducted in the Glenn L. Martin Wind Tunnel with the same four sets of rotor blades. The rotors tested were 5.417 ft in diameter and differed only in planform geometry. The planforms were (1) rectangular, (2) 3:1 linear taper starting at 94 percent radius, (3) 3:1 linear taper starting at 75 percent radius, and (4) 3:1 linear taper starting at 50 percent radius. Each planform had a thrust-weighted solidity of 0.098. The forward-flight investigation included advance ratios from 0.14 to 0.43 for a range of rotor lift and drag coefficients.

Symbols

The positive directions of forces, angles, and velocities are shown in figure 1.

A	balance axial force, lb
a	speed of sound, ft/sec
C_D	rotor drag coefficient, $\frac{D}{\rho\pi R^2(\Omega R)^2}$
C_L	rotor lift coefficient, $\frac{L}{\rho\pi R^2(\Omega R)^2}$
C_Q	rotor torque coefficient, $\frac{Q}{\rho\pi R^2(\Omega R)^2 R}$
c	local blade chord, ft
c_q	torque-weighted equivalent blade chord, $\frac{\int_0^1 c(r/R)^3\, d(r/R)}{\int_0^1 (r/R)^3\, d(r/R)}$, ft
c_t	thrust-weighted equivalent blade chord, $\frac{\int_0^1 c(r/R)^2\, d(r/R)}{\int_0^1 (r/R)^2\, d(r/R)}$, ft
D	rotor drag, $N \sin \alpha_s + A \cos \alpha_s$, lb
D_{veh}	$= f_D\left(\frac{1}{2}\rho V^2\right)$, lb
f_D	vehicle equivalent parasite area, ft^2
L	rotor lift, $N \cos\ \alpha_s - A \sin\ \alpha_s$, lb
M_T	rotor hover tip Mach number, $\frac{\Omega R}{a}$
N	balance normal force, lb
Q	rotor shaft torque, ft-lb
R	rotor radius, ft
r	spanwise distance along blade radius measured from center of rotation, ft
SLS	sea-level atmospheric density conditions at 59°F
V	free-stream velocity, ft/sec
W	weight, lb
α_s	rotor shaft angle of attack, positive aft, deg
Θ	rotor blade collective pitch angle at $\frac{r}{R} = 0.75$, positive nose up, deg
Θ_1	twist angle built into rotor blade, positive nose up, deg
μ	rotor advance ratio, $\frac{V}{\Omega R}$
ρ	mass density of test medium, slugs/ft^3
σ	area solidity, $\frac{4\int_0^1 c\, d(r/R)}{\pi R}$
σ_Q	torque-weighted solidity, $\frac{4c_q}{\pi R}$
σ_T	thrust-weighted solidity, $\frac{4c_t}{\pi R}$
ψ	rotor blade azimuth angle, deg
Ω	rotor rotational velocity, rad/sec

Subscript:

rect	rectangular

Wind Tunnel and Models

Wind Tunnel

The Glenn L. Martin Wind Tunnel (located at the University of Maryland, College Park) is a closed-circuit, single-return, subsonic tunnel that can be operated at Mach numbers up to 0.32 at atmospheric pressure (ref. 10). Figure 2 shows a schematic of the tunnel. The tunnel test section is 7.75 ft high, 11 ft wide, and 15 ft long, and it has corner fillets. This facility permits tests of small-scale model rotors at full-scale tip Mach numbers at low Reynolds numbers.

Model Description

Rotor blades. Figure 3 shows the planform geometry, airfoil distribution, and twist distribution of the four blade sets. As previously mentioned, the planform geometry was the only difference between the blade sets, so the effect of planform geometry on forward-flight performance can be quantified.

The four blade sets were 13-percent-size representations of blades for a conceptual high-speed, lightweight military helicopter. The full-scale values

of some important parameters for this helicopter are as follows:

R, ft	20.6
ΩR, ft/sec	729
f_D, ft^2	10.5
W, lb	8500
C_L (4000 ft/95°F)	0.00625
C_L (SLS)	0.00505

The thrust-weighted solidity ($\sigma_T = 0.098$), twist ($\Theta_1 = -13°$), and airfoil distribution were thus selected for this class of vehicle. The tapered blades incorporated a 3:1 taper ratio (root chord over tip chord), with the tapers initiated at three different radial stations. A 3:1 taper ratio was chosen because it was a good compromise between aerodynamic performance and fabrication limitations. For some conditions, a rotor with 4:1 taper ratio blades was predicted to provide a small reduction in power compared with a rotor with 3:1 taper ratio blades. (See ref. 1.) However, the smaller tip size for a 4:1 taper ratio blade of 13 percent size makes it more difficult to build and still retain the desired structural characteristics. A linear twist distribution was used to simplify the model fabrication. The area solidity σ, thrust-weighted solidity σ_T, and torque-weighted solidity σ_Q for the rotor blades are listed in table 1. No attempt was made to aeroelastically scale the internal structure of the blades to represent full-scale blades. The blades were made with a D-spar of graphite epoxy, a trailing edge of balsa wood, and an outer skin of fiberglass; this combination of materials resulted in very stiff blades.

Table 1. Solidity for Rotor Blades

Rotor	σ	σ_T	σ_Q
Rectangular	0.098	0.098	0.098
94-percent taper	0.102	0.098	0.096
75-percent taper	0.114	0.098	0.092
50-percent taper	0.126	0.098	0.090

The three rotorcraft (RC) airfoils used for these rotors were developed by the U.S. Army. (See fig. 4.) The RC(4)-10 airfoil, designed for application to the inboard blade region, has high maximum lift coefficients and moderately high drag divergence Mach numbers at low lift coefficients. The RC(3)-08 airfoil has a high drag divergence Mach number at low lift coefficients, so this airfoil was applied to the rotor blade tip region to reduce compressibility effects on the advancing side of the rotor disk. The RC(3)-10 airfoil has drag divergence Mach number characteristics and maximum lift coefficients between those of the RC(4)-10 and the RC(3)-08. Thus, the RC(3)-10 airfoil was used to make the transition between those two airfoil sections. Smooth transitions were made between the different airfoil sections over 5 percent of the blade radius. The two-dimensional aerodynamic characteristics of the RC(4)-10 are described in reference 11, and those of both the RC(3)-10 and RC(3)-08 are described in reference 12.

Test bed. The four sets of rotor blades were tested with the model rotor system shown in figure 5. This system consists of a fully articulated four-bladed rotor hub with coincident lead-lag and blade-flap hinges, a drive shaft, rotor controls, and a gear box of 90° with a 2.75:1 speed reduction ratio. The system is powered by a variable-frequency synchronous motor that is rated at 100 hp at 13 500 rpm. The rotor hub and controls are suspended on a six-component strain-gauge balance and are isolated from the gearbox and motor by a flexible diaphragm coupling. The entire assembly is enclosed in a streamlined fiberglass outer shell and is supported on a post rigidly attached to the tunnel floor. The assembly contains a pitch hinge to tilt the rotor shaft in the fore and aft directions.

To vary the shaft angle of attack, the entire assembly is pitched by means of a remotely controlled hydraulic actuator. Blade collective pitch and lateral and longitudinal cyclic pitch are input to the rotor through a swashplate. The swashplate is remotely positioned with three electromechanical actuators mounted 90° apart. The collective actuator assembly moves both the swashplate and the cyclic control actuator assembly and thus independently determines the blade collective pitch. This arrangement eliminates the mixing of collective and cyclic pitch inputs through use of control laws.

Instrumentation. Operation of the model is conducted through use of the instrumentation mounted on the model rotor system. This instrumentation permits a continuous display of the control settings, rotor forces and moments, and blade angular positions. The swashplate position and thus blade pitch inputs are determined by calibrated linear potentiometers mounted at each actuator. The blade-flap and lead-lag angles are measured by Hall-effect transducers mounted at the blade-flap and lead-lag hinges. The rotating-blade data are transferred through a 60-channel slip-ring assembly mounted on the gearbox along the shaft axis. All strain-gauge

signals are conditioned by bridge amplifiers with anti-aliasing filters set to 1 kHz. The rotor shaft speed is measured with 1-per-rev and 60-per-rev disks and a photocell pickup. The rotor forces and moments are measured by a six-component strain-gauge balance that is fixed with respect to the rotor shaft but pitches with the assembly. Rotor lift and drag are determined from the measured balance normal and axial forces. Forces and moments on the generalized-body fairing are not detected by the balance. The rotor torque is measured independently with a torque disk that is instrumented with a strain-gauge bridge and is attached to the rotor shaft. The rotor shaft tilt is measured with an electronic inclinometer mounted near the rotor balance.

Procedures

This investigation determined the effect of planform variation on the aerodynamic performance of four sets of rotors. As much as possible, the rotors were tested at the same nominal conditions defined by μ, Ω, α_s, and Θ. The range of μ covered in this test was 0.14 to 0.43. The rotor tip speed ($\mu = 0$) was nominally 729 ft/sec, which resulted in an M_T range of 0.627 ($\mu = 0.43$) to 0.635 ($\mu = 0.14$) because of changes in the tunnel temperature. With the tip speed set for each test point in forward flight, the tunnel conditions were adjusted to give the desired value of μ. Then with a constant rotor shaft angle of attack, a collective pitch sweep was initiated. To facilitate data acquisition and reduce blade loads, the rotor cyclic pitch was used to remove the first harmonic flapping with respect to the rotor shaft at each test point. The maximum obtainable values of μ, C_L, and C_D were constrained by the inability of the control system to limit the blade-flapping response quickly when the blades were operated at high loading conditions.

Model deadweight tares were determined throughout the range of shaft angle of attack with the blades installed and with them removed. Aerodynamic rotor hub tares were determined with the hub rotating and the blades removed throughout the ranges of shaft angle of attack and advance ratio that were investigated. Both deadweight and aerodynamic hub tares have been removed from the data. Corrections for tunnel wall effects were applied to the data to obtain a corrected free-stream dynamic pressure and rotor shaft angle. (See refs. 13 and 14.) The maximum correction to α_s because of tunnel wall effects was about 1.4°. The corrected rotor shaft angle was displayed, so the operator of the rotor model could make small adjustments to the preset value of α_s until the corrected α_s matched the desired value. The values of C_L, C_D, and C_Q were obtained from the average of 2048 data samples taken over a nominal 128 rotor revolutions at each test condition.

Data Quality

The performance data measured during this investigation was examined for repeatability and is reported in the appendix. For the four blade sets, collective pitch sweeps were typically repeated for a single α_s at some advance ratios. To minimize the data acquisition time for these repeat sweeps, no attempt was made to exactly duplicate the collective and cyclic angles used for the first sweep. Thus, the repeatability is based on the closeness of the two faired curves drawn through the two sets of data points rather than on each pair of data points. The repeatability of these data is judged to be very good.

Presentation of Results

The results of this investigation were reduced to coefficient form and are presented in figures 6 to 43, as shown in table 2. These performance parameters were not divided by the rotor solidity because the four different types of blades (tapered and rectangular) had the same thrust-weighted solidity.

Discussion of Results

The basic data are presented in figures 6 to 35, and the C_D versus C_Q results at constant values of the rotor lift coefficients (figs. 36 to 39) were determined from a cross plot of the basic data. The C_Q versus μ results at constant rotor lift coefficients (figs. 40 to 42) were determined from a cross plot of the C_D versus C_Q results. For example, the C_Q versus μ result for $C_L = 0.006$ (fig. 41) was obtained from a record of the C_Q value, at each advance ratio, that corresponds to the appropriate value of the rotor drag coefficient (equal in magnitude to the vehicle drag coefficient) obtained from figure 38. The vehicle drag coefficient was determined from the vehicle drag D_{veh} that was defined through use of an equivalent parasite area as follows: $D_{veh} = f_D\left(\frac{1}{2}\rho V^2\right)$. A value of 10.5 ft^2 was selected to represent f_D for a modern, lightweight military helicopter. The C_Q versus μ results are presented for lift coefficients of 0.005 and 0.006. These values were chosen because they are close to the level-flight values at SLS ($C_L = 0.00505$) and 4000 ft/95°F ($C_L = 0.00625$) atmospheric conditions for the selected helicopter and they are convenient to use in making cross plots. Also, a C_Q versus μ result is presented for a lift coefficient ($C_L = 0.007$) above the level-flight values.

Table 2. Performance Parameters for Rotors

(a) Basic characteristics

Parameter	μ	Figures for rotor planform—			
		Rectangular	94-percent taper	75-percent taper	50-percent taper
C_L vs C_D and C_L vs C_Q	0.14	6	12	20	28
	0.19	7	13	21	29
	0.23	8		22	30
	0.24		14		
	0.27	9	15	23	31
	0.30			24	32
	0.31	10	16		
	0.35			25	33
	0.36	11	17		
	0.40		18	26	34
	0.43		19	27	35

(b) Comparison of rotors

Parameter	C_L	μ	Figures for rotor planform—			
			Rectangular	94-percent taper	75-percent taper	50-percent taper
C_D vs C_Q	0.004	0.14-0.40	36	36	36	36
	0.005	0.14-0.36	37	37	37	37
	0.006	0.14-0.36	38	38	38	38
	0.007	0.14-0.27	39	39	39	39
C_Q vs μ	0.005	0.14-0.31	40	40	40	40
	0.006	0.14-0.31	41	41	41	41
	0.007	0.14-0.27	42	42	42	42
$\frac{C_Q - C_{Q,\text{rect}}}{C_{Q,\text{rect}}}$	0.005	0.14-0.30	43	43	43	43
	0.006	0.14-0.30	43	43	43	43
	0.007	0.14-0.27	43	43	43	43

For the four rotors at lift coefficients from 0.004 to 0.007, C_D varies linearly with C_Q at all advance ratios (figs. 36 to 39). Among the four rotors, the rectangular rotor requires the highest C_Q (and thus the greatest power) for the entire range of C_D attained at advance ratios greater than 0.14 for the four rotor lift coefficients. Only at the lowest advance ratio for $C_L = 0.006$ and 0.007 and for $C_D \leq 0.00025$ is the C_Q required for any of the tapered rotors (the 94-percent tapered rotor in this case) as high as the C_Q required for the rectangular rotor. Among the rotors with tapered blades, either the 75-percent tapered rotor or the 50-percent tapered rotor requires the least amount of torque at each advance ratio. For $C_L = 0.004$ to 0.006, the 75-percent tapered rotor has the lower torque coefficients for all values of C_D at $\mu = 0.14$ and 0.19, whereas the 50-percent tapered rotor has the lower values of C_Q for all values of C_D at $\mu = 0.30$ and 0.31. The 75-percent tapered rotor and the 50-percent tapered rotor have nearly the same performance at $\mu = 0.23$ and 0.27 for many values of C_D at the four rotor lift coefficients. The performance of the 94-percent tapered rotor is generally between that of the rectangular rotor and the 75- and 50-percent tapered rotors at each advance ratio at the four rotor lift coefficients.

The performance of the four rotors in terms of C_Q versus μ is compared in figures 40 to 42 for lift coefficients from 0.005 to 0.007. The trends due to planform variation shown in these figures are consistent with the previous discussion. The advance ratio for the minimum C_Q changes as the lift coefficient increases. For $C_L = 0.005$, the minimum C_Q for each rotor occurs at $\mu = 0.14$, but for $C_L = 0.007$ the minimum C_Q for each rotor occurs near $\mu = 0.19$. As expected, the C_Q level for the four rotors increases as C_L increases.

Figure 43 shows the performance of the tapered rotors expressed in terms relative to the rectangular rotor $\left(\left(C_Q - C_{Q,\text{rect}}\right)/C_{Q,\text{rect}}\right)$. For $\mu \leq 0.23$, the 75-percent tapered rotor provides the maximum improvement, which is about 8 percent for the three rotor lift coefficients. For $\mu > 0.23$, the 50-percent tapered rotor or, for some conditions, both the 50- and 75-percent tapered rotors provide the maximum improvement. The maximum improvement for this range of μ is between 7 and 10 percent for the three rotor lift coefficients. These effects of blade planform variation on rotor performance are not in agreement with the analytical trends presented in reference 1 for an advance ratio of 0.40. Among the four rotors of this investigation, the results of reference 1 suggest that the 94-percent tapered rotor should require the least amount of torque. In this study, however, the 50- and 75-percent tapered rotors required the least amount of torque.

Conclusions

An investigation was conducted in the Glenn L. Martin Wind Tunnel to determine the effects of blade planform variation on the forward-flight performance of four small-scale rotors. The rotors were 5.417 ft in diameter and differed only in planform geometry. The four planforms were (1) rectangular, (2) 3:1 linear taper starting at 94 percent radius, (3) 3:1 linear taper starting at 75 percent radius, and (4) 3:1 linear taper starting at 50 percent radius. Each planform had a thrust-weighted solidity of 0.098. The investigation included forward-flight simulation at advance ratios from 0.14 to 0.43 for a range of rotor lift and drag coefficients. Examination of these data led to the following conclusions.

1. Among the four rotors, the rectangular rotor required the highest torque for the entire range of rotor drag coefficients attained at values of advance ratio μ from 0.19 to 0.36 for rotor lift coefficients C_L of 0.004 and 0.005. For $C_L = 0.006$ and 0.007, this same trend was indicated for μ's from 0.19 to 0.31 and 0.19 to 0.27, respectively. Among the rotors with tapered blades and for $C_L = 0.004$ to 0.007, either the 75-percent tapered rotor or the 50-percent tapered rotor required the least amount of torque for the full range of rotor drag coefficients attained at each advance ratio tested. For this range of C_L, the performance of the 94-percent tapered rotor was generally between that of the rectangular rotor and the 75- and 50-percent tapered rotors at each μ.

2. For $C_L = 0.005$ and 0.006 and a vehicle equivalent parasite area f_D of 10.5 ft^2, the rectangular rotor required the most torque at advance ratios from 0.14 to 0.31. For the same range of C_L, the torque required for the 94-percent tapered rotor at all values of μ was generally less than that for the rectangular rotor but higher than that for the 75- and 50-percent tapered rotors. The 75-percent tapered rotor required the lowest torque for $\mu \leq 0.23$ and the 50-percent tapered rotor required the lowest torque for $\mu = 0.27$ to 0.30.

3. The torque required for the 75-percent tapered rotor at $\mu \leq 0.23$, $f_D = 10.5$ ft^2, and $C_L = 0.005$ to 0.007 represents an improvement of 5 to 8 percent over that for the rectangular rotor. For $0.23 < \mu \leq 0.30$ with the same f_D and range of C_L, the torque required for the 50-percent tapered rotor represents an improvement of 7 to 10 percent over that for the rectangular rotor.

NASA Langley Research Center
Hampton, VA 23665-5225
March 11, 1992

References

1. Noonan, Kevin W. Aerodynamic Design of a Helicopter Main Rotor Blade With Consideration of Flap-Lag Flutter in Hover. M.S. Thesis, Univ. of Maryland, 1985.

2. Howes, H. E., and Tomashofski, C. A. *Integrated Technology Rotor/Flight Research Rotor (ITR/FRR) Concept Definition.* NASA CR-166415, USAAVRADCOM TR 83-A-5, 1983.

3. Bingham, Gene J. The Aerodynamic Influences of Rotor Blade Airfoils, Twist, Taper and Solidity on Hover and Forward Flight Performance. *37th Annual Forum Proceedings*, American Helicopter Soc., 1981, pp. 37–50.

4. Berry, John D. *Performance Testing of a Main Rotor System for a Utility Helicopter at 1/4 Scale.* NASA TM-83271, AVRADCOM TR 82-B-3, 1982.

5. Yeager, William T., Jr., Mantay, Wayne R., Wilbur, Matthew L., Cramer, Robert G., Jr., and Singleton, Jeffrey D. *Wind-Tunnel Evaluation of an Advanced Main-Rotor Blade Design for a Utility-Class Helicopter.* NASA TM-89129, AVSCOM TM 87-B-8, 1987.

6. Kelley, Henry L.: *Aerodynamic Performance of a 0.27-Scale Model of an AH-64 Helicopter With Baseline and Alternate Rotor Blade Sets.* NASA TM-4201, AVSCOM TM-90-B-015, 1990.

7. Kelley, Henry L.: *Effect of Planform Taper on Hover Performance of an Advanced AH-64 Model Rotor.* NASA TM-89145, AVSCOM TM-87-B-10, 1987.

8. McVeigh, Michael A.; and McHugh, Francis J.: Influence of Tip Shape, Chord, Blade Number, and Airfoil on Advanced Rotor Performance. *J. American Helicopter Soc.*, vol. 29, no. 4, Oct. 1984, pp. 55-62.

9. Althoff, Susan L.; and Noonan, Kevin W.: *Effect of Blade Planform Variation on a Small-Scale Hovering Rotor.* NASA TM-4146, AVSCOM TM-89-B-009, 1990.

10. Pirrello, C. J.; Hardin, R. D.; Heckart, M. V., and Brown, K. R.: *An Inventory of Aeronautical Ground Research Facilities. Volume I—Wind Tunnels.* NASA CR-1874, 1971.

11. Noonan, Kevin W.: *Aerodynamic Characteristics of Two Rotorcraft Airfoils Designed for Application to the Inboard Region of a Main Rotor Blade.* NASA TP-3009, AVSCOM TR-90-B-005, 1990.

12. Bingham, Gene J.; and Noonan, Kevin W.: *Two-Dimensional Aerodynamic Characteristics of Three Rotorcraft Airfoils at Mach Numbers From 0.35 to 0.90.* NASA TP-2000, AVRADCOM TR 82-B-2, 1982.

13. Heyson, Harry H.: *FORTRAN Programs for Calculating Wind-Tunnel Boundary Interference.* NASA TM X-1740, 1969.

14. Heyson, Harry H.: *Use of Superposition in Digital Computers To Obtain Wind-Tunnel Interference Factors for Arbitrary Configurations, With Particular Reference to V/STOL Models.* NASA TR R-302, 1969.

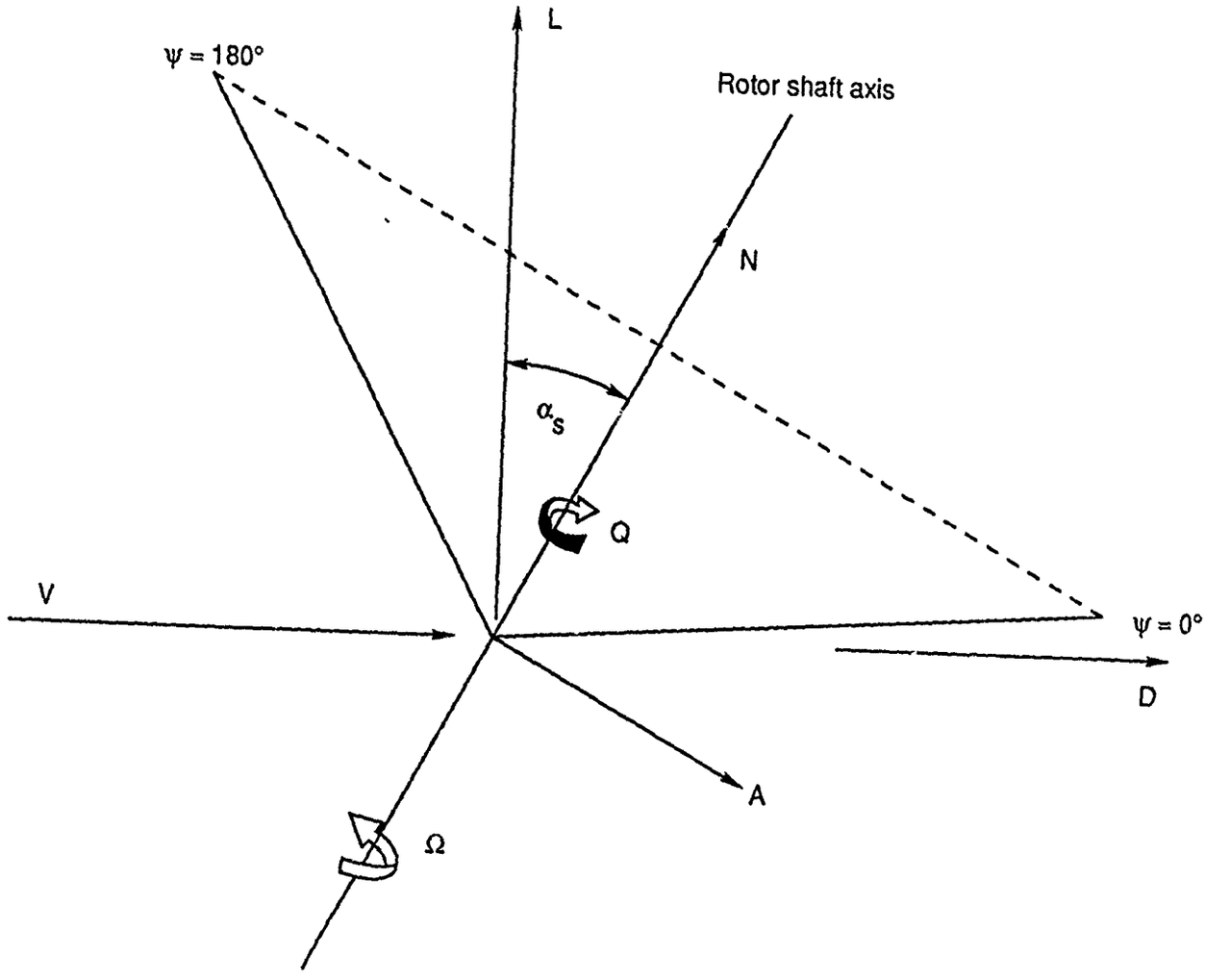

Figure 1. Positive directions of forces, angles, and velocities.

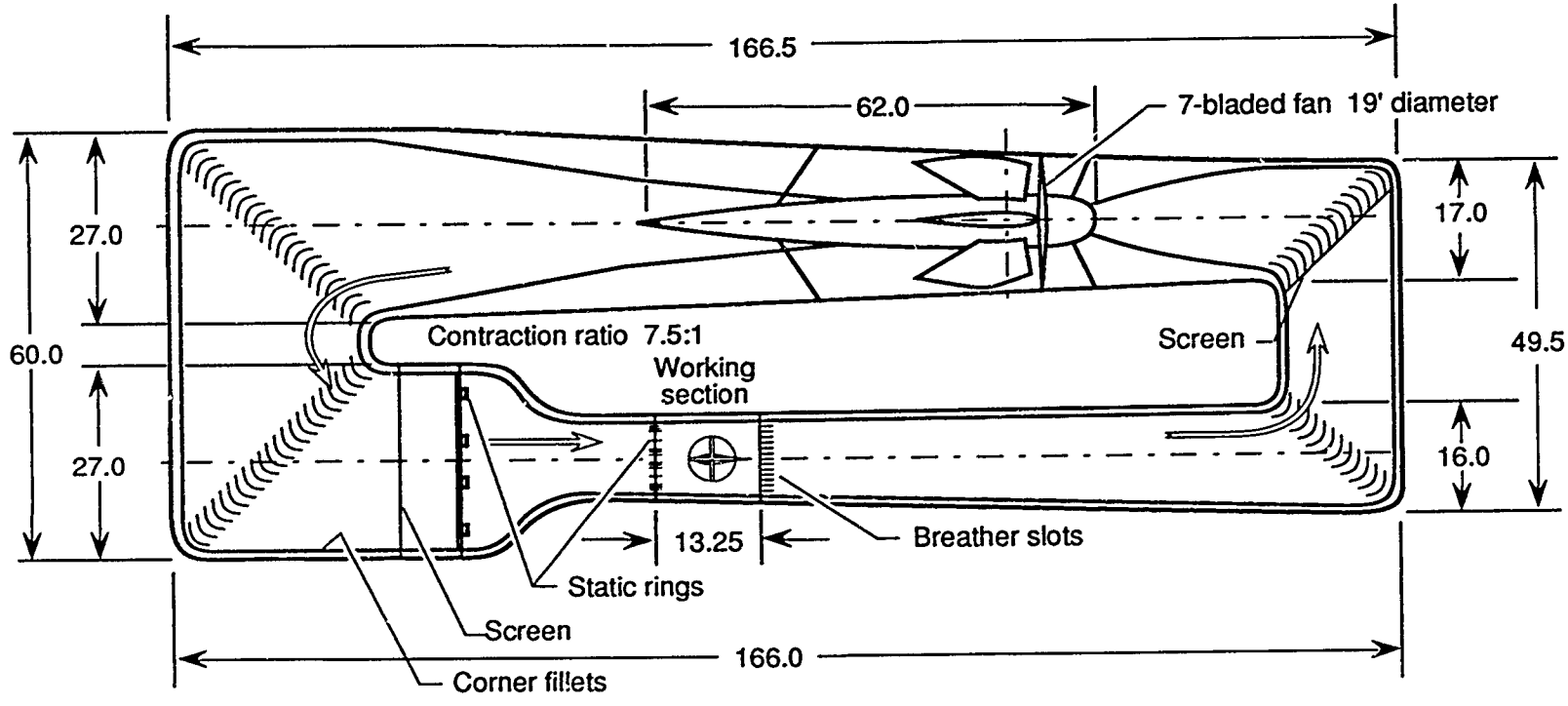

Figure 2. Planview of Glenn L. Martin Wind Tunnel. Linear dimensions in feet.

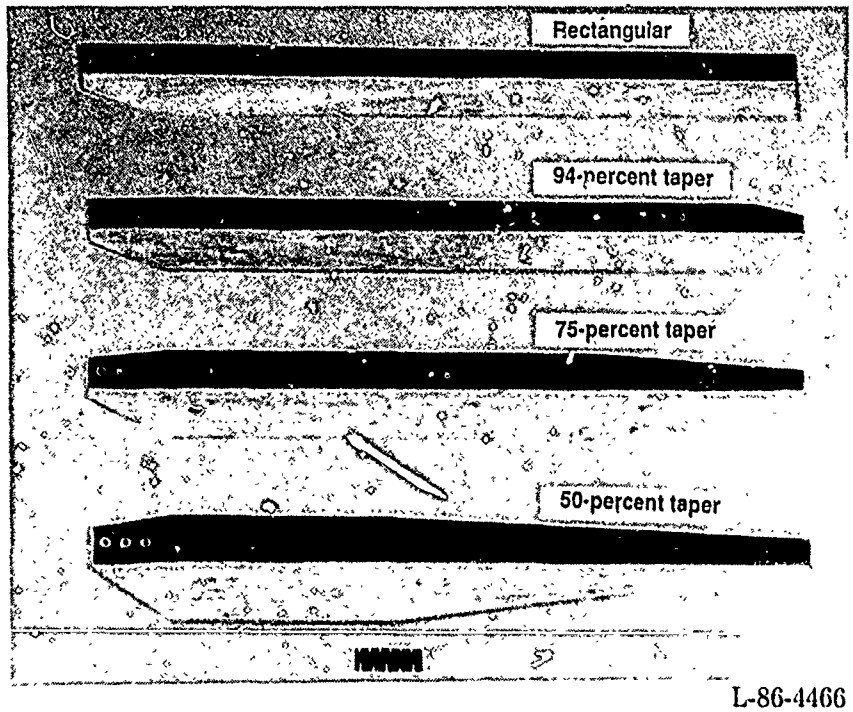

(a) Four blade planforms.

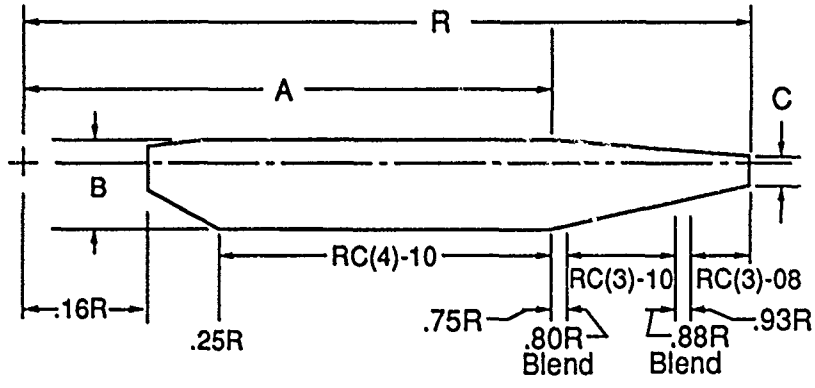

Blade	Twist, deg	R, ft	A	B	C
Rectangular	-13	2.708	1.00R	0.0770R	0.0770R
94-percent taper	-13	2.708	0.94R	.0817R	.0272R
75-percent taper	-13	2.708	.75R	.0972R	.0324R
50-percent taper	-13	2.708	.50R	.1194R	.0398R

(b) Planform and airfoil distribution.

Figure 3. Description of rotor blades.

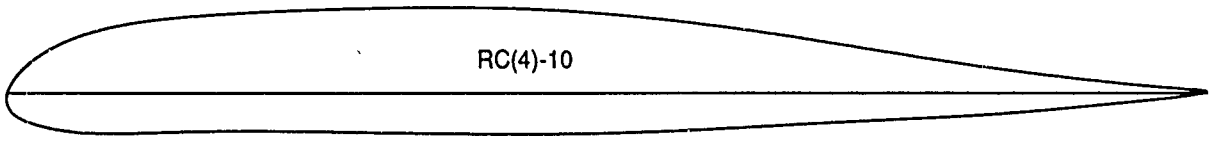

r/R = 0.25 to 0.75

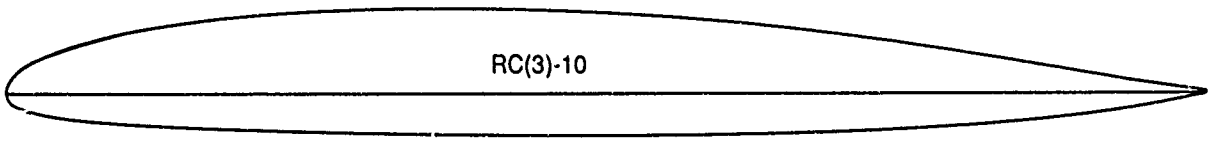

r/R = 0.80 to 0.88

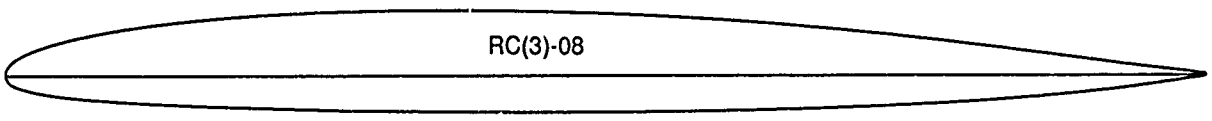

r/R = 0.93 to 1.0

Figure 4. Airfoils used on rotor blades.

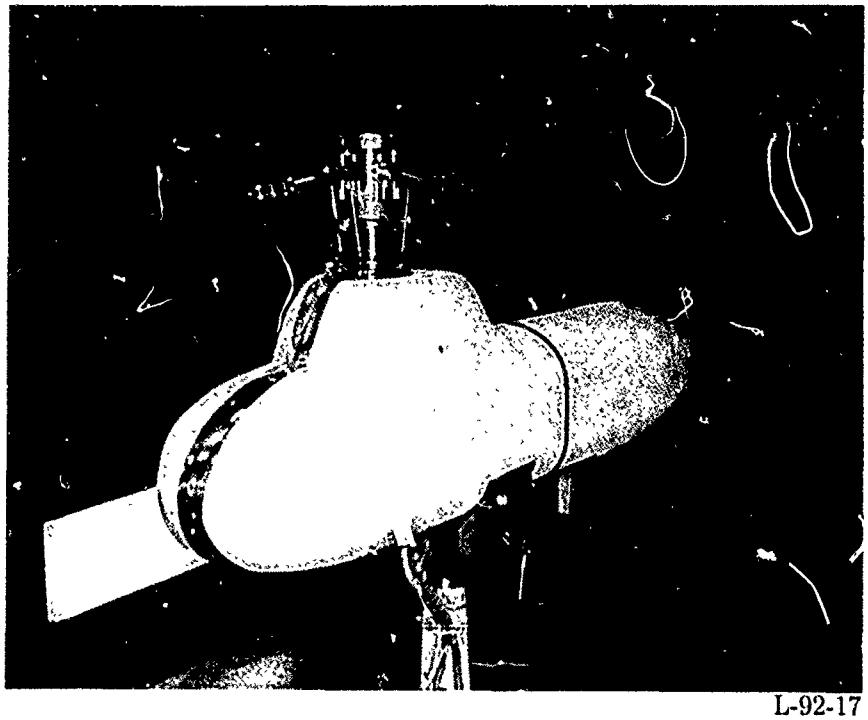

L-92-17

(a) Generalized-body fairing installed.

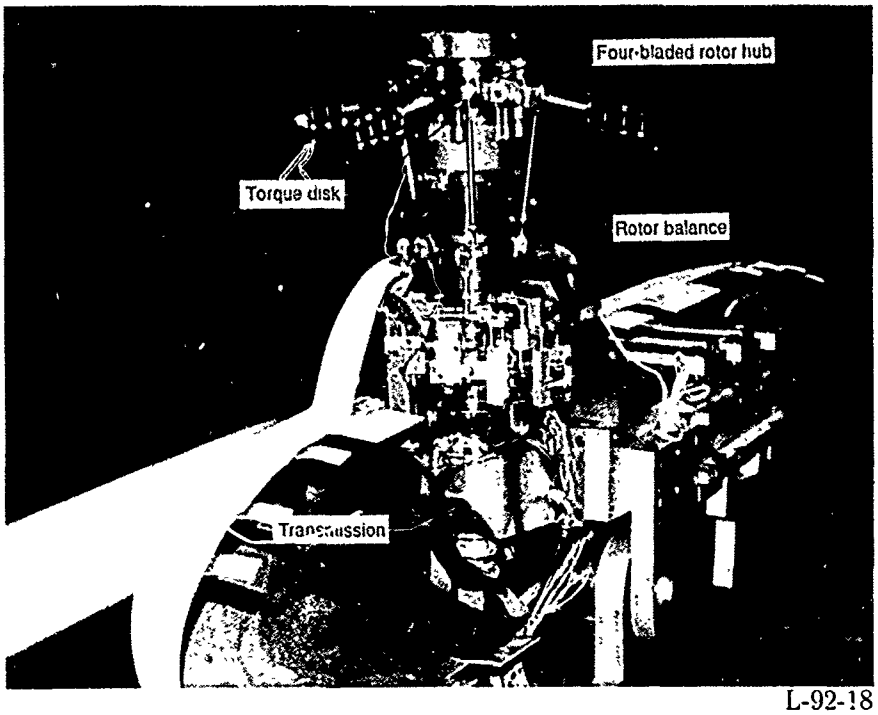

L-92-18

(b) Cutaway view.

Figure 5. Model rotor system installed in the Glenn L. Martin Wind Tunnel.

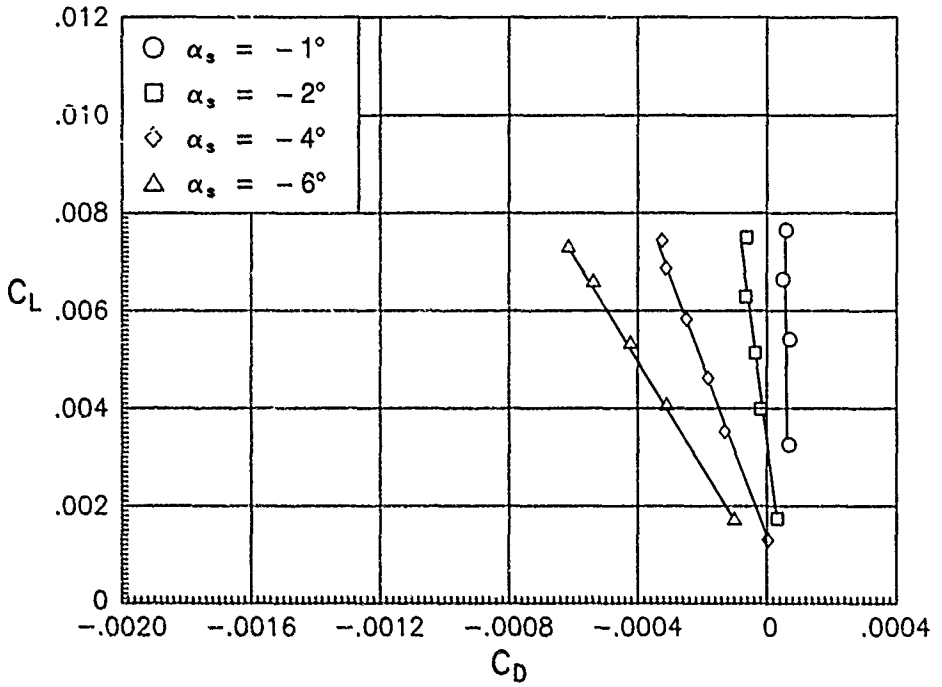

(a) C_L versus C_D.

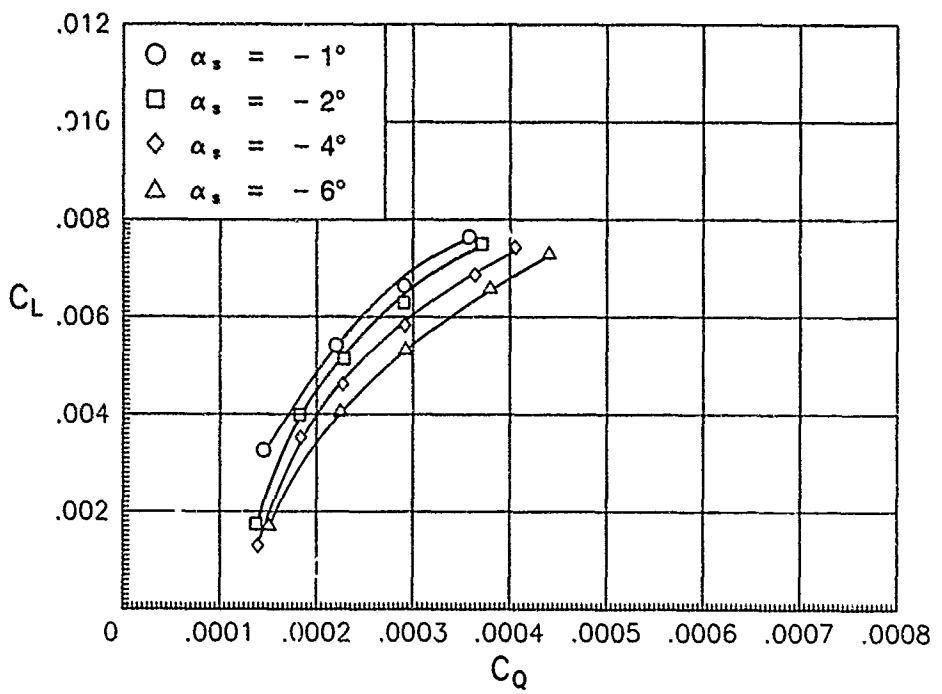

(b) C_L versus C_Q.

Figure 6. Basic forward-flight characteristics of rectangular rotor for $\mu = 0.14$.

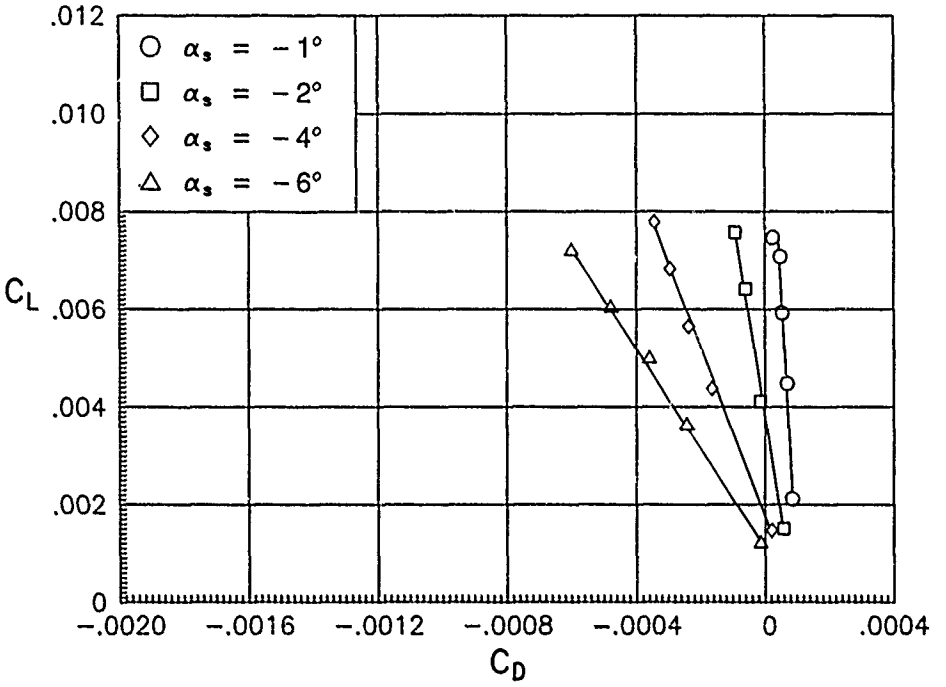

(a) C_L versus C_D.

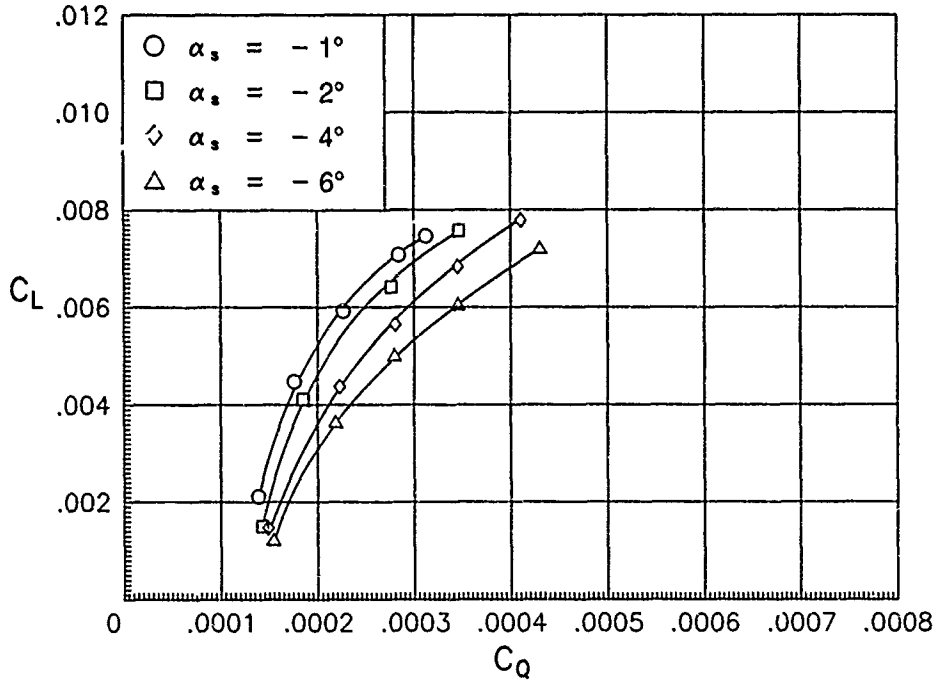

(b) C_L versus C_Q.

Figure 7. Basic forward-flight characteristics of rectangular rotor for $\mu = 0.19$.

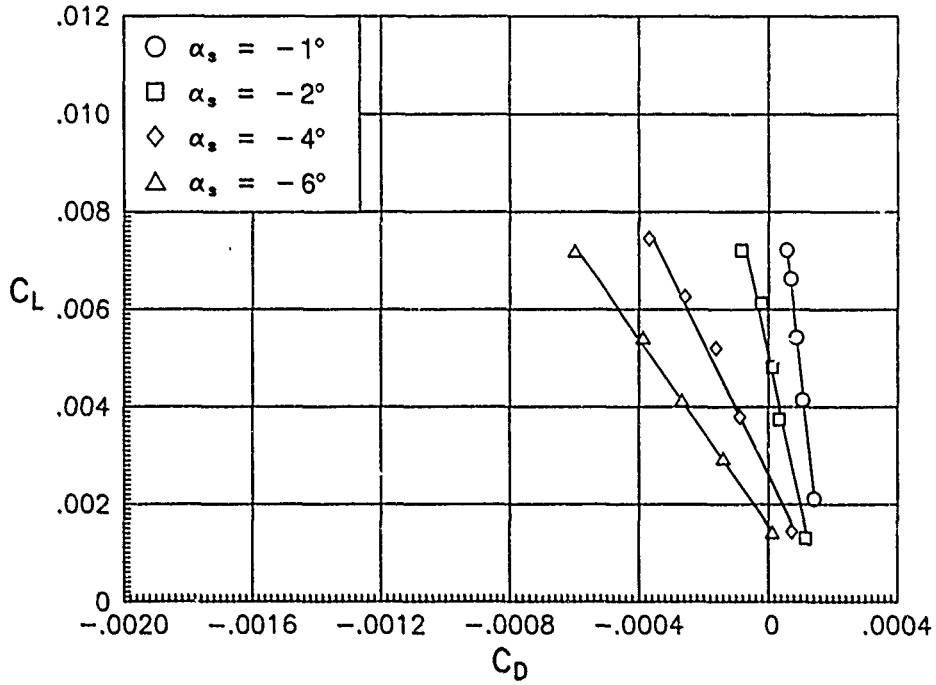

(a) C_L versus C_D.

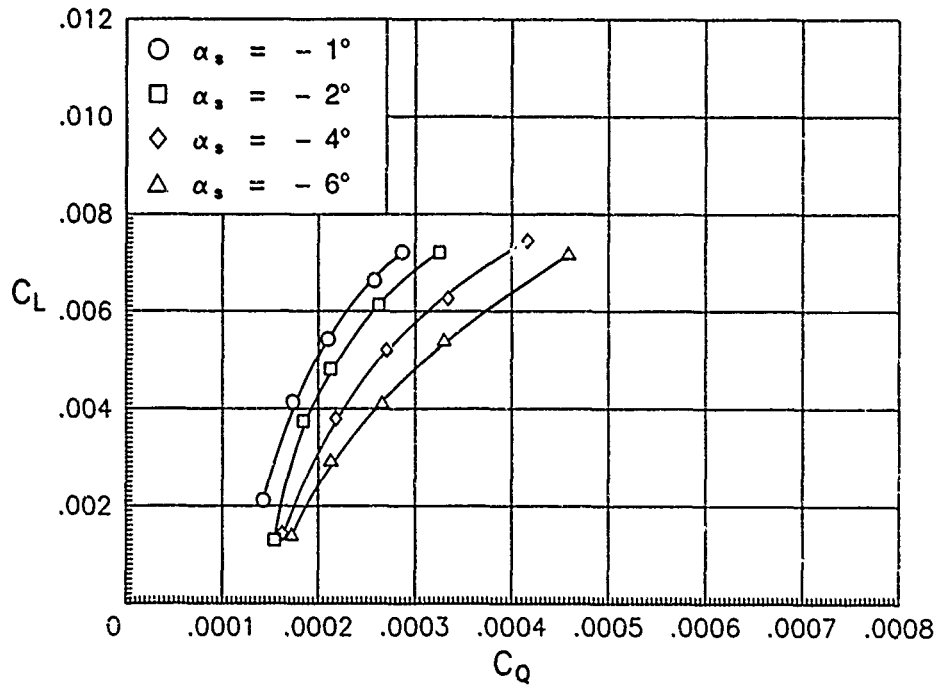

(b) C_L versus C_Q.

Figure 8. Basic forward-flight characteristics of rectangular rotor for $\mu = 0.23$.

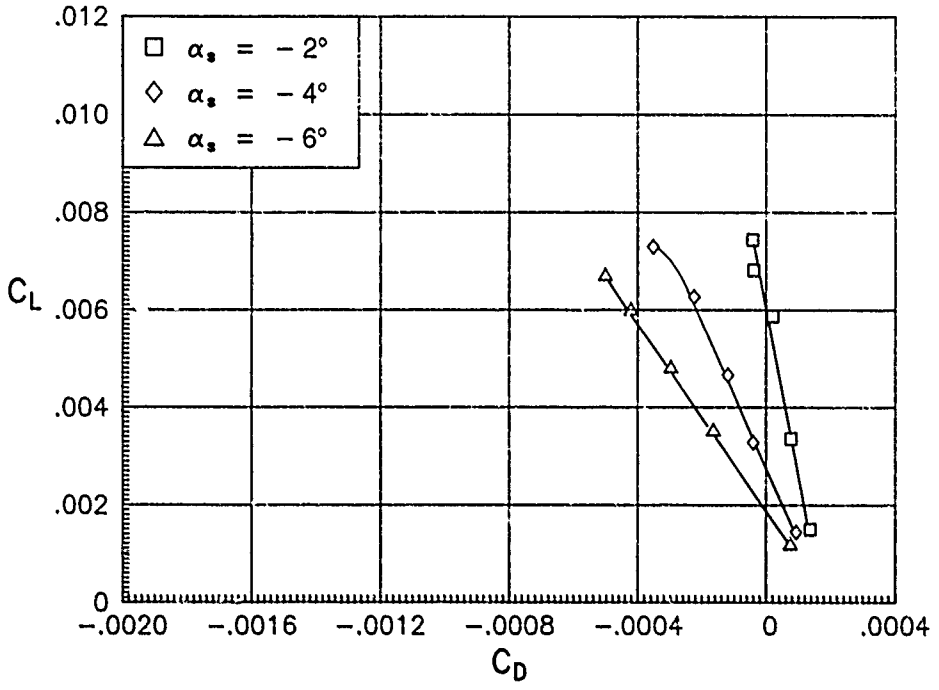

(a) C_L versus C_D.

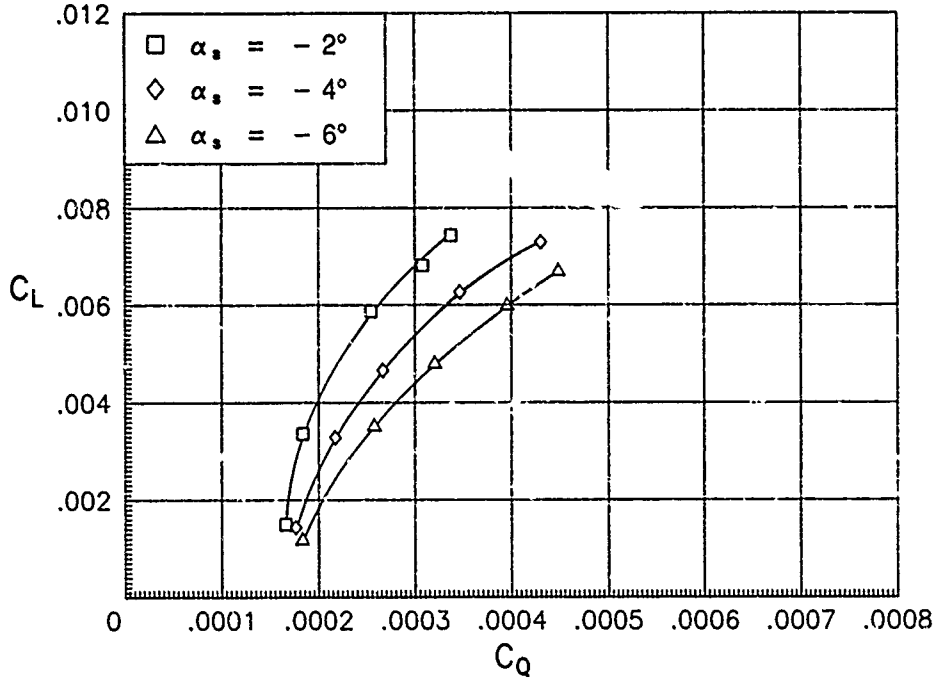

(b) C_L versus C_Q.

Figure 9. Basic forward-flight characteristics of rectangular rotor for $\mu = 0.27$.

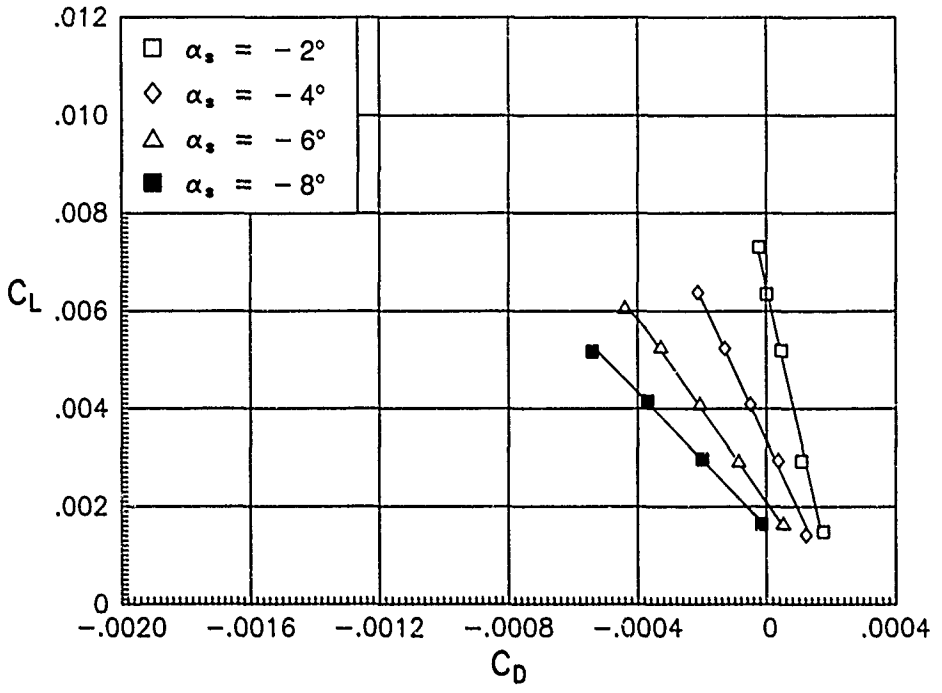

(a) C_L versus C_D.

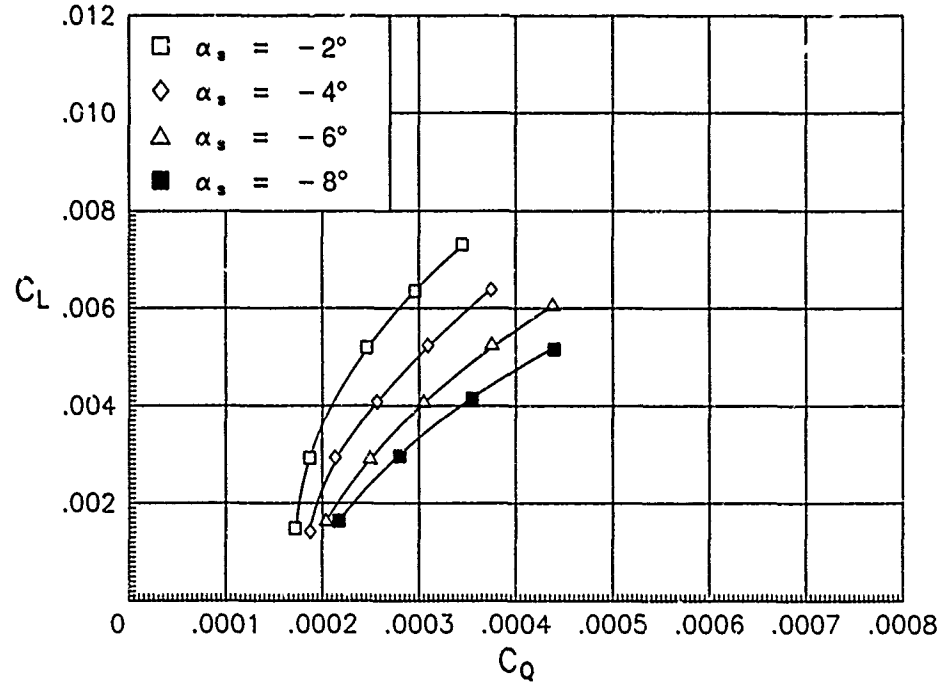

(b) C_L versus C_Q.

Figure 10. Basic forward-flight characteristics of rectangular rotor for $\mu = 0.31$.

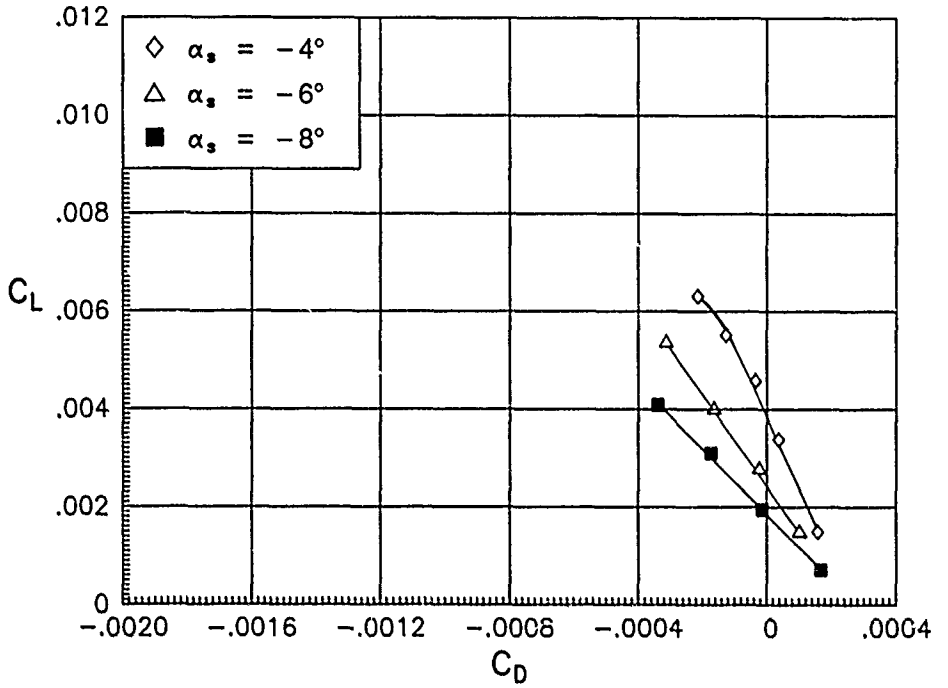

(a) C_L versus C_D.

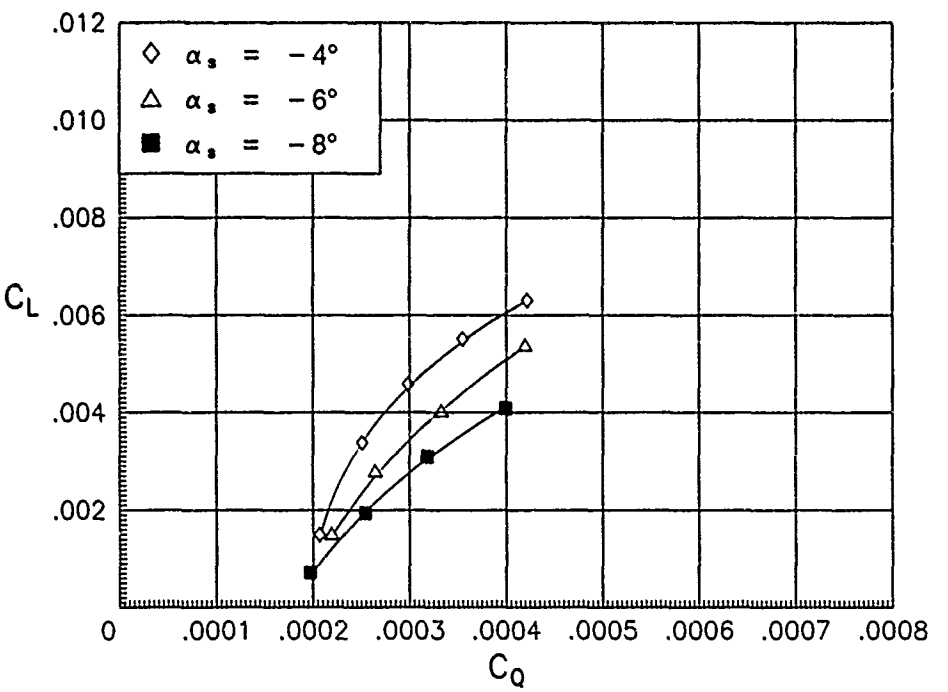

(b) C_L versus C_Q.

Figure 11. Basic forward-flight characteristics of rectangular rotor for $\mu = 0.36$.

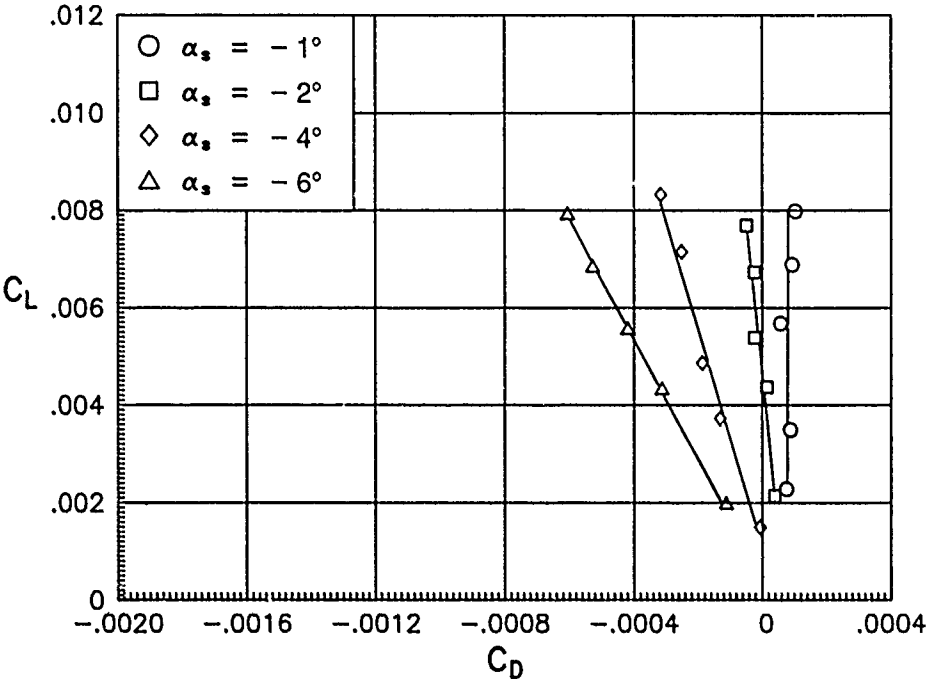

(a) C_L versus C_D.

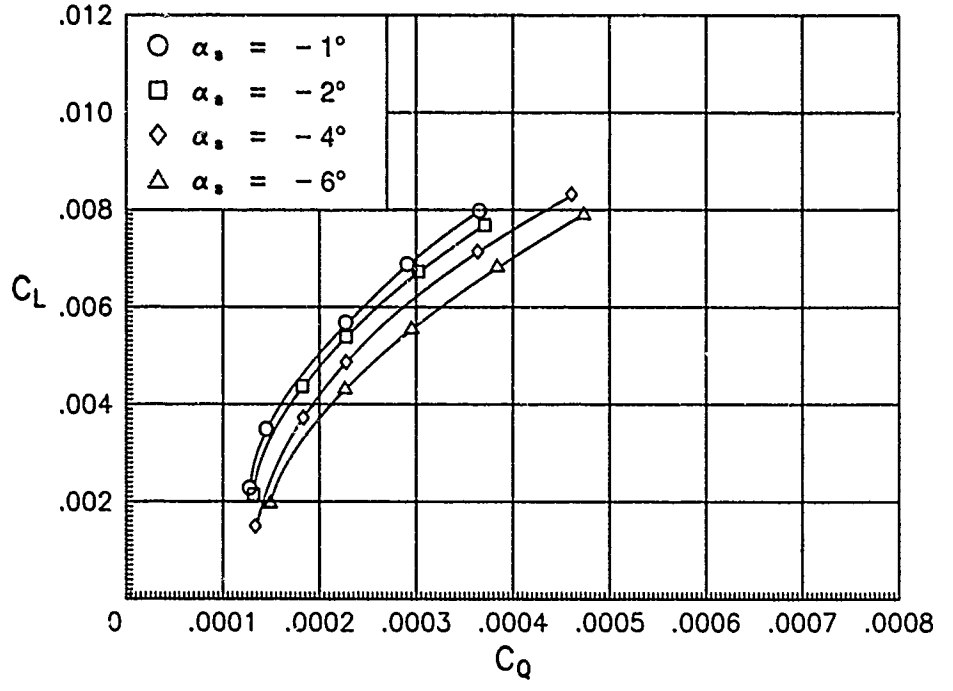

(b) C_L versus C_Q.

Figure 12. Basic forward-flight characteristics of 94-percent tapered rotor for $\mu = 0.14$.

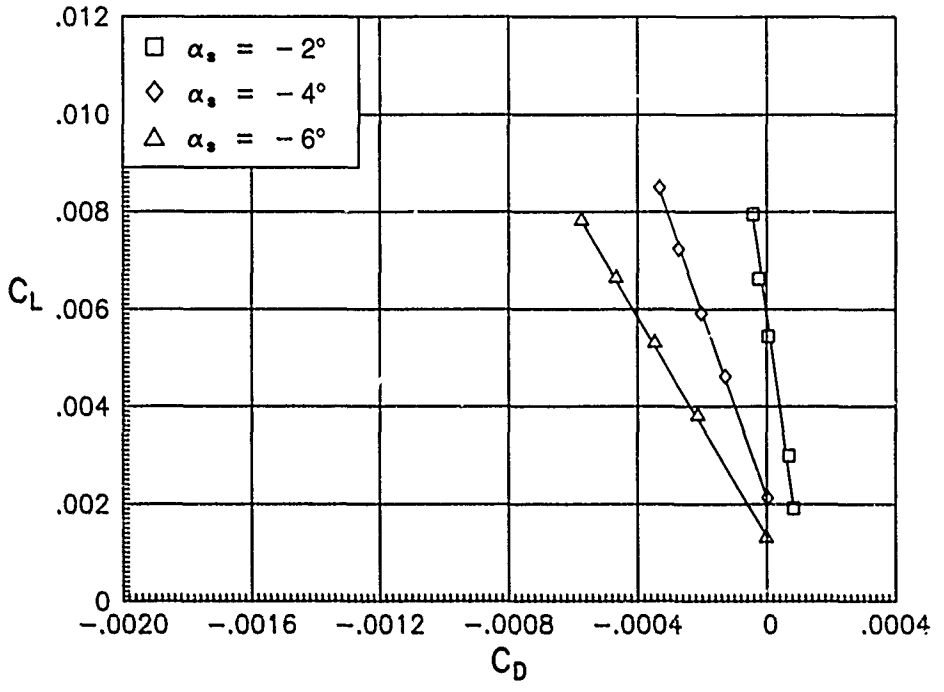

(a) C_L versus C_D.

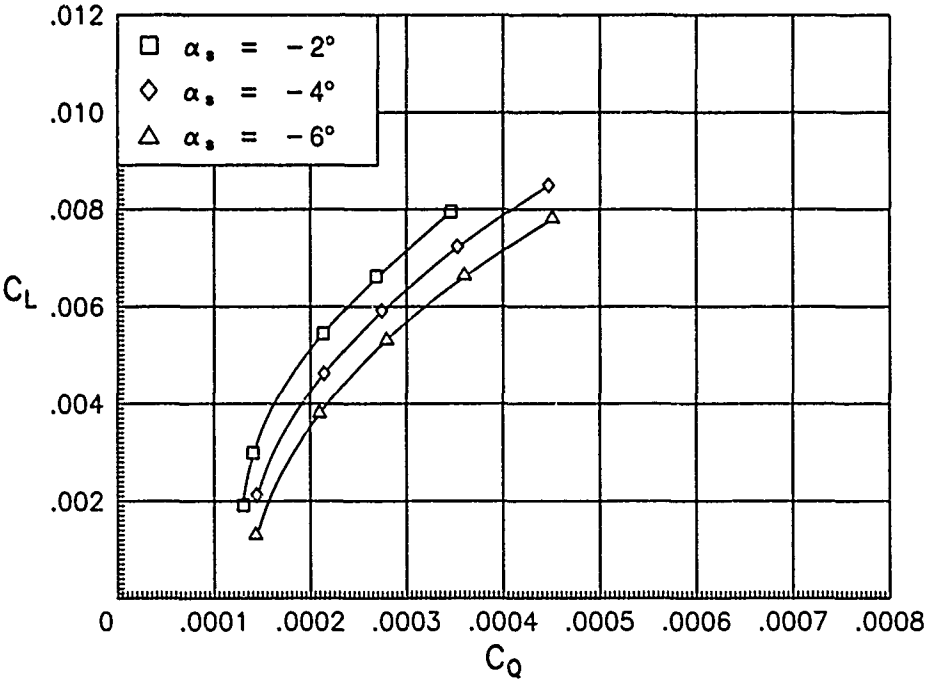

(b) C_L versus C_Q.

Figure 13. Basic forward-flight characteristics of 94-percent tapered rotor for $\mu = 0.19$.

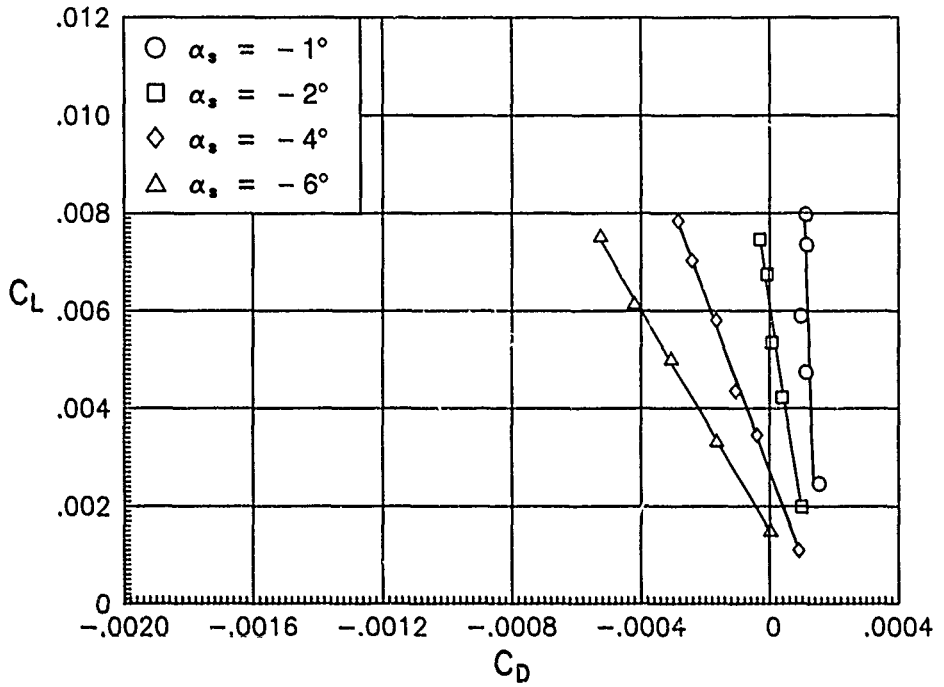

(a) C_L versus C_D.

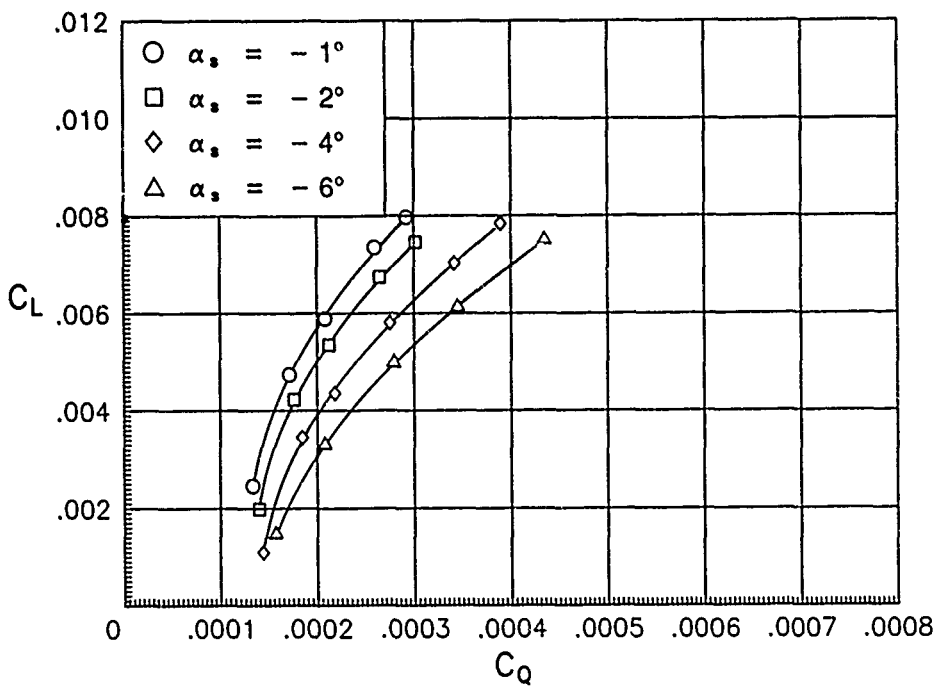

(b) C_L versus C_Q.

Figure 14. Basic forward-flight characteristics of 94-percent tapered rotor for $\mu = 0.24$.

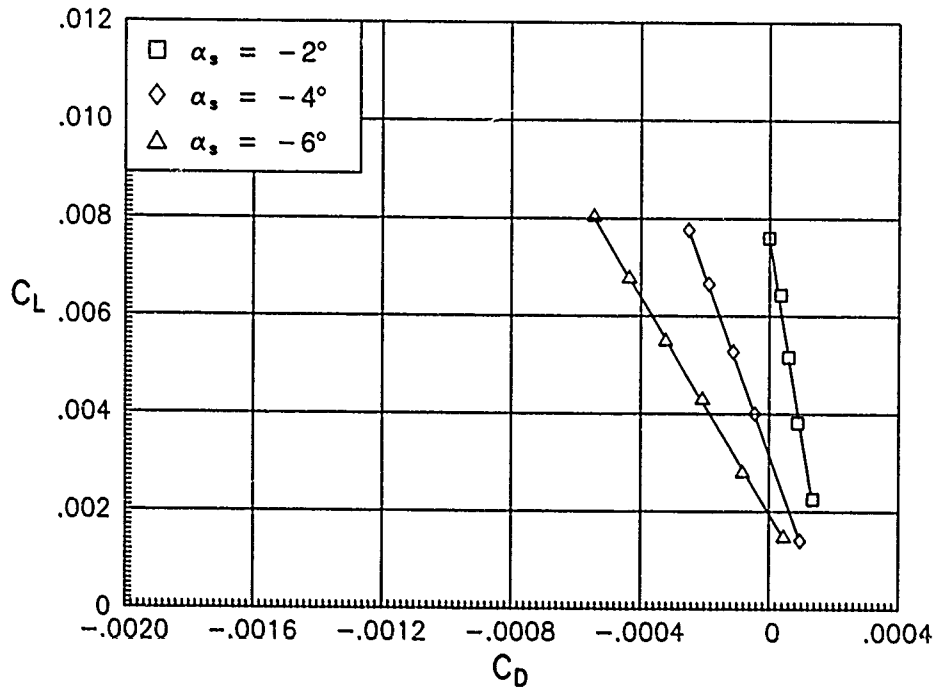

(a) C_L versus C_D.

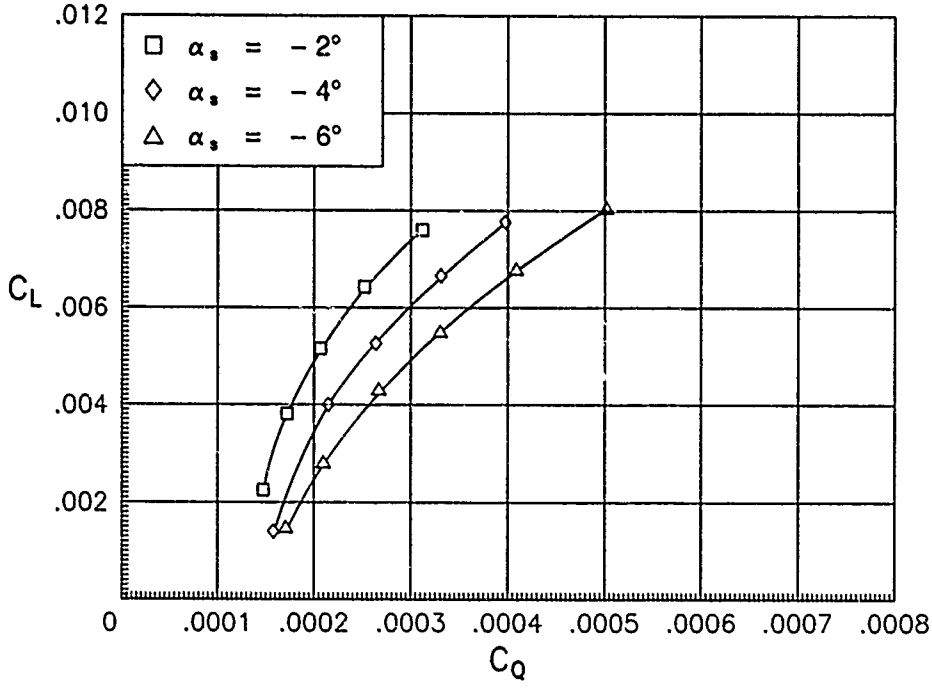

(b) C_L versus C_Q.

Figure 15. Basic forward-flight characteristics of 94-percent tapered rotor for $\mu = 0.27$.

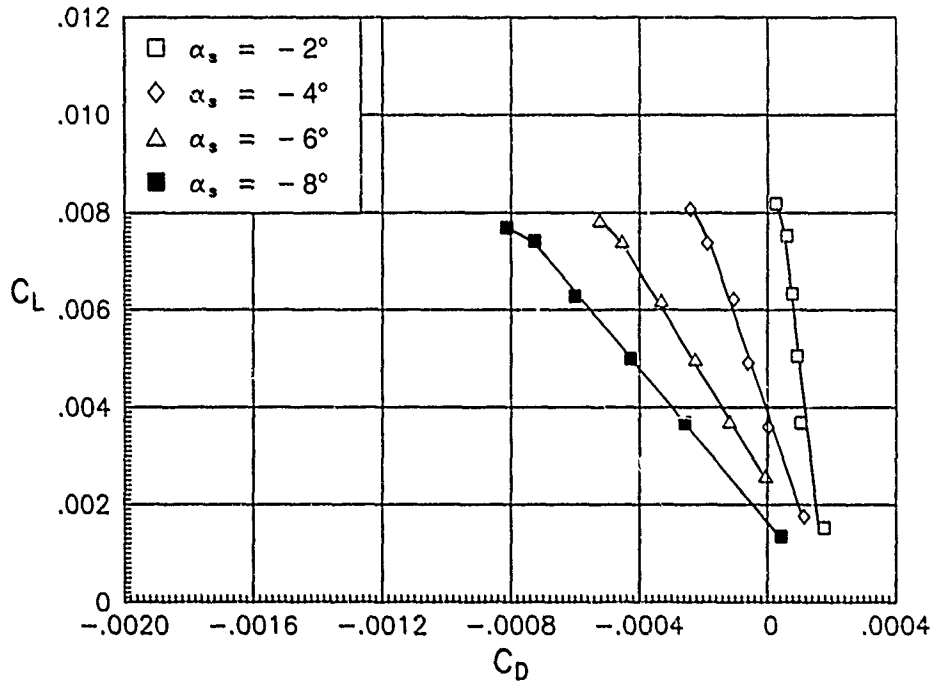

(a) C_L versus C_D.

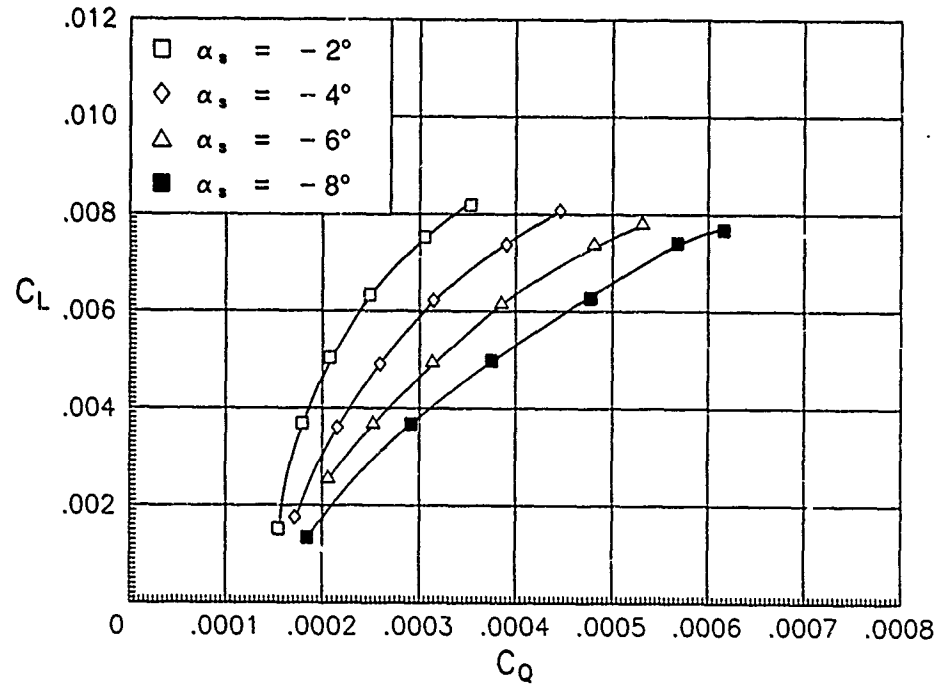

(b) C_L versus C_Q.

Figure 16. Basic forward-flight characteristics of 94-percent tapered rotor for $\mu = 0.31$.

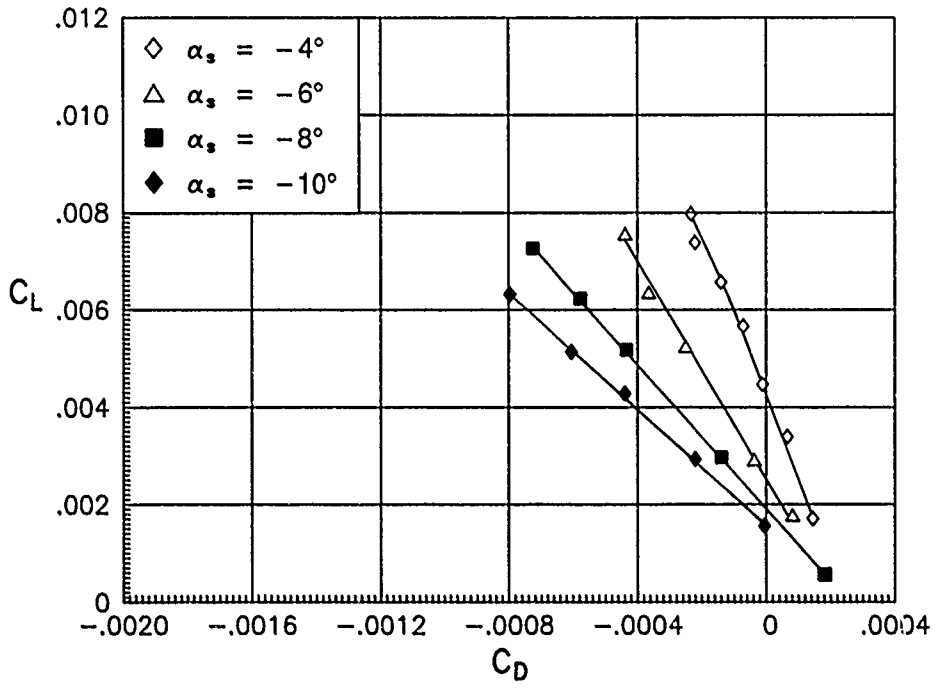

(a) C_L versus C_D.

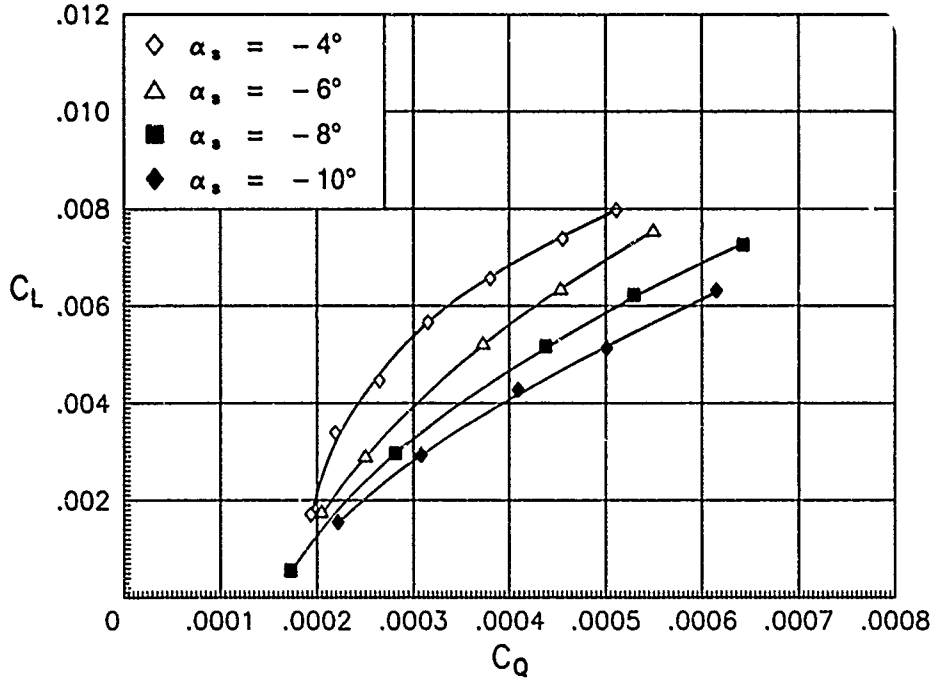

(b) C_L versus C_Q.

Figure 17. Basic forward-flight characteristics of 94-percent tapered rotor for $\mu = 0.36$.

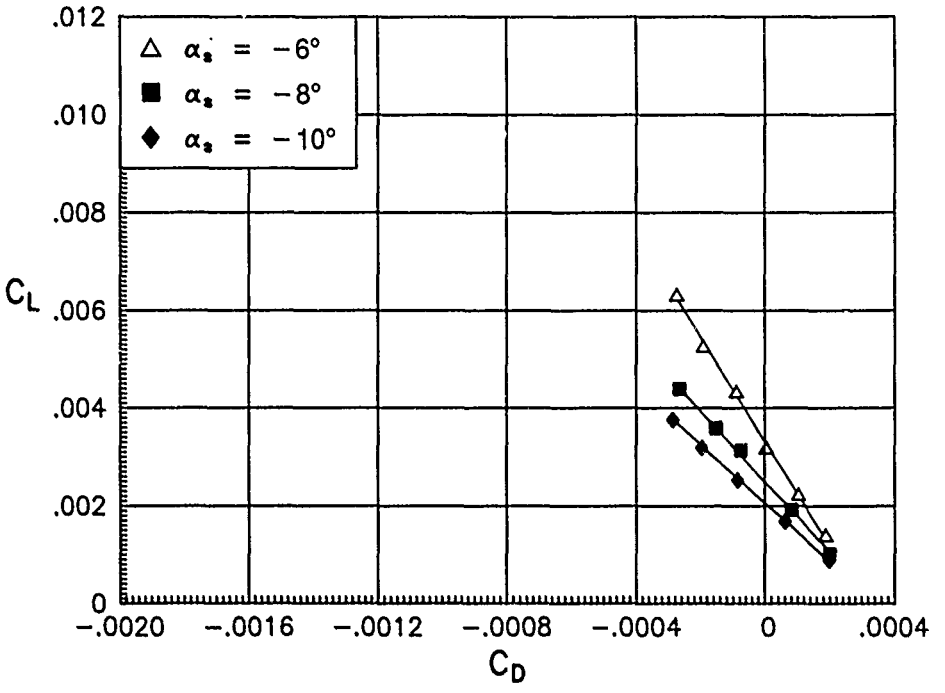

(a) C_L versus C_D.

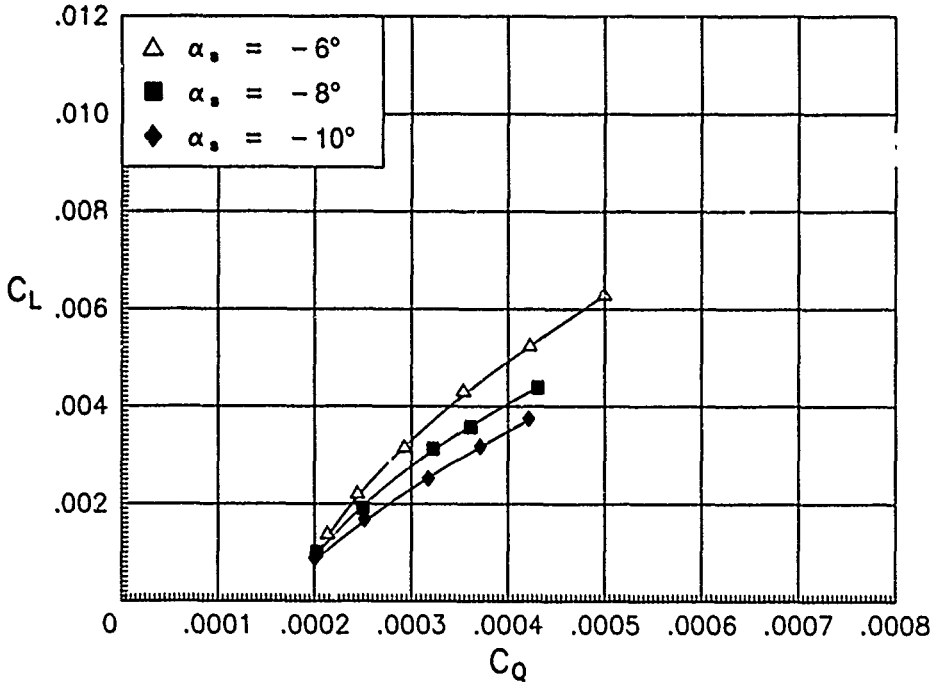

(b) C_L versus C_Q.

Figure 18. Basic forward-flight characteristics of 94-percent tapered rotor for $\mu = 0.40$.

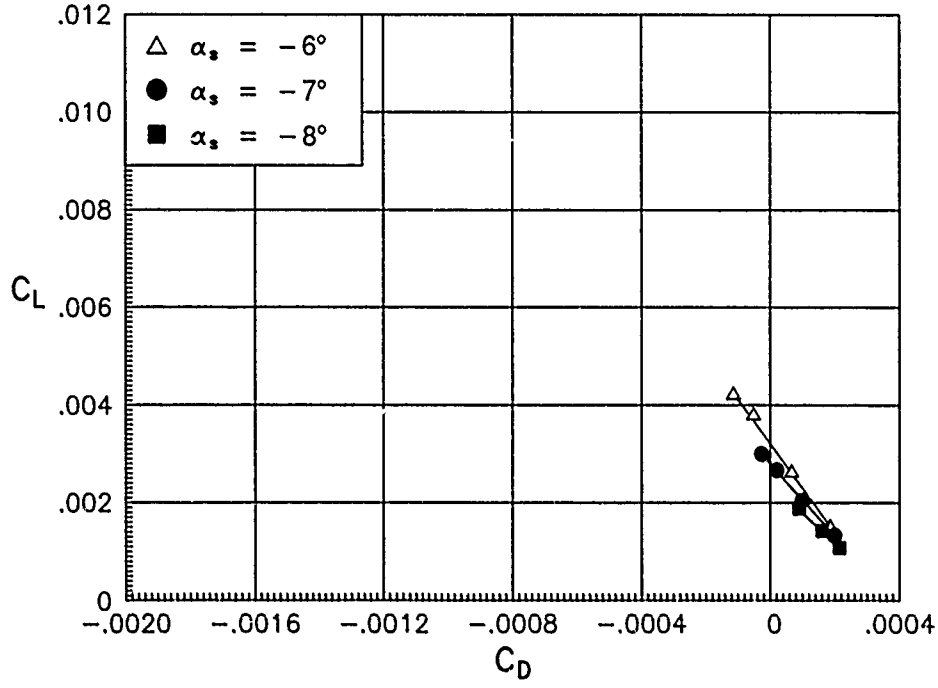

(a) C_L versus C_D.

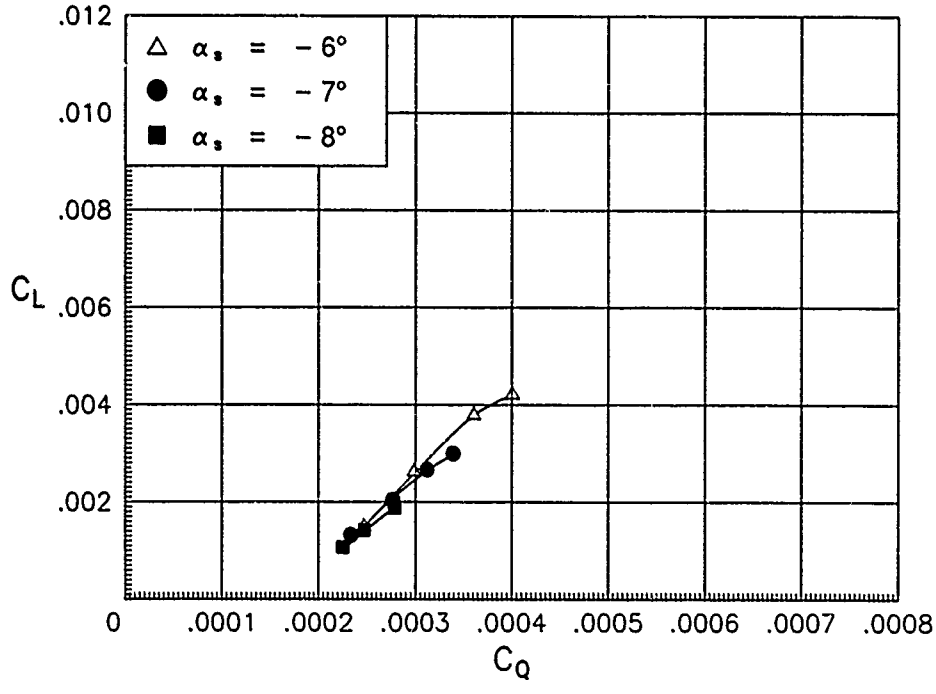

(b) C_L versus C_Q.

Figure 19. Basic forward-flight characteristics of 94-percent tapered rotor for $\mu = 0.43$.

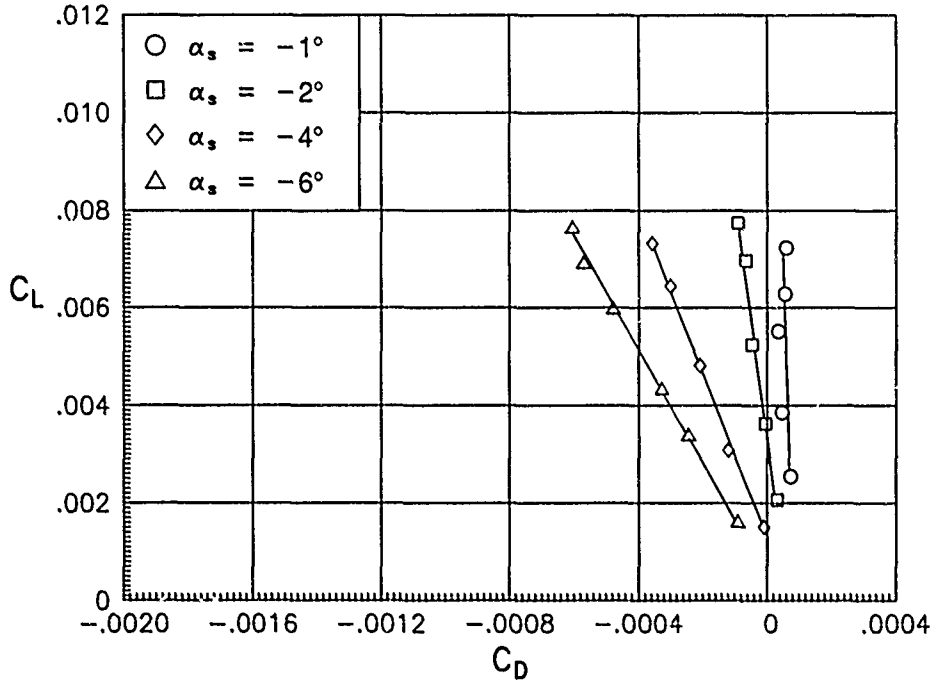

(a) C_L versus C_D.

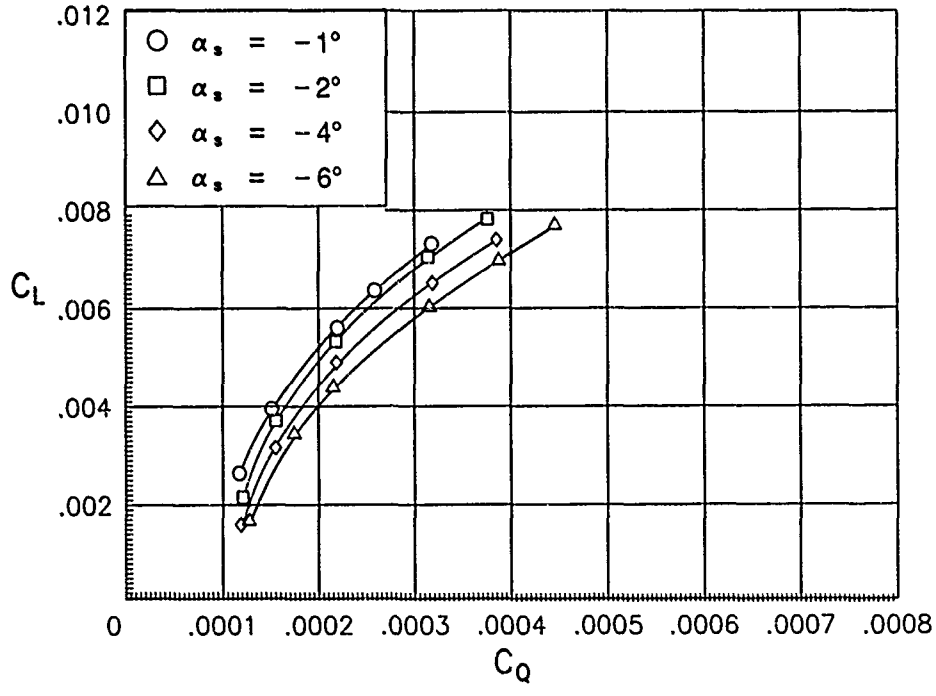

(b) C_L versus C_Q.

Figure 20. Basic forward-flight characteristics of 75-percent tapered rotor for $\mu = 0.14$.

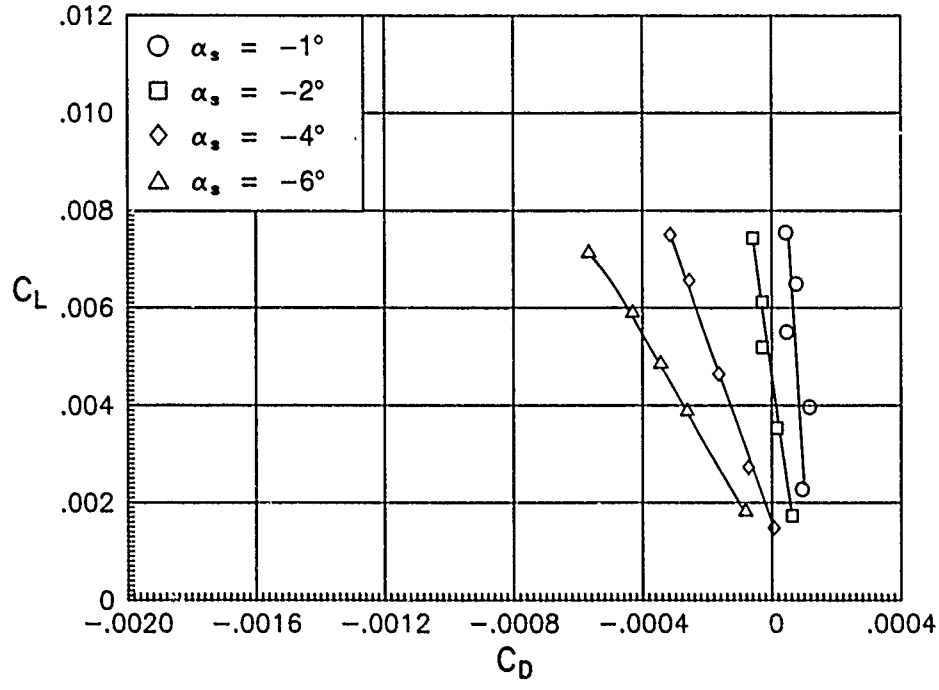

(a) C_L versus C_D.

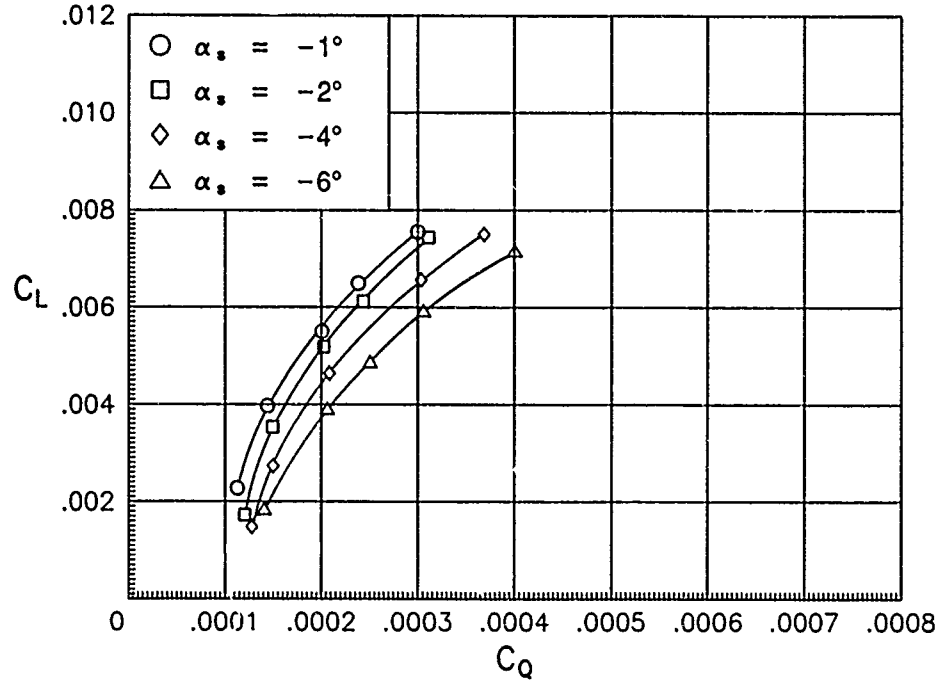

(b) C_L versus C_Q.

Figure 21. Basic forward-flight characteristics of 75-percent tapered rotor for $\mu = 0.19$.

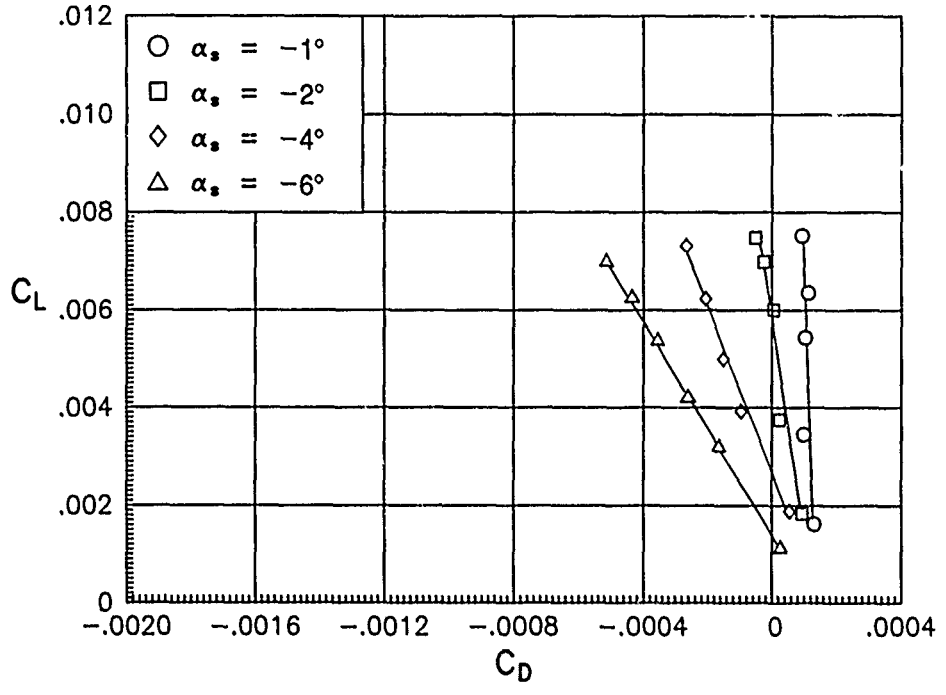

(a) C_L versus C_D.

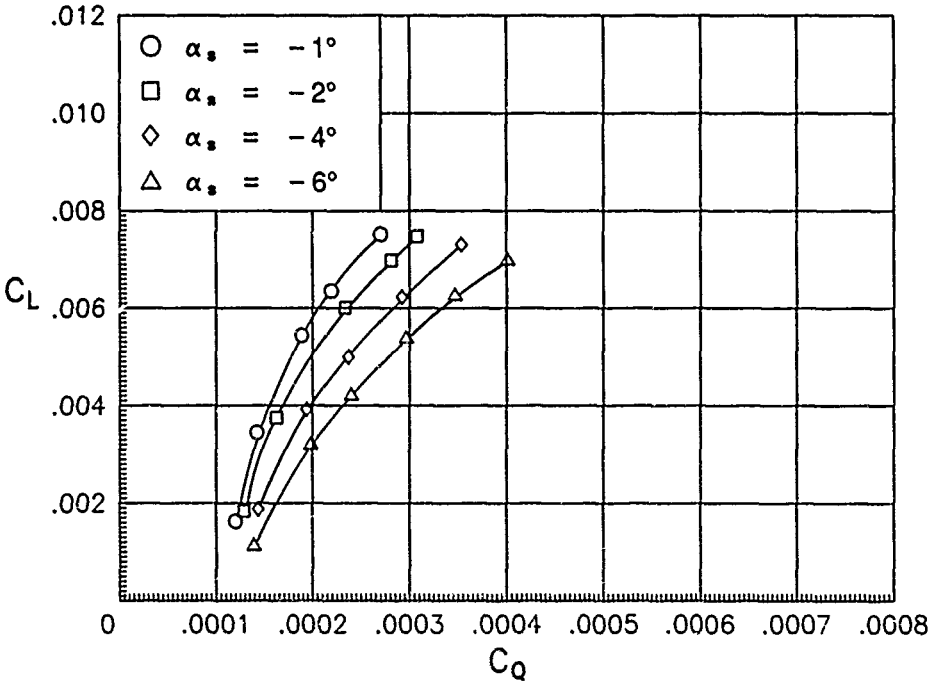

(b) C_L versus C_Q.

Figure 22. Basic forward-flight characteristics of 75-percent tapered rotor for $\mu = 0.23$

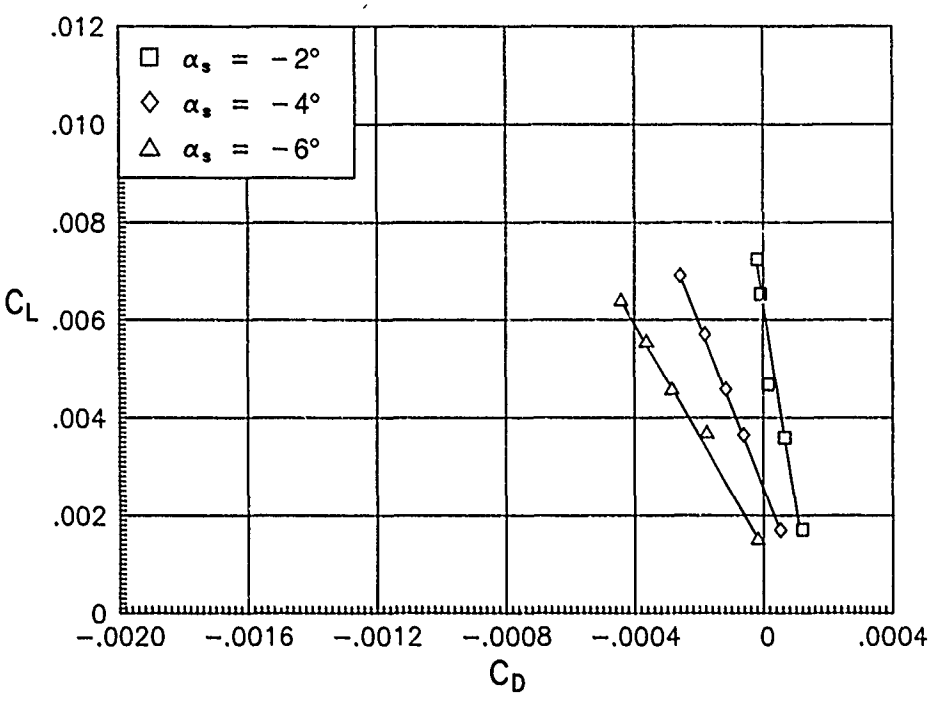

(a) C_L versus C_D.

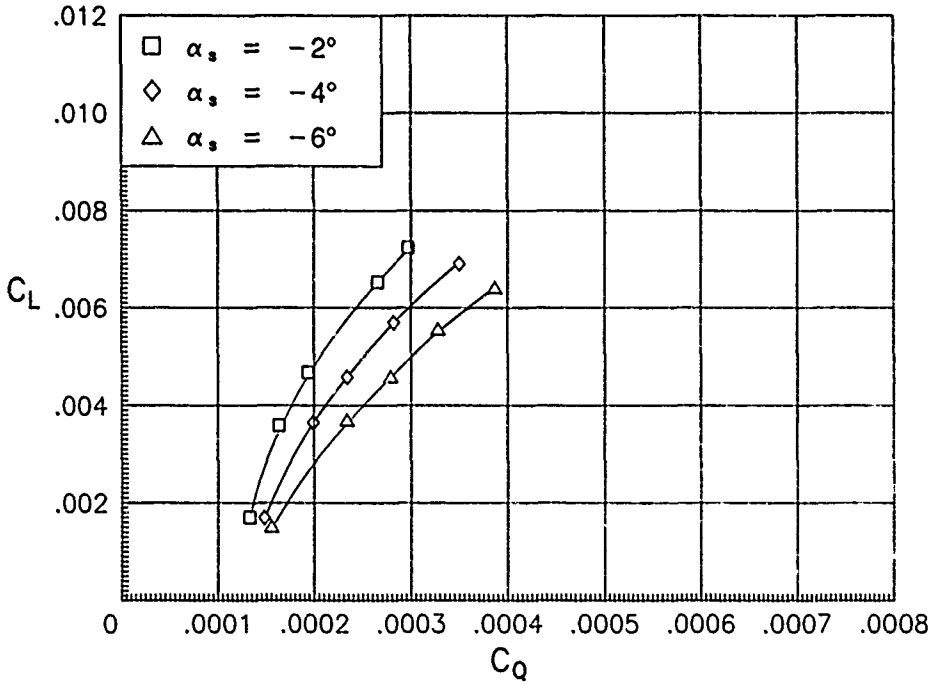

(b) C_L versus C_Q.

Figure 23. Basic forward-flight characteristics of 75-percent tapered rotor for $\mu = 0.27$.

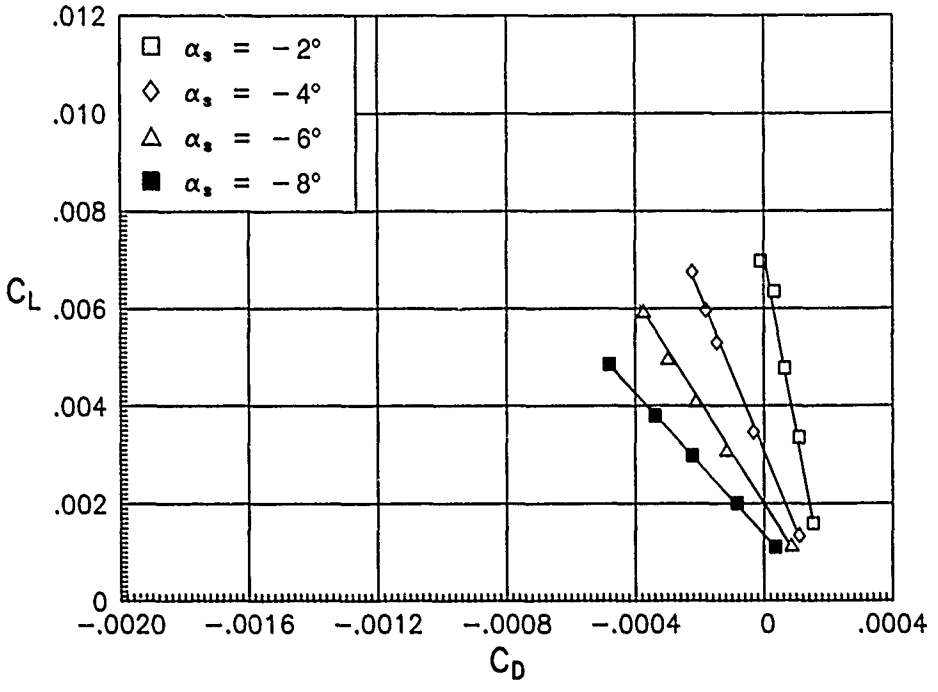

(a) C_L versus C_D.

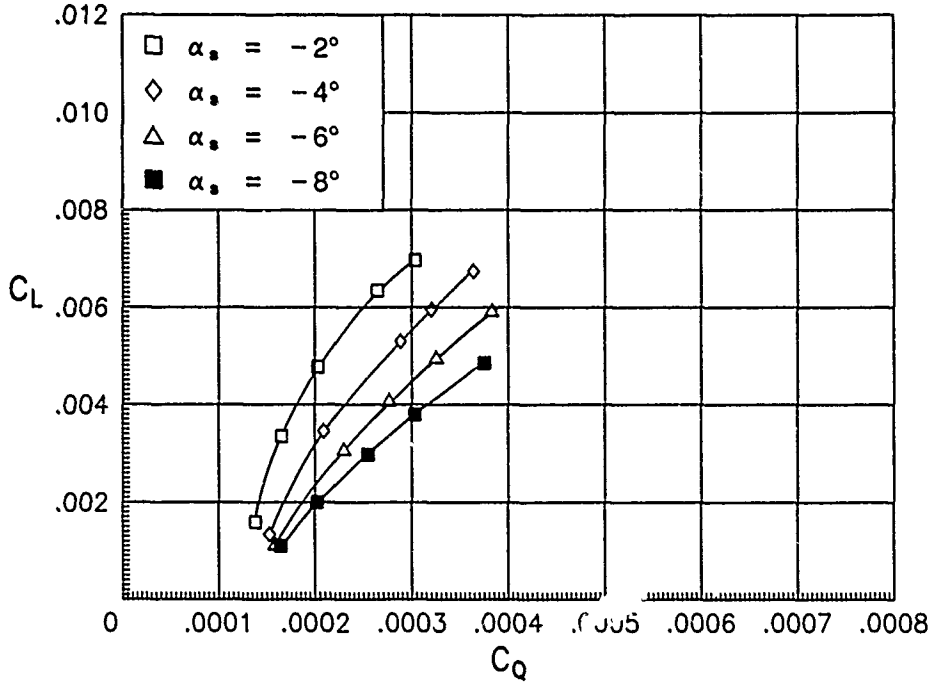

(b) C_L versus C_Q.

Figure 24. Basic forward-flight characteristics of 75-percent tapered rotor for $\mu = 0.30$.

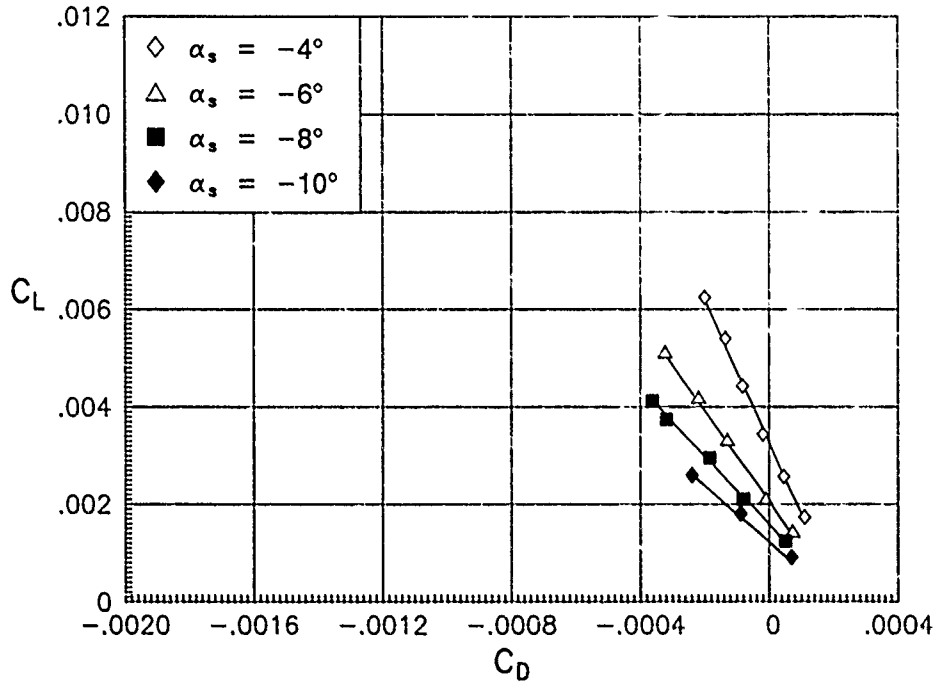

(a) C_L versus C_D.

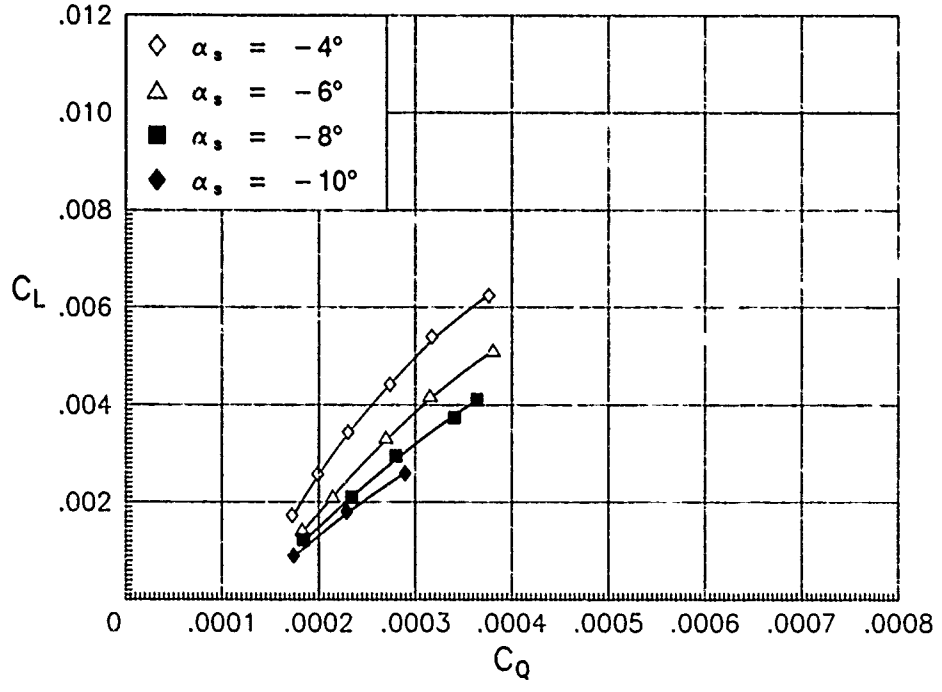

(b) C_L versus C_Q.

Figure 25. Basic forward-flight characteristics of 75-percent tapered rotor for $\mu = 0.35$.

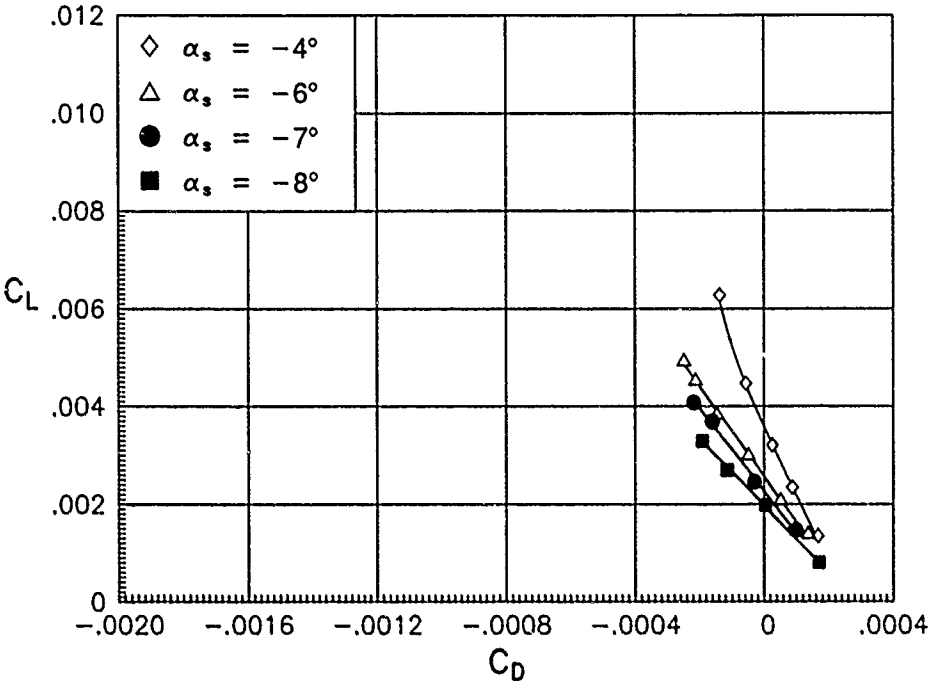

(a) C_L versus C_D.

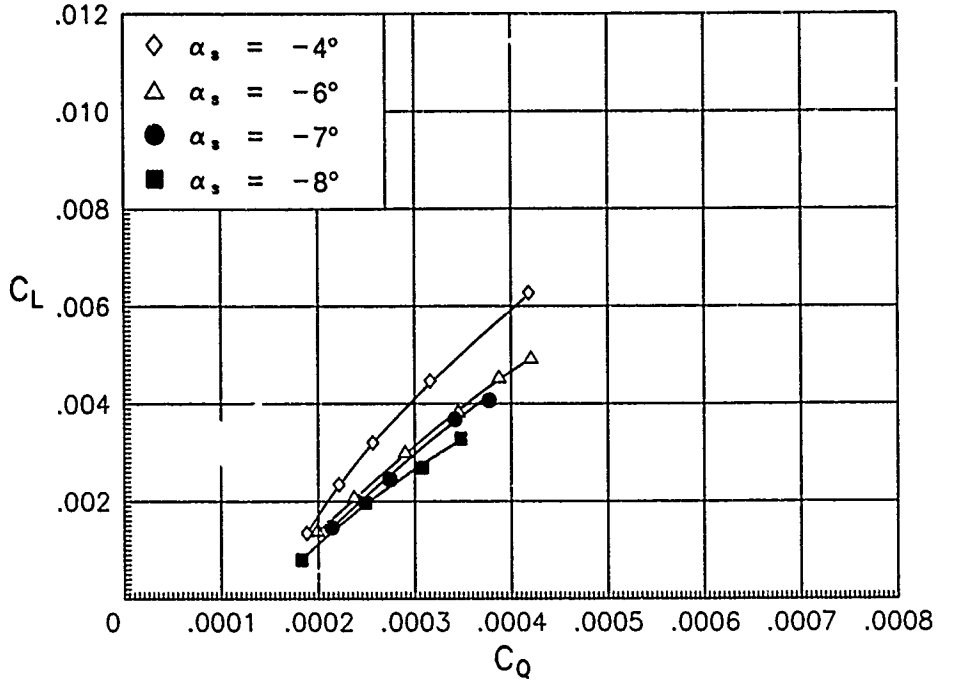

(b) C_L versus C_Q.

Figure 26. Basic forward-flight characteristics of 75-percent tapered rotor for $\mu = 0.40$.

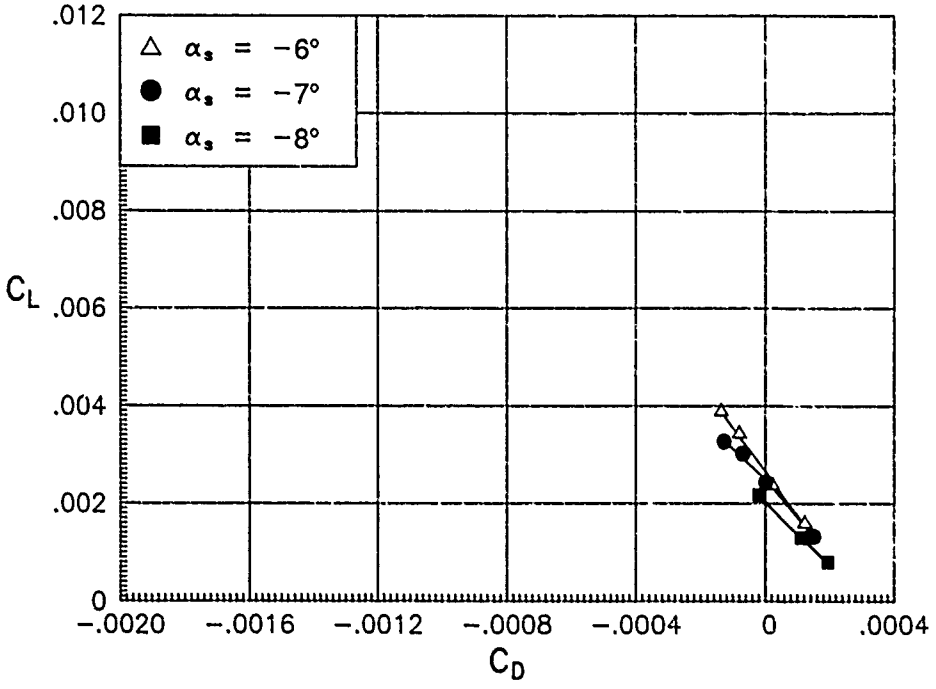

(a) C_L versus C_D.

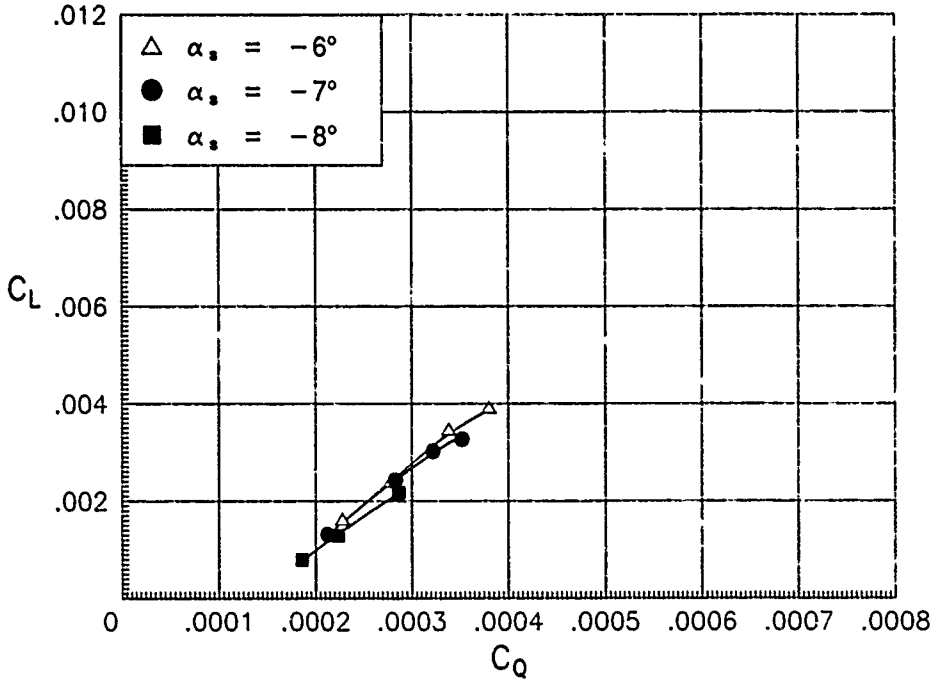

(b) C_L versus C_Q.

Figure 27. Basic forward-flight characteristics of 75-percent tapered rotor for $\mu = 0.43$.

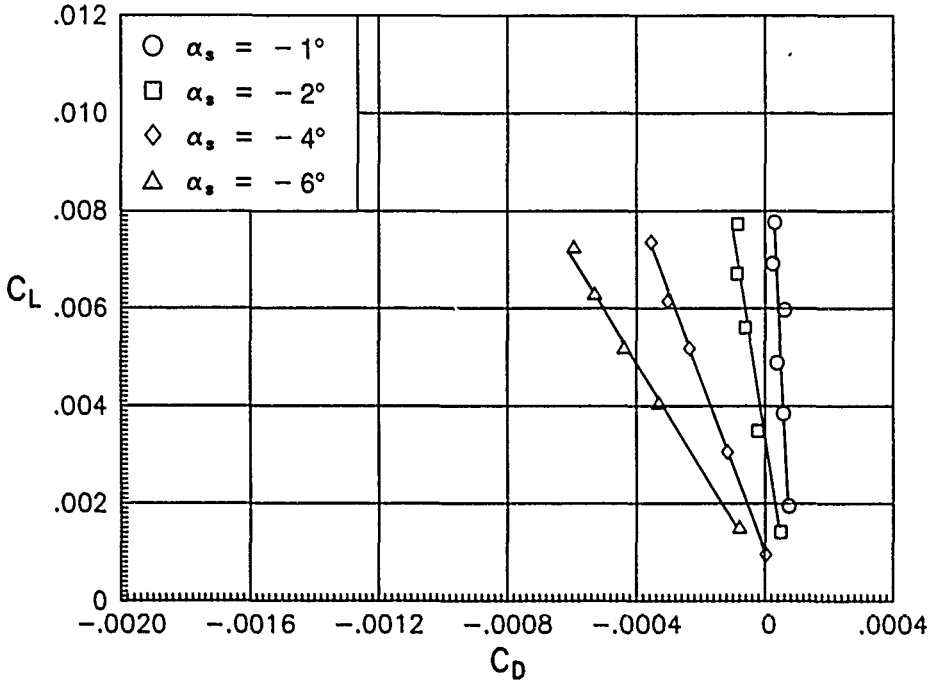

(a) C_L versus C_D.

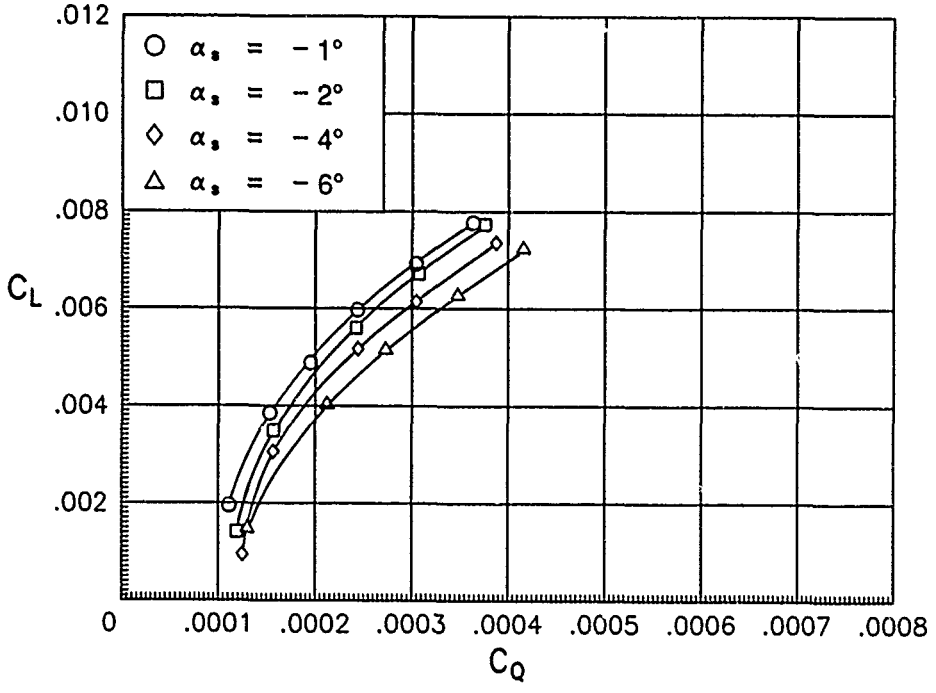

(b) C_L versus C_Q.

Figure 28. Basic forward-flight characteristics of 50-percent tapered rotor for $\mu = 0.14$.

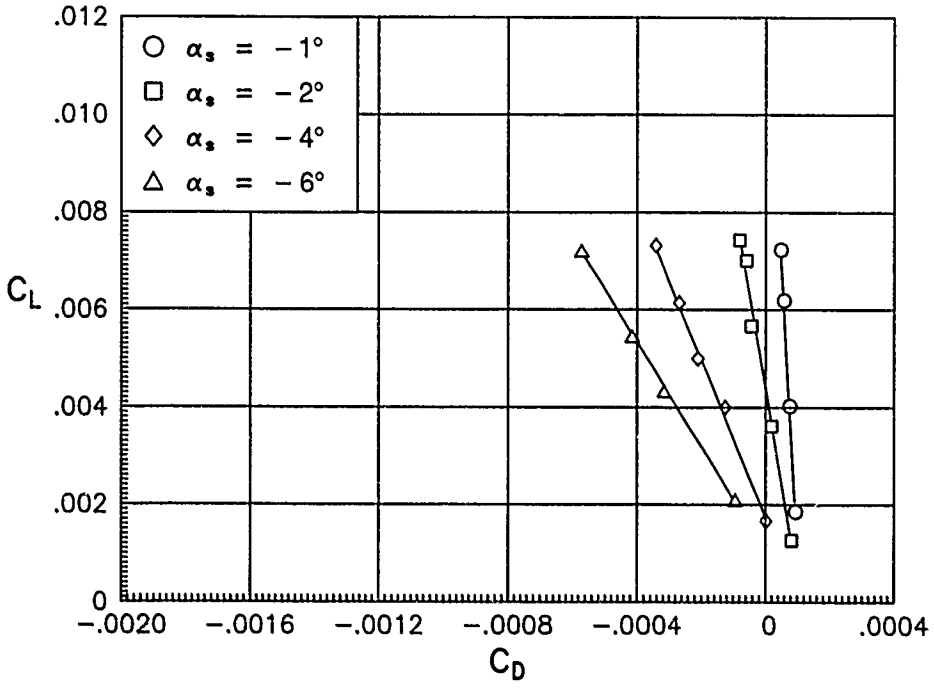

(a) C_L versus C_D.

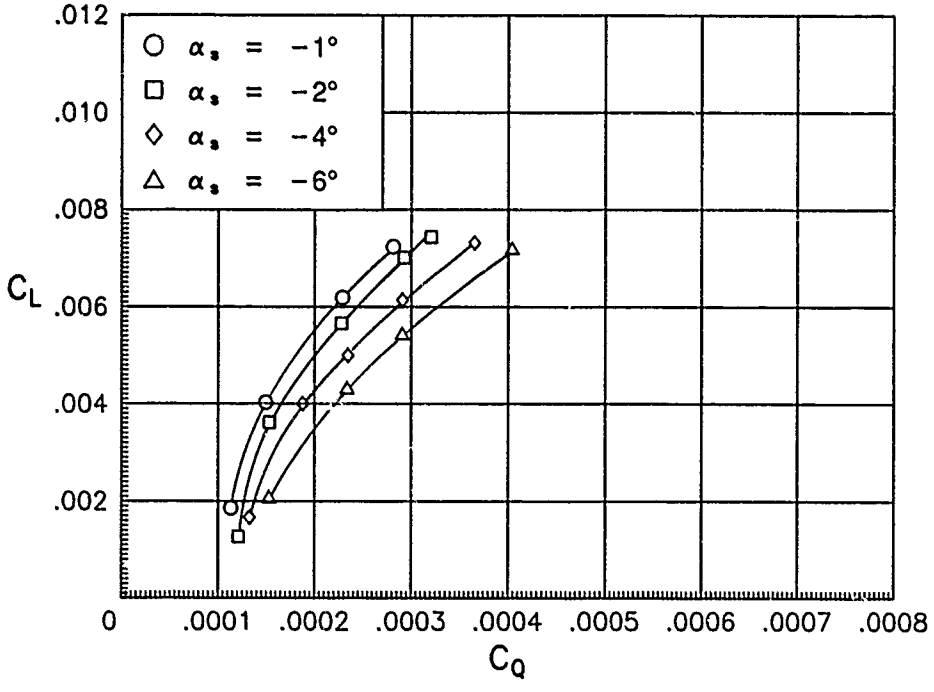

(b) C_L versus C_Q.

Figure 29. Basic forward-flight characteristics of 50-percent tapered rotor for $\mu = 0.19$.

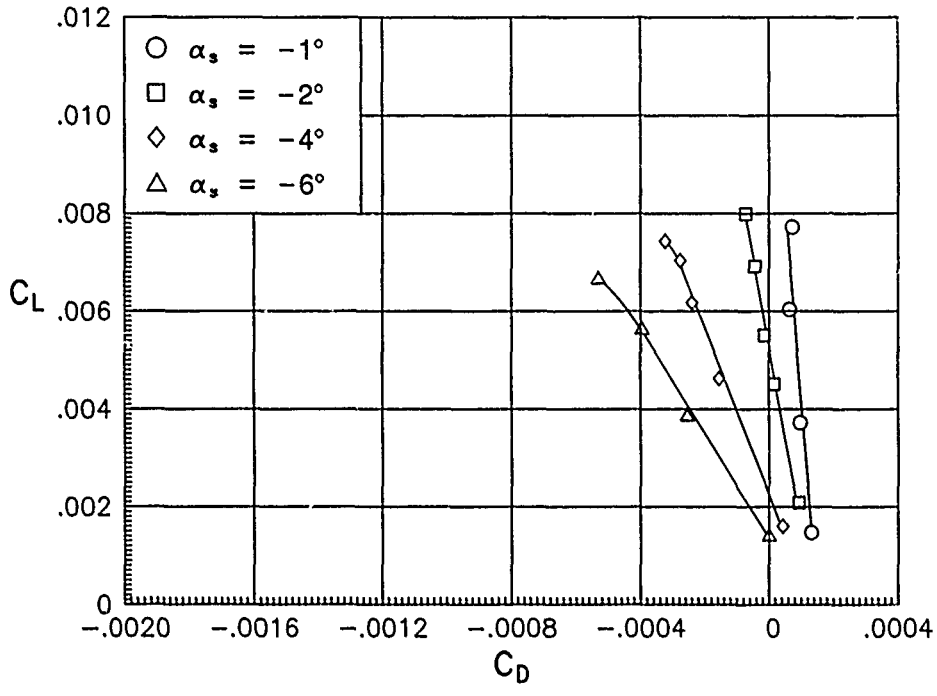

(a) C_L versus C_D.

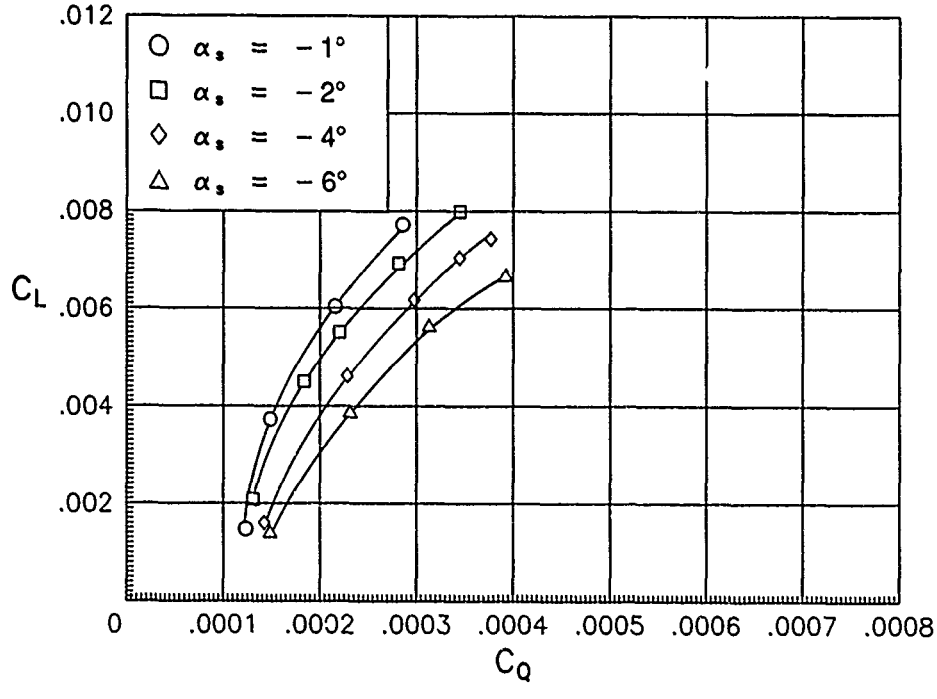

(b) C_L versus C_Q.

Figure 30. Basic forward-flight characteristics of 50-percent tapered rotor for $\mu = 0.23$.

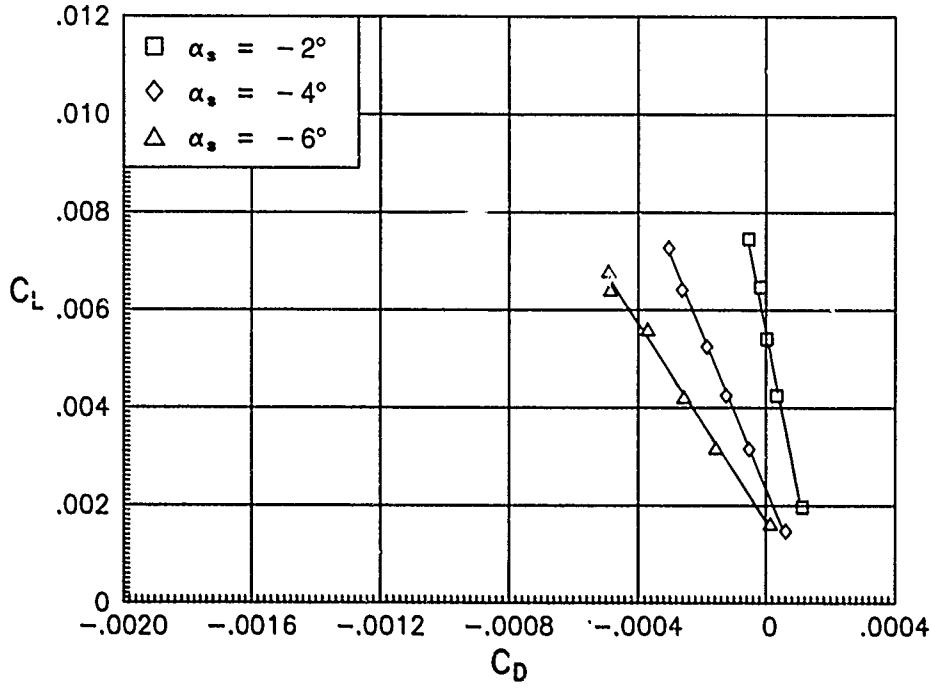

(a) C_L versus C_D.

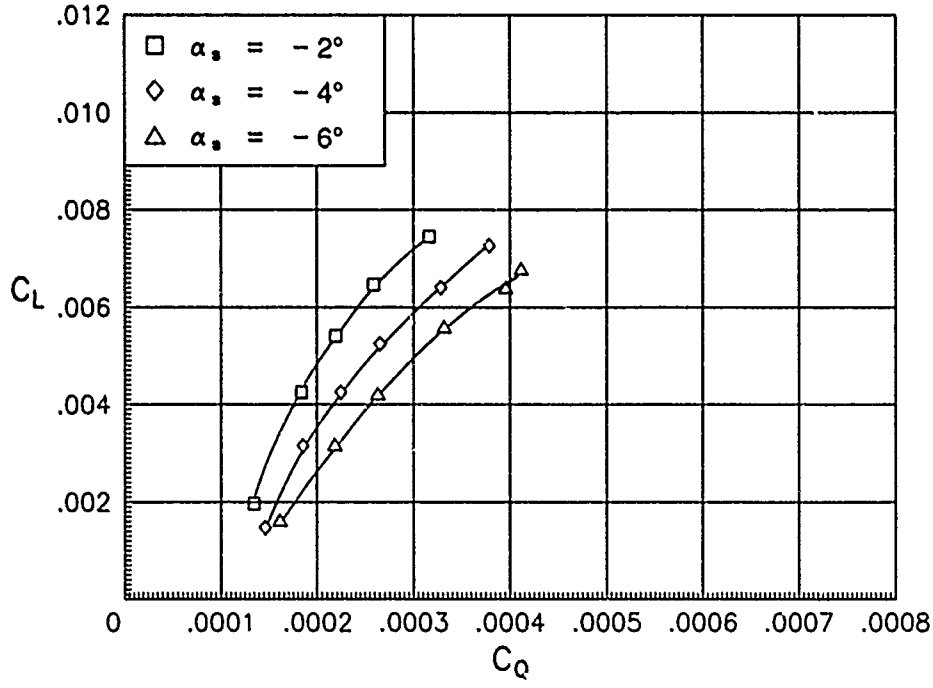

(b) C_L versus C_Q.

Figure 31. Basic forward-flight characteristics of 50-percent tapered rotor for $\mu = 0.27$.

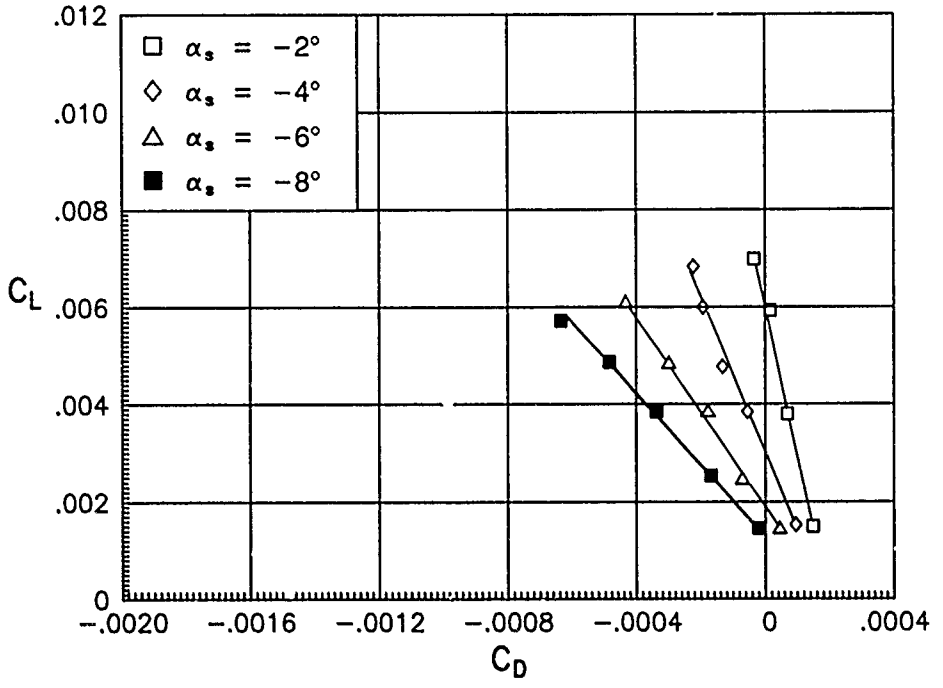

(a) C_L versus C_D.

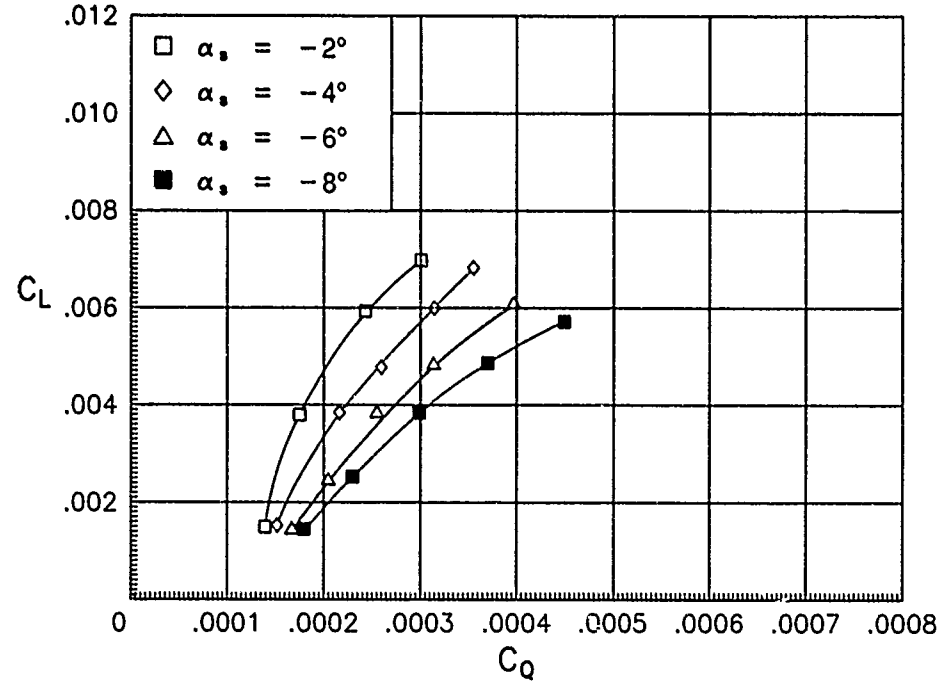

(b) C_L versus C_Q.

Figure 32. Basic forward-flight characteristics of 50-percent tapered rotor for $\mu = 0.30$.

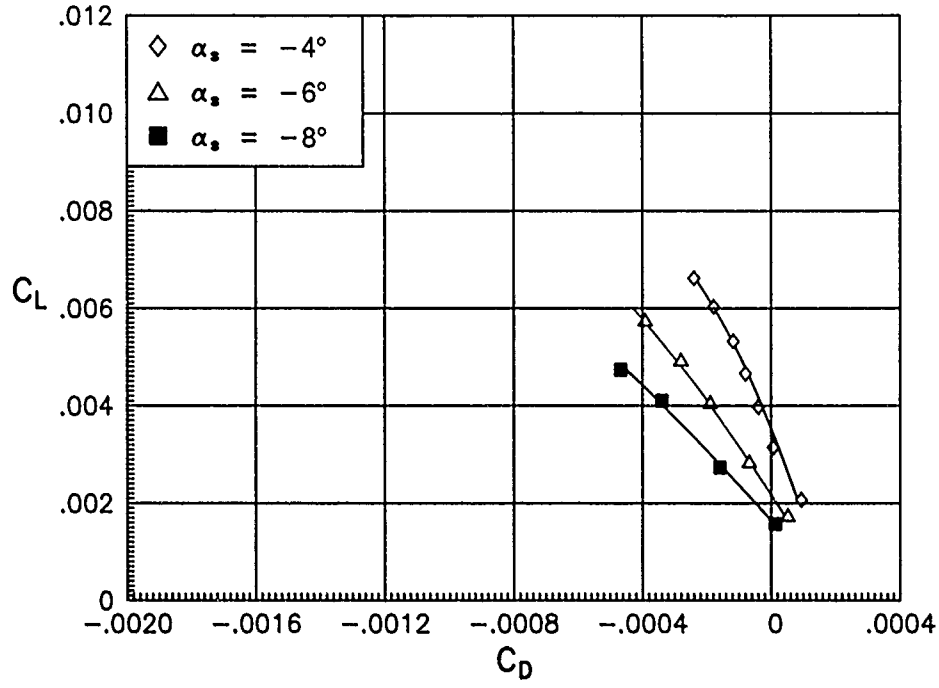

(a) C_L versus C_D.

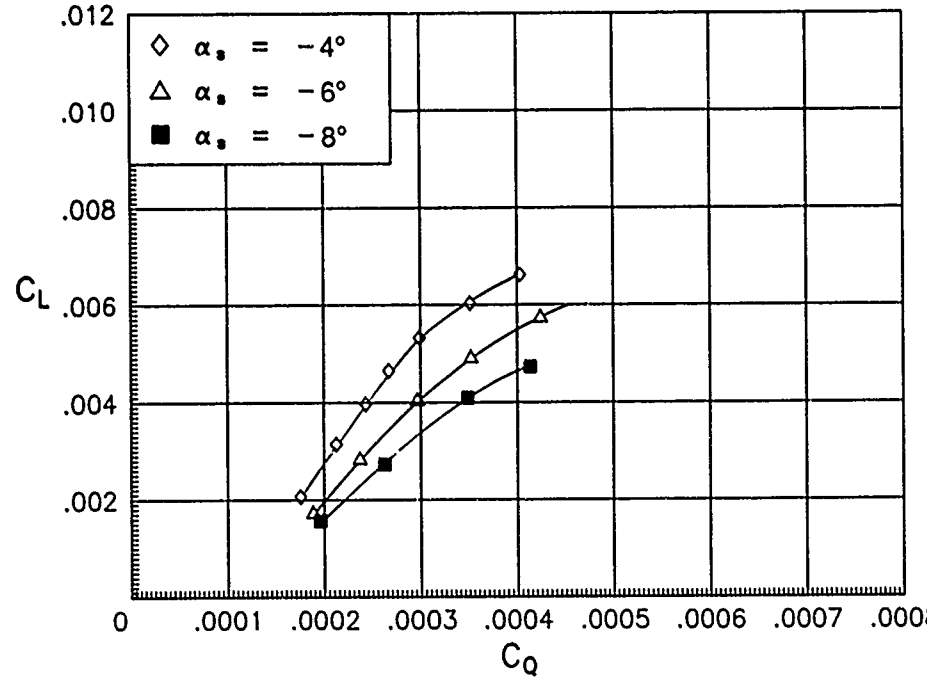

(b) C_L versus C_Q.

Figure 33. Basic forward-flight characteristics of 50-percent tapered rotor for $\mu = 0.35$.

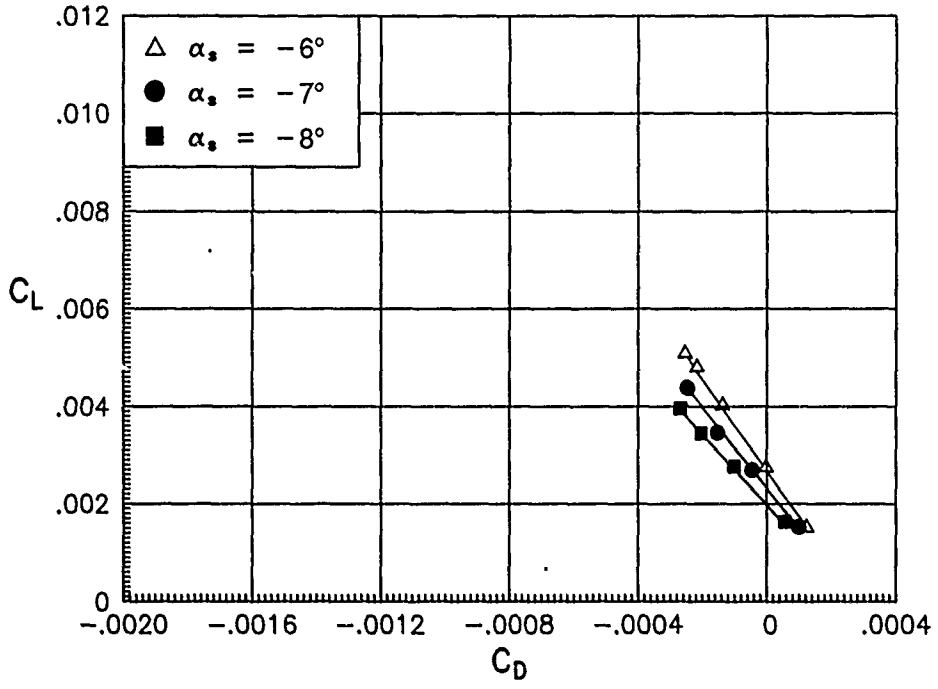

(a) C_L versus C_D.

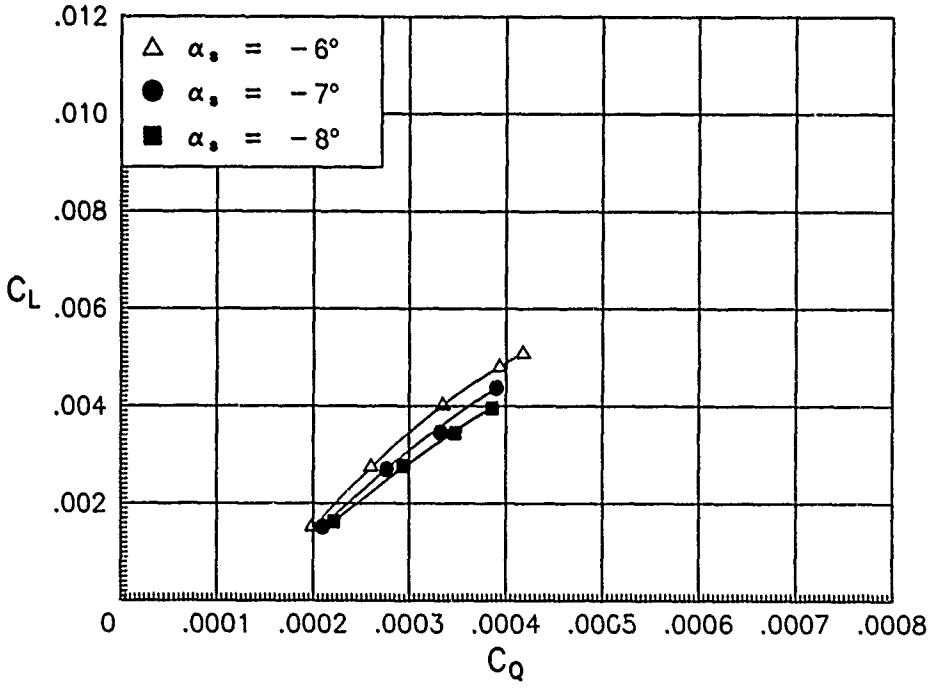

(b) C_L versus C_Q.

Figure 34. Basic forward-flight characteristics of 50-percent tapered rotor for $\mu = 0.40$.

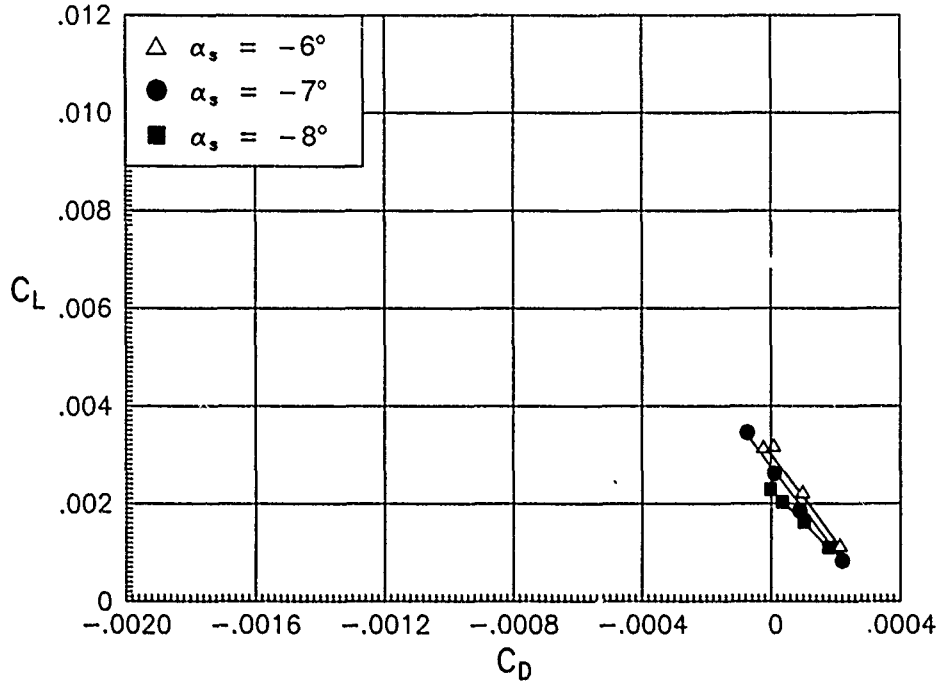

(a) C_L versus C_D.

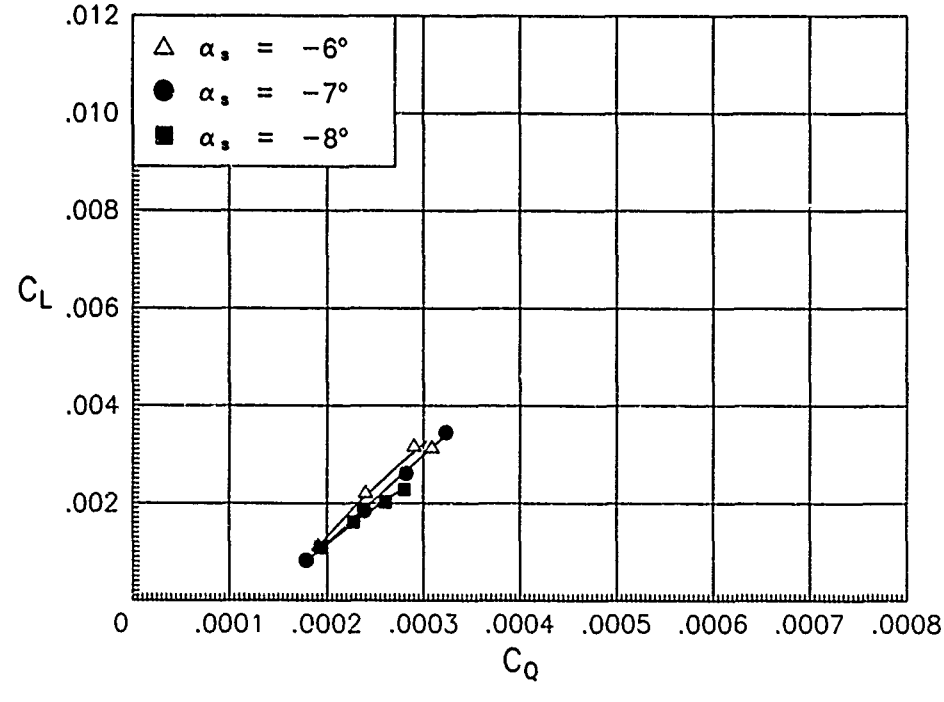

(b) C_L versus C_Q.

Figure 35. Basic forward-flight characteristics of 50-percent tapered rotor for $\mu = 0.43$.

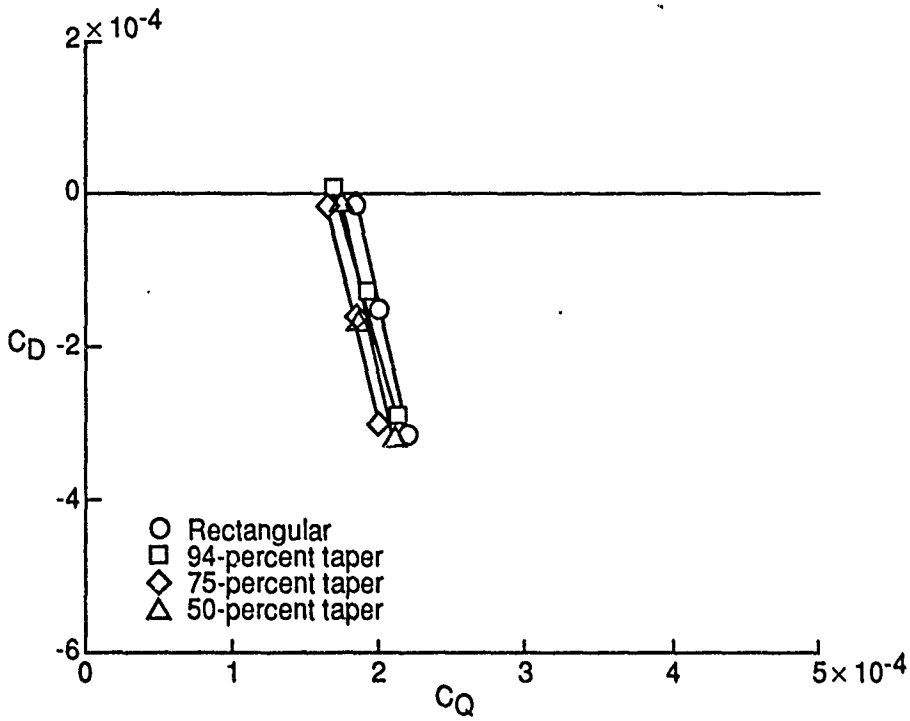

(a) $\mu = 0.14$.

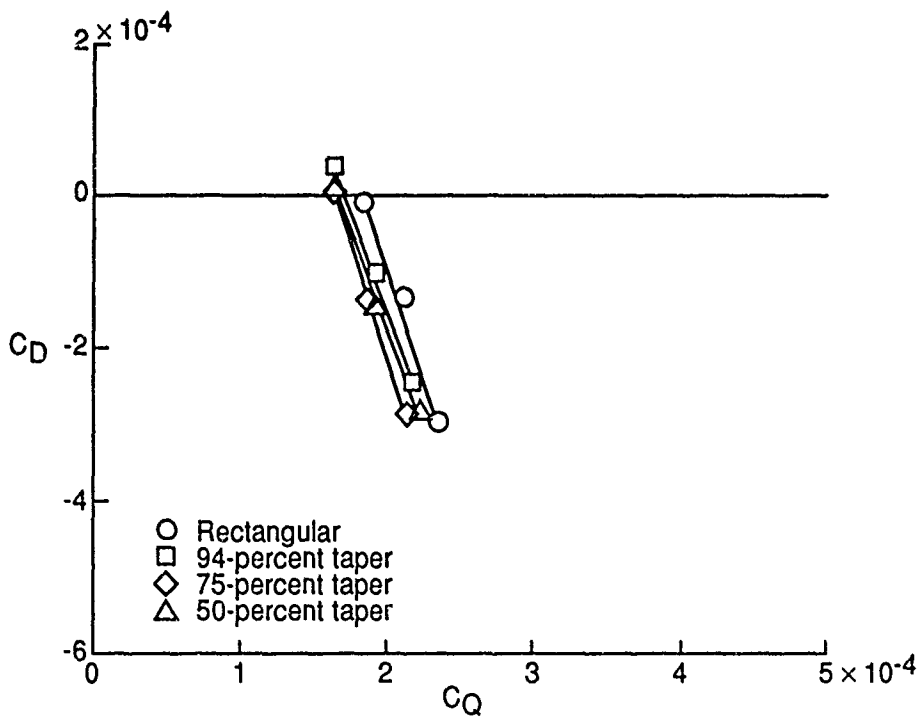

(b) $\mu = 0.19$.

Figure 36. Variation of rotor drag coefficient with rotor torque coefficient for $C_L = 0.004$.

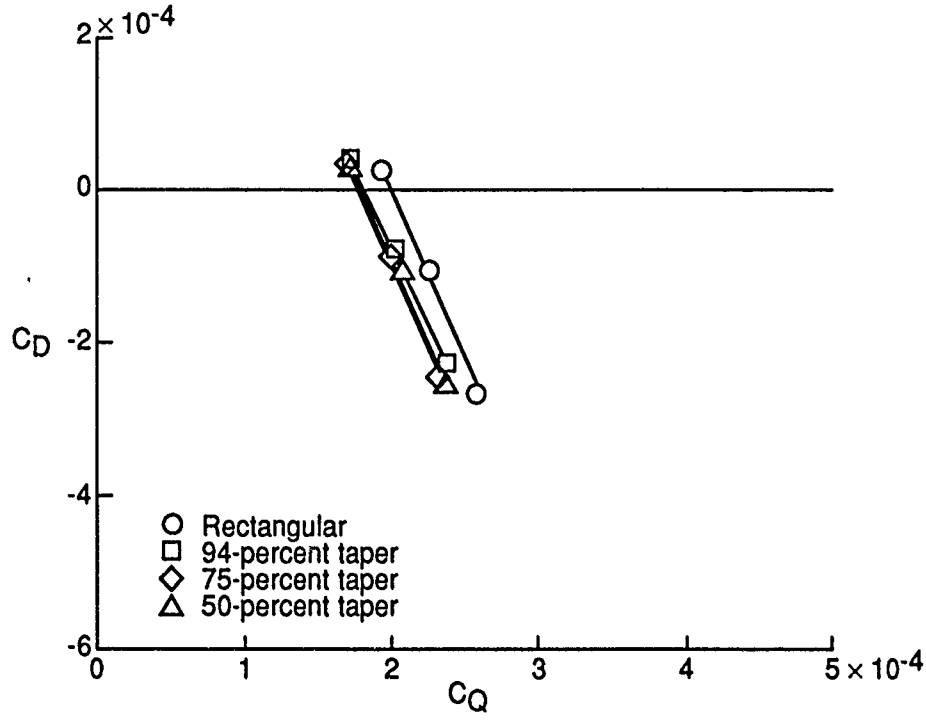

(c) $\mu = 0.23$ and 0.24.

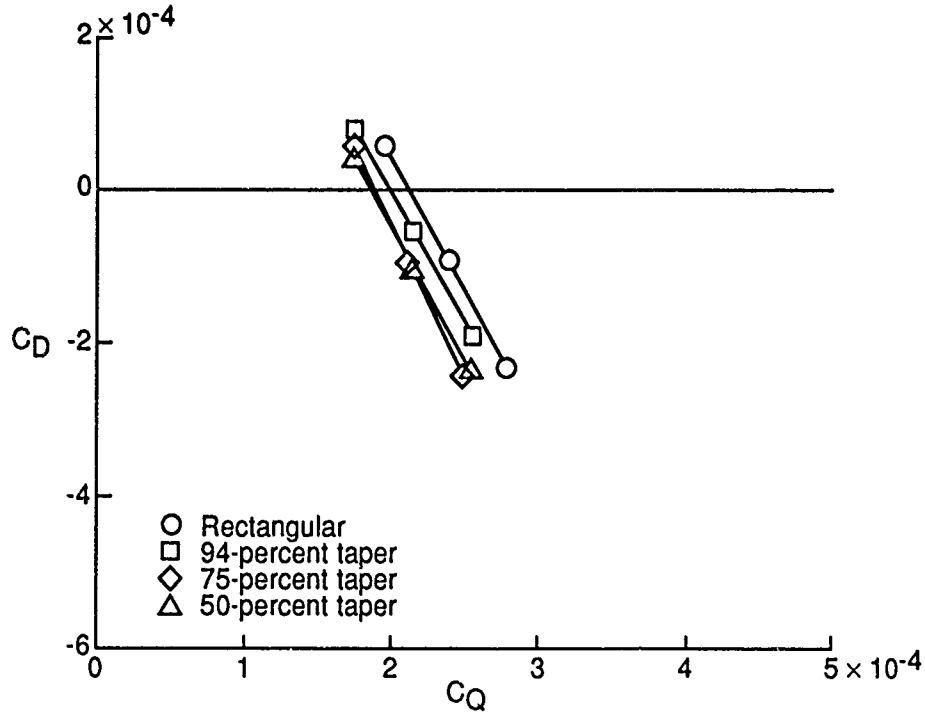

(d) $\mu = 0.27$.

Figure 36. Continued.

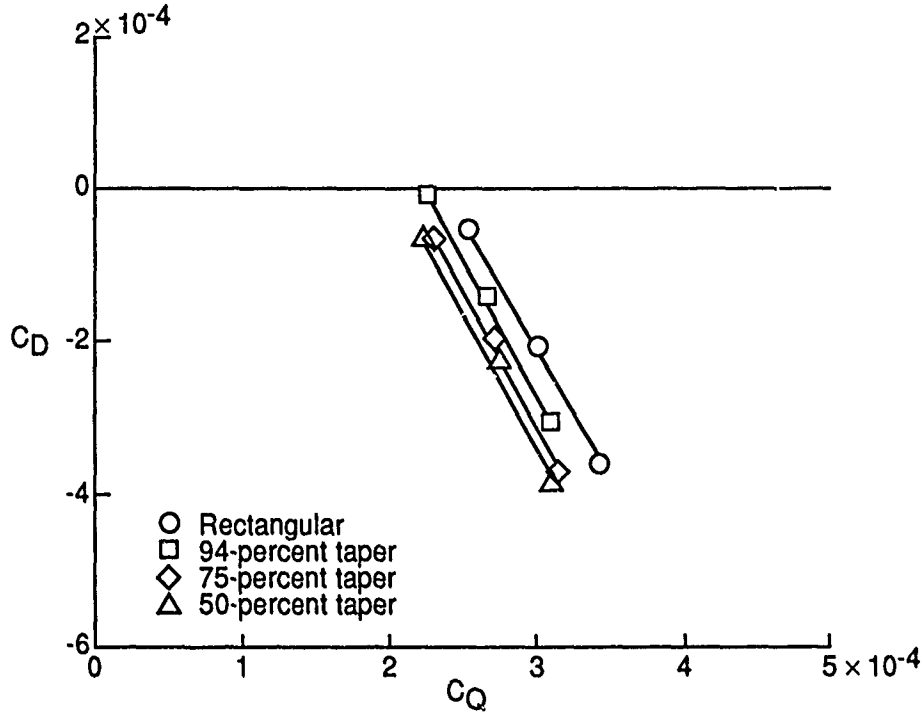

(e) $\mu = 0.30$ and 0.31.

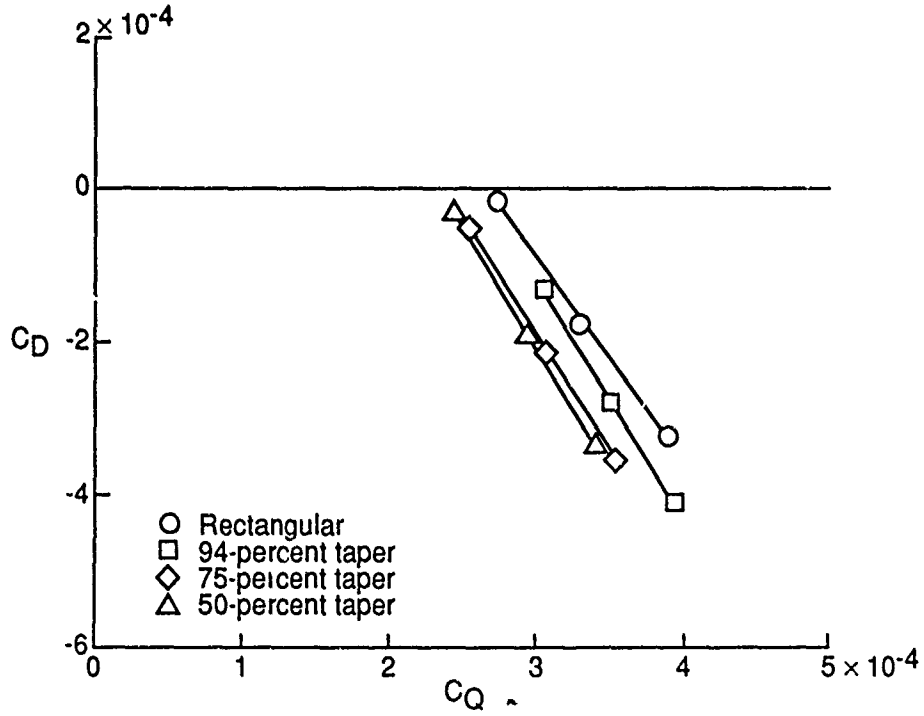

(f) $\mu = 0.35$ and 0.36.

Figure 36. Continued.

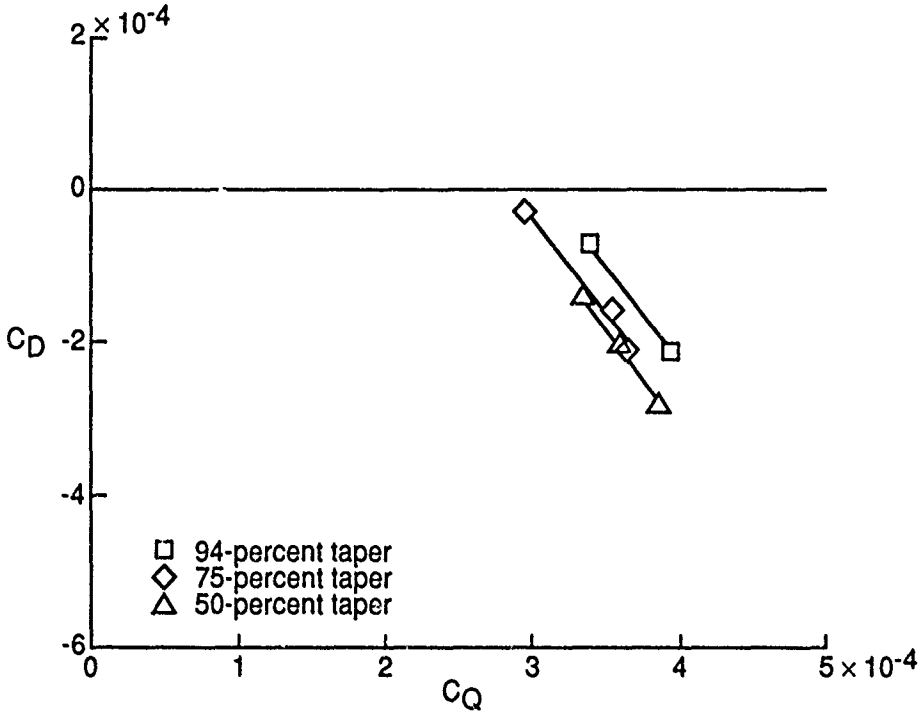

(g) $\mu = 0.40$.

Figure 36. Concluded.

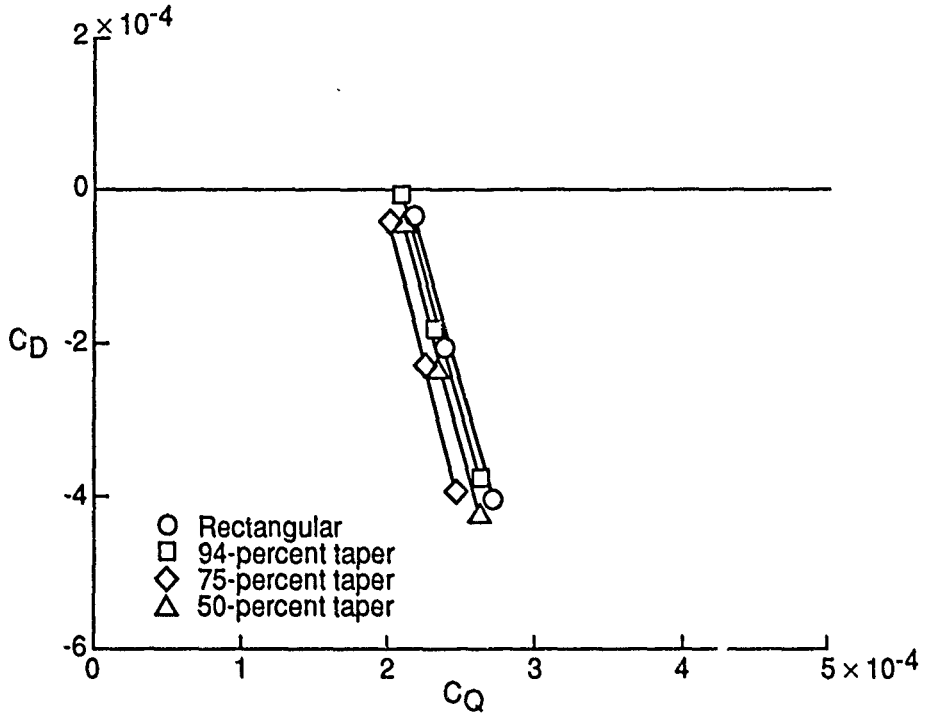

(a) $\mu = 0.14$.

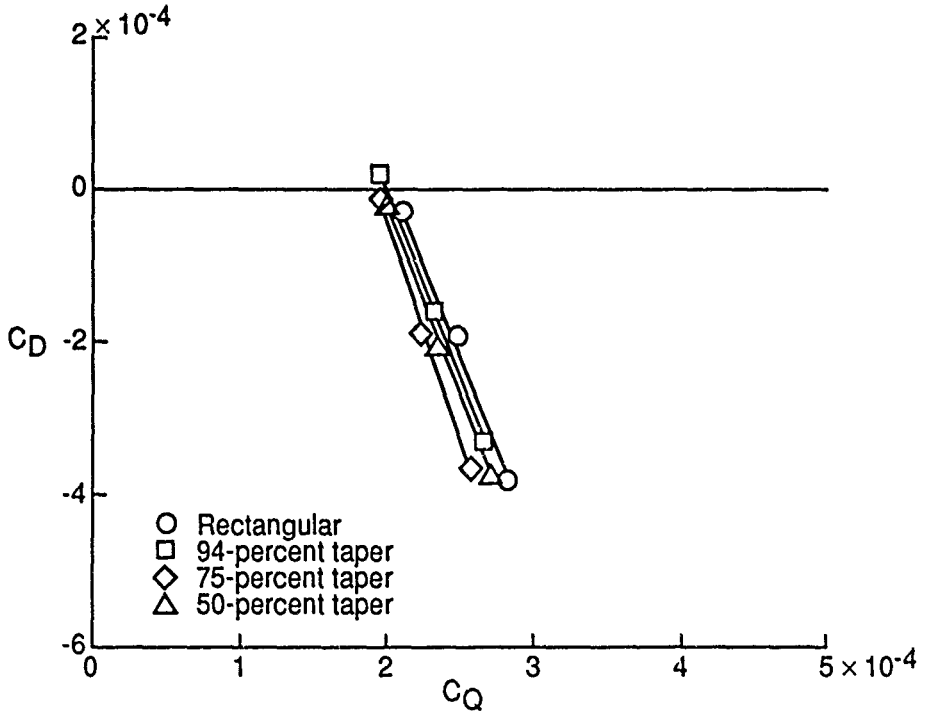

(b) $\mu = 0.19$.

Figure 37. Variation of rotor drag coefficient with rotor torque coefficient for $C_L = 0.005$.

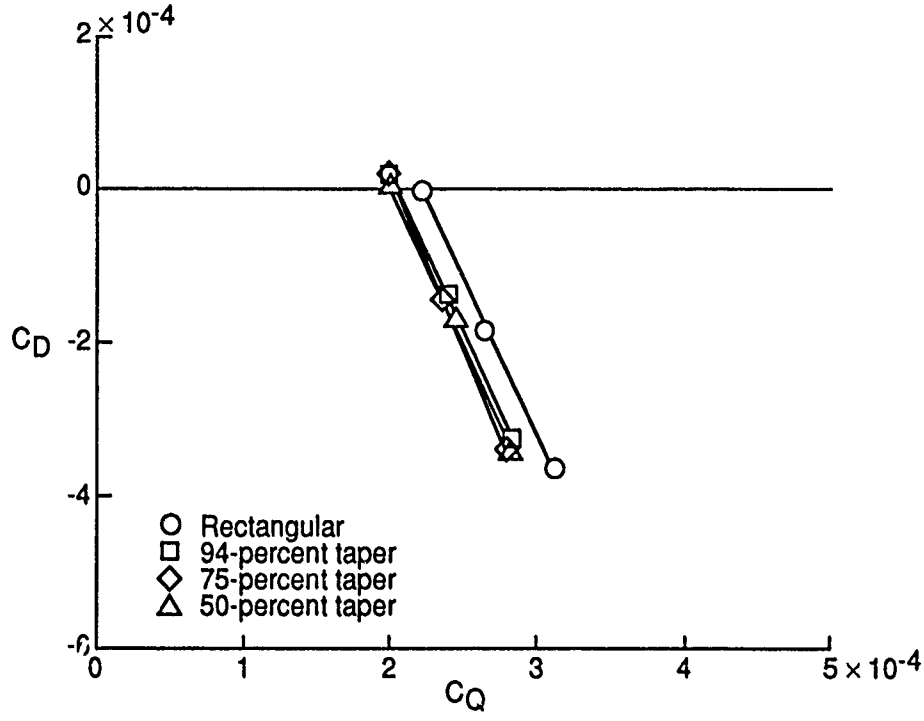

(c) $\mu = 0.23$ and 0.24.

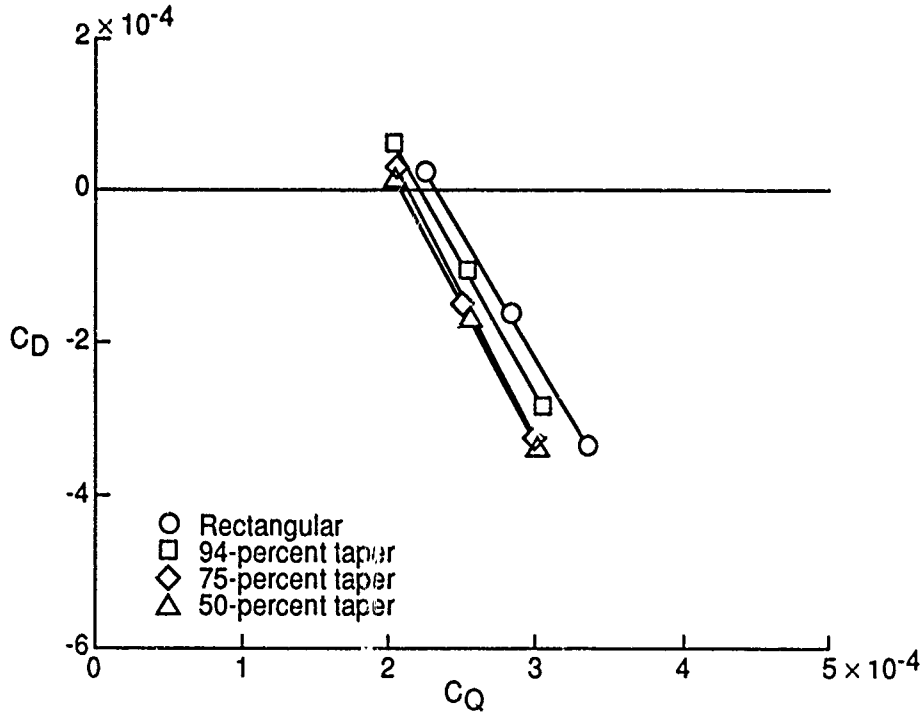

(d) $\mu = 0.27$.

Figure 37. Continued.

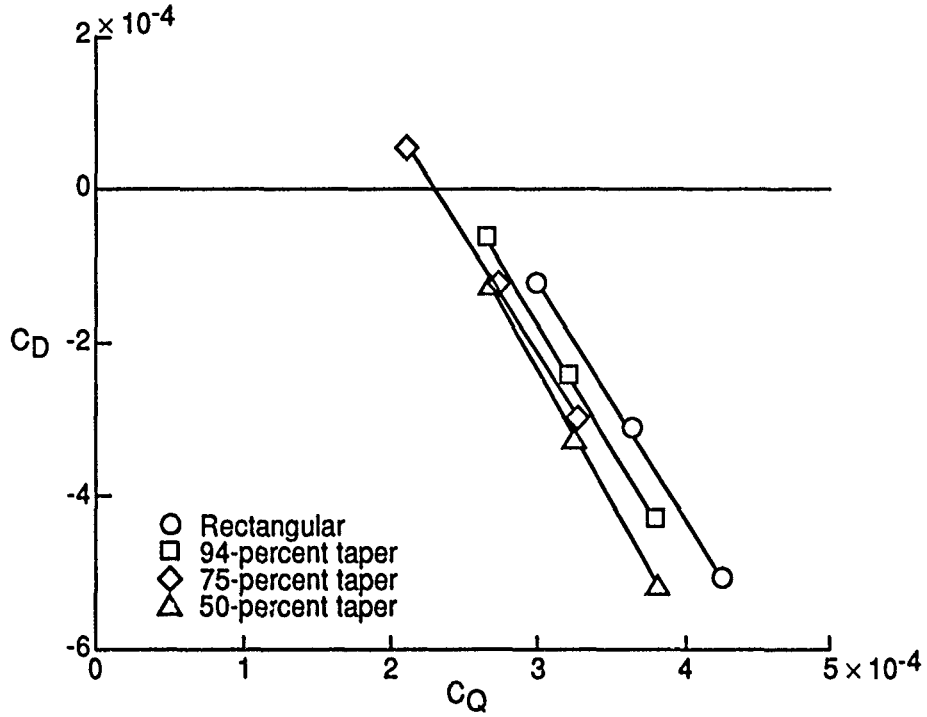

(e) $\mu = 0.30$ and 0.31.

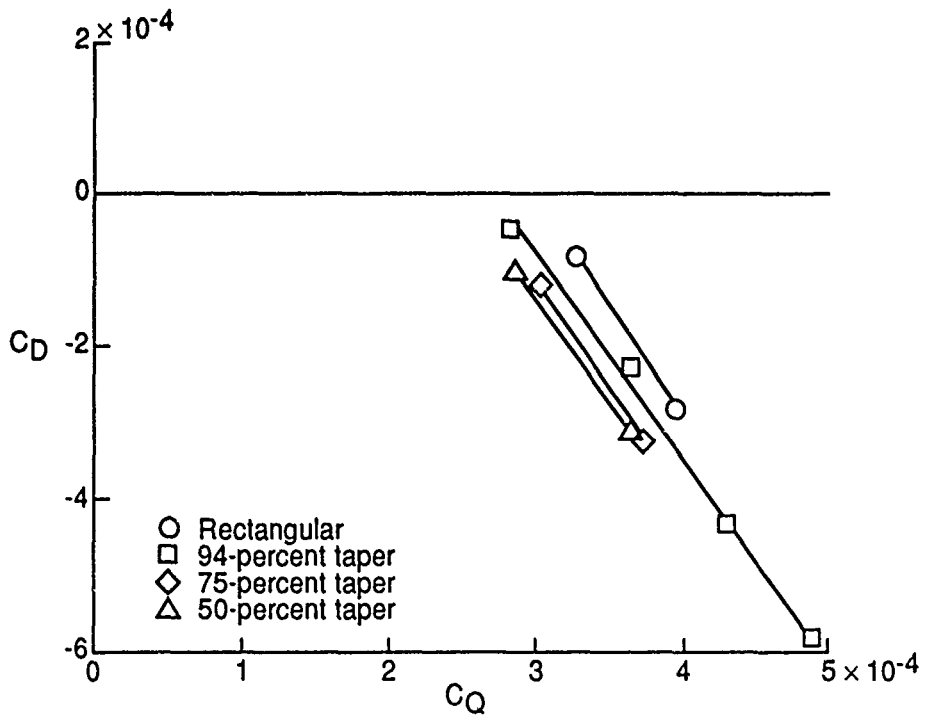

(f) $\mu = 0.35$ and 0.36.

Figure 37. Concluded.

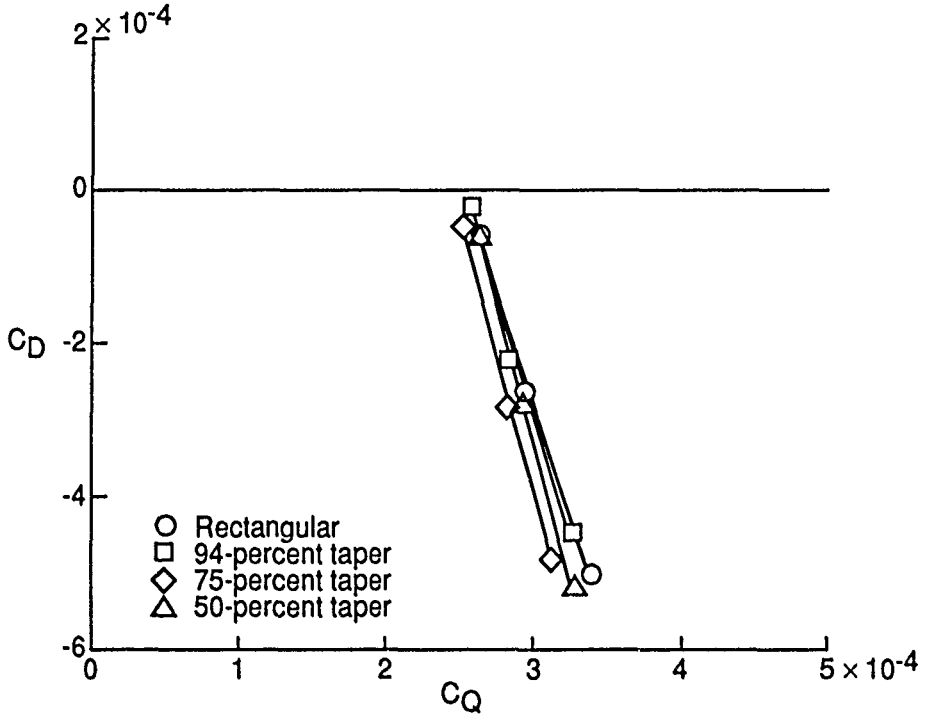

(a) $\mu = 0.14$.

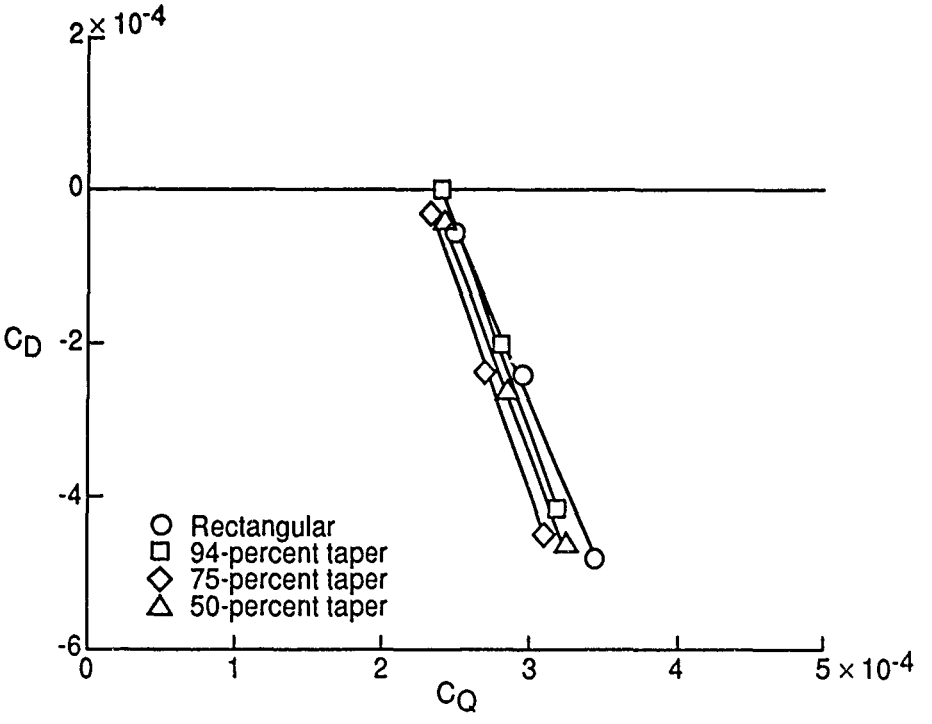

(b) $\mu = 0.19$.

Figure 38. Variation of rotor drag coefficient with rotor torque coefficient for $C_L = 0.006$.

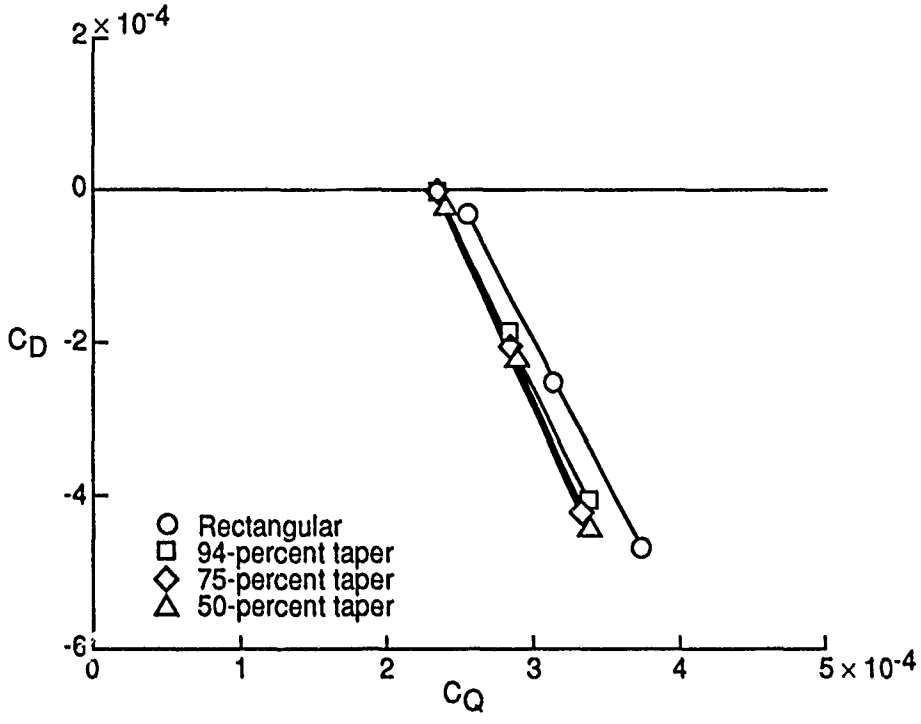

(c) $\mu = 0.23$ and 0.24.

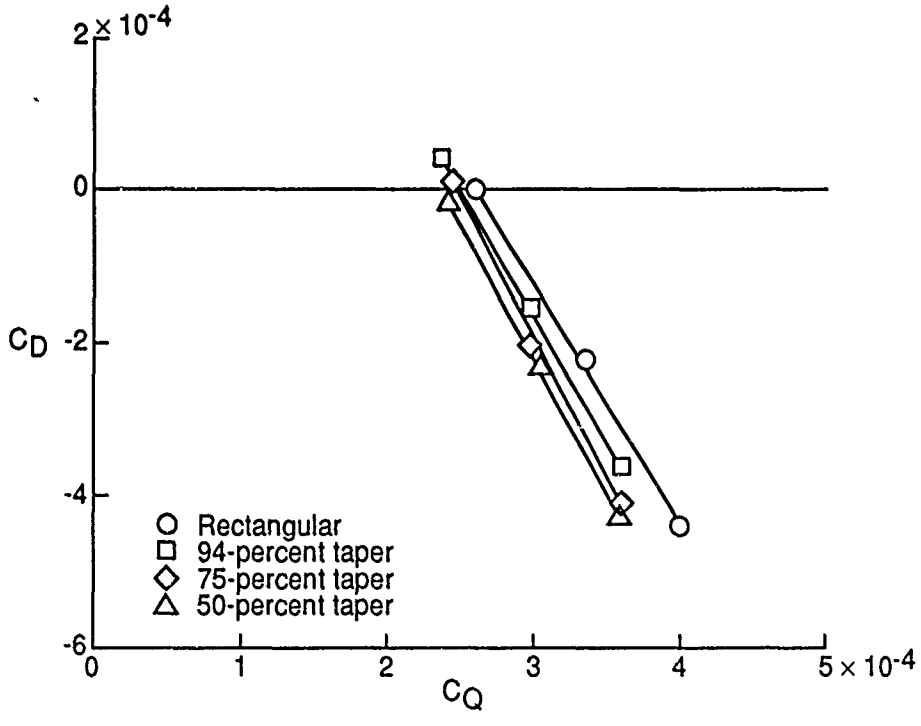

(d) $\mu = 0.27$.

Figure 38. Continued.

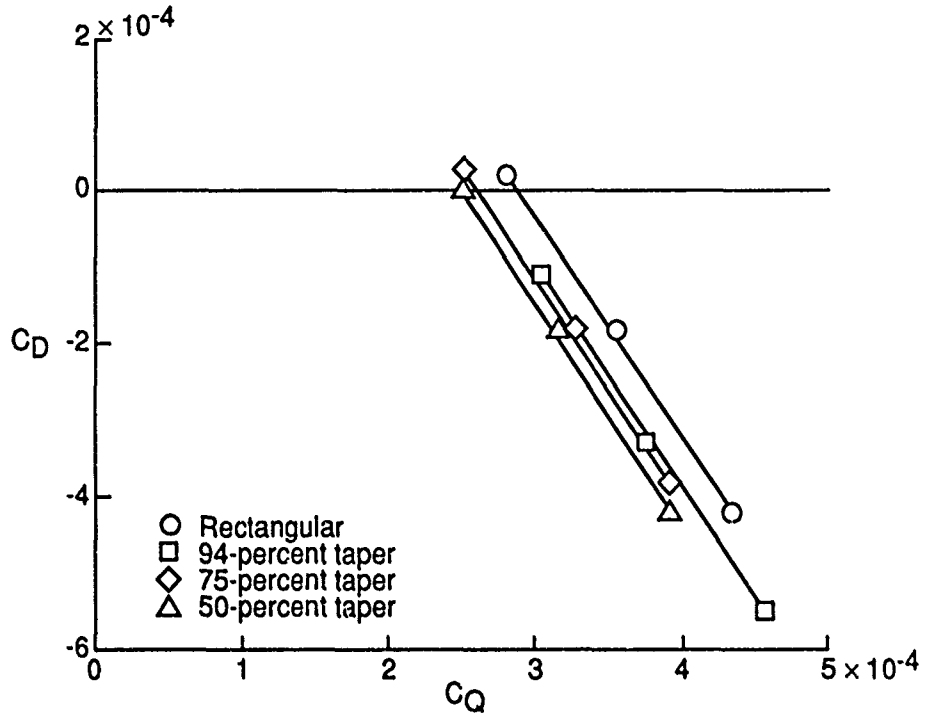

(e) $\mu = 0.30$ and 0.31.

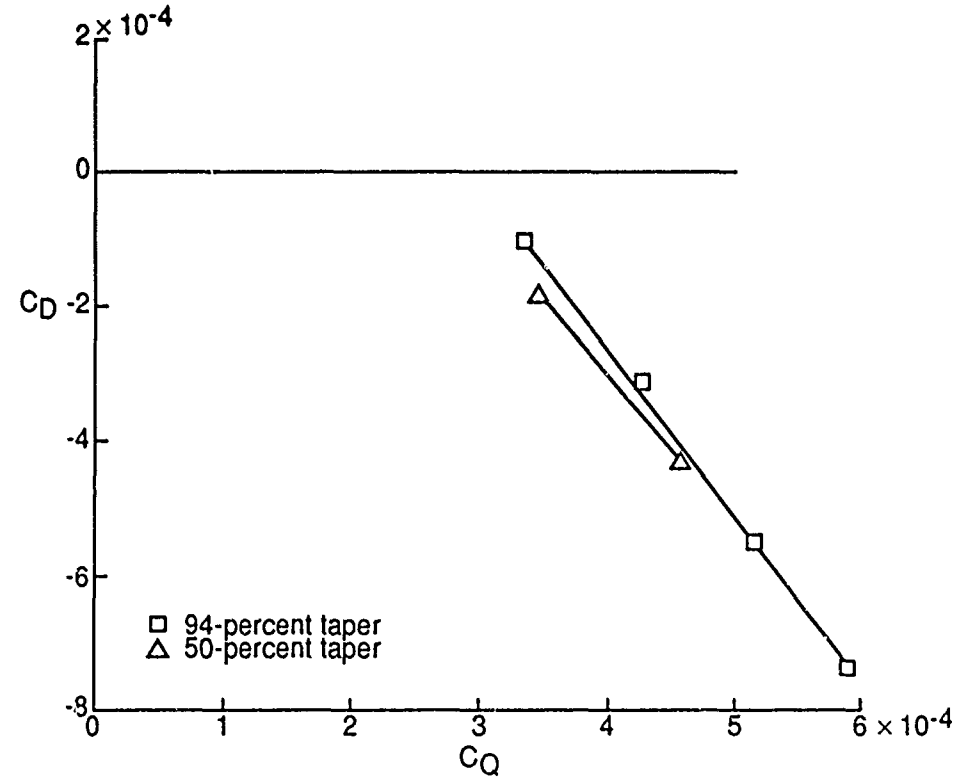

(f) $\mu = 0.35$ and 0.36

Figure 38. Concluded.

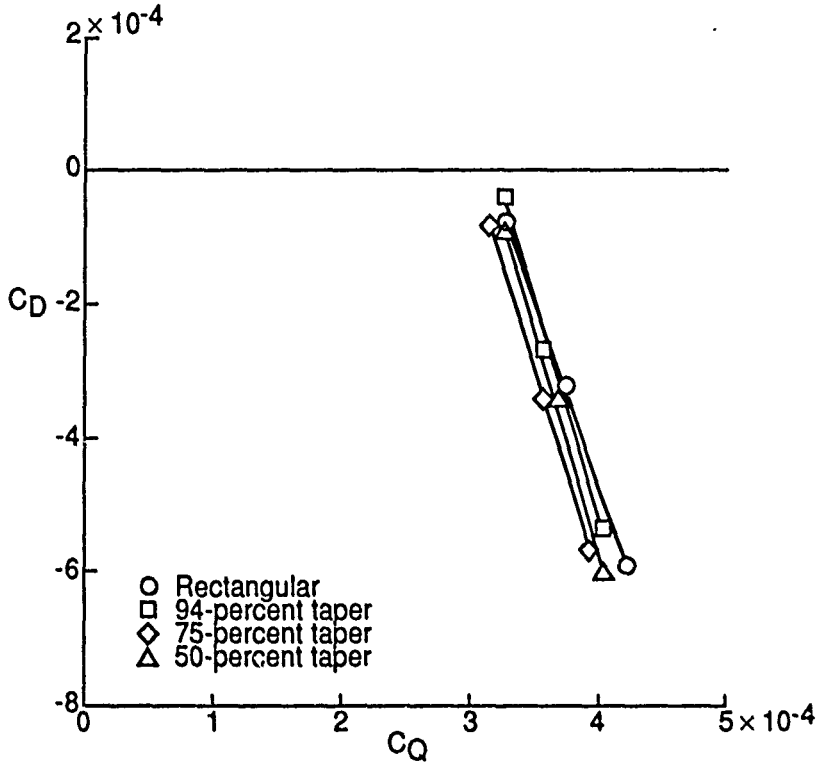

(a) $\mu = 0.14$.

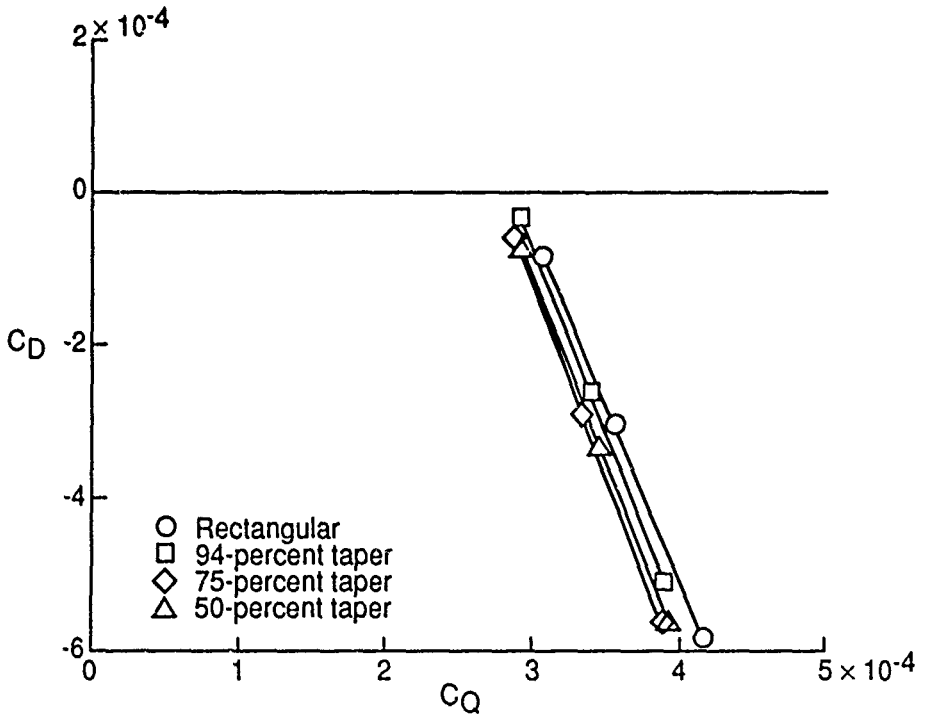

(b) $\mu = 0.19$.

Figure 39. Variation of rotor drag coefficient with rotor torque coefficient for $C_l = 0.007$.

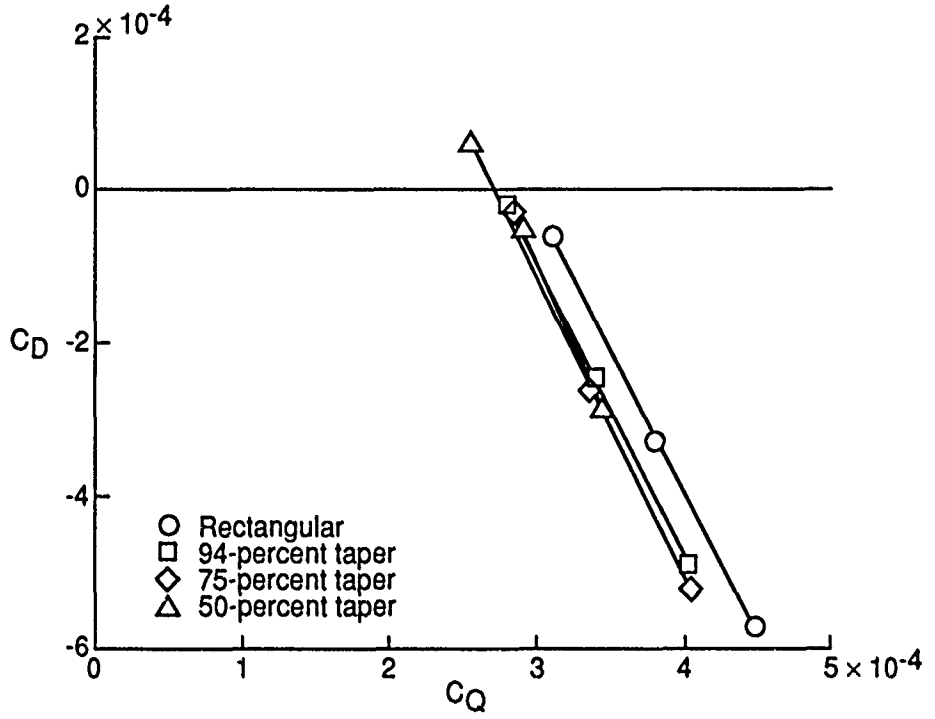

(c) $\mu = 0.23$ and 0.24.

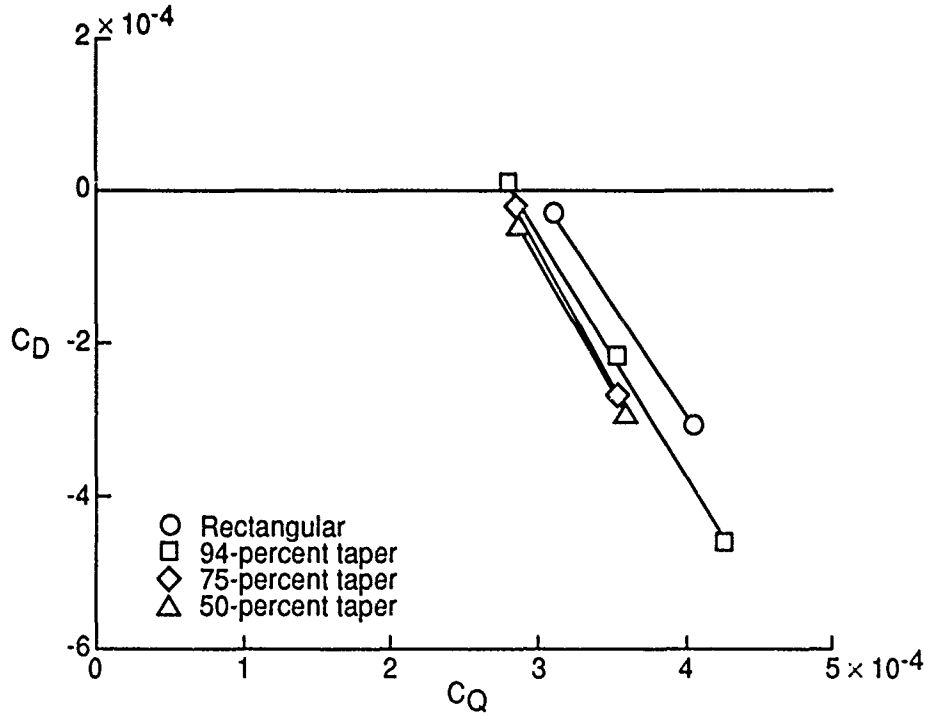

(d) $\mu = 0.27$.

Figure 39. Concluded.

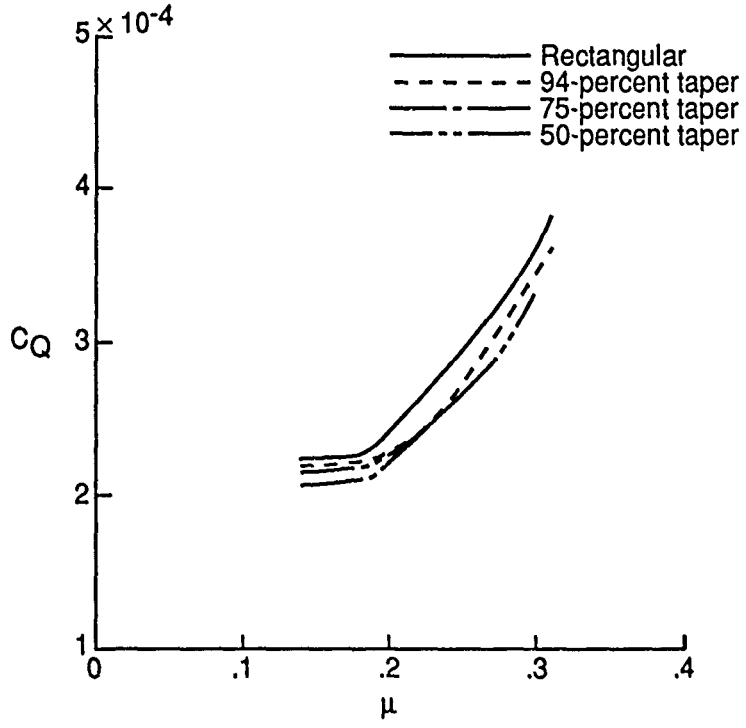

Figure 40. Variation of rotor torque coefficient with advance ratio for $C'_L = 0.005$ and $f_D = 10.5$ ft^2.

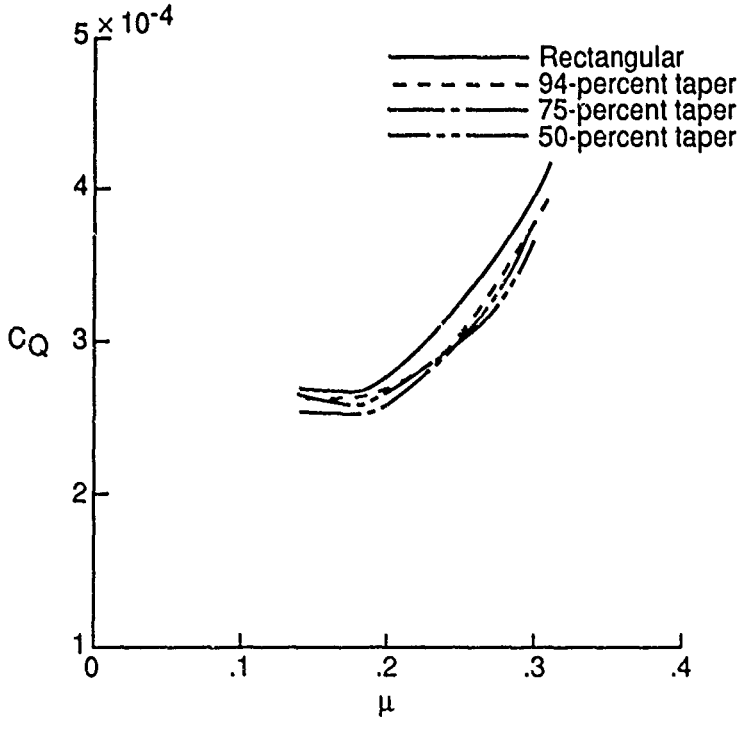

Figure 41. Variation of rotor torque coefficient with advance ratio for $C'_L = 0.006$ and $f_D = 10.5$ ft^2.

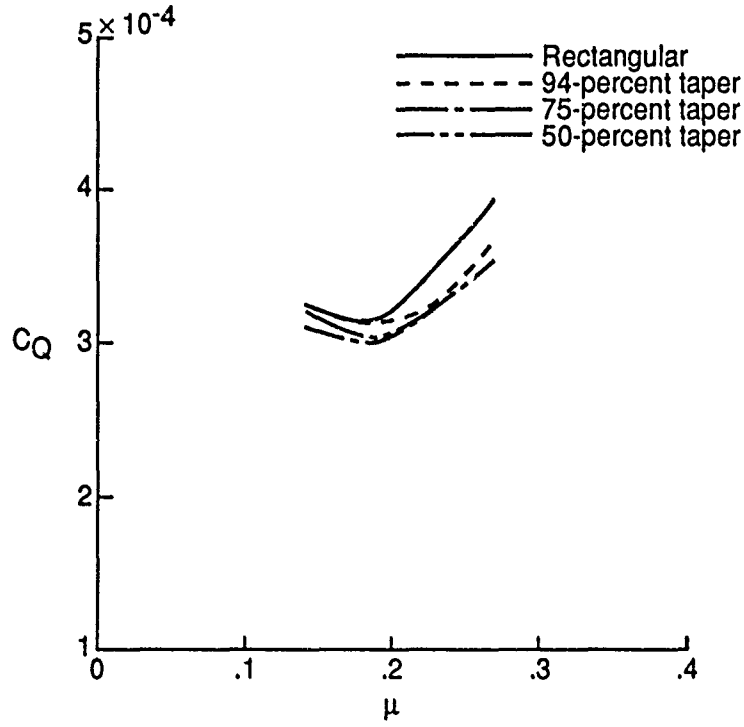

Figure 42. Variation of rotor torque coefficient with advance ratio for $C_L = 0.007$ and $f_D = 10.5$ ft^2.

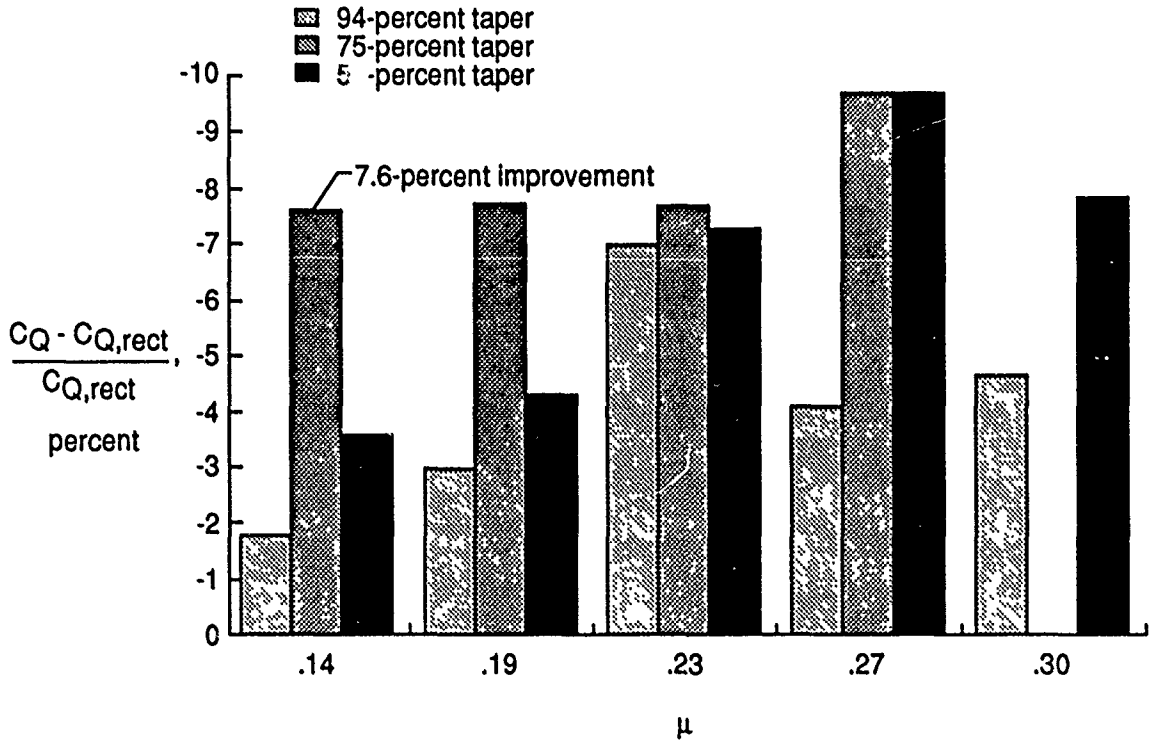

(a) $C_L = 0.005$.

Figure 43. Performance of tapered blades relative to rectangular blades for $f_D = 10.5$ ft^2.

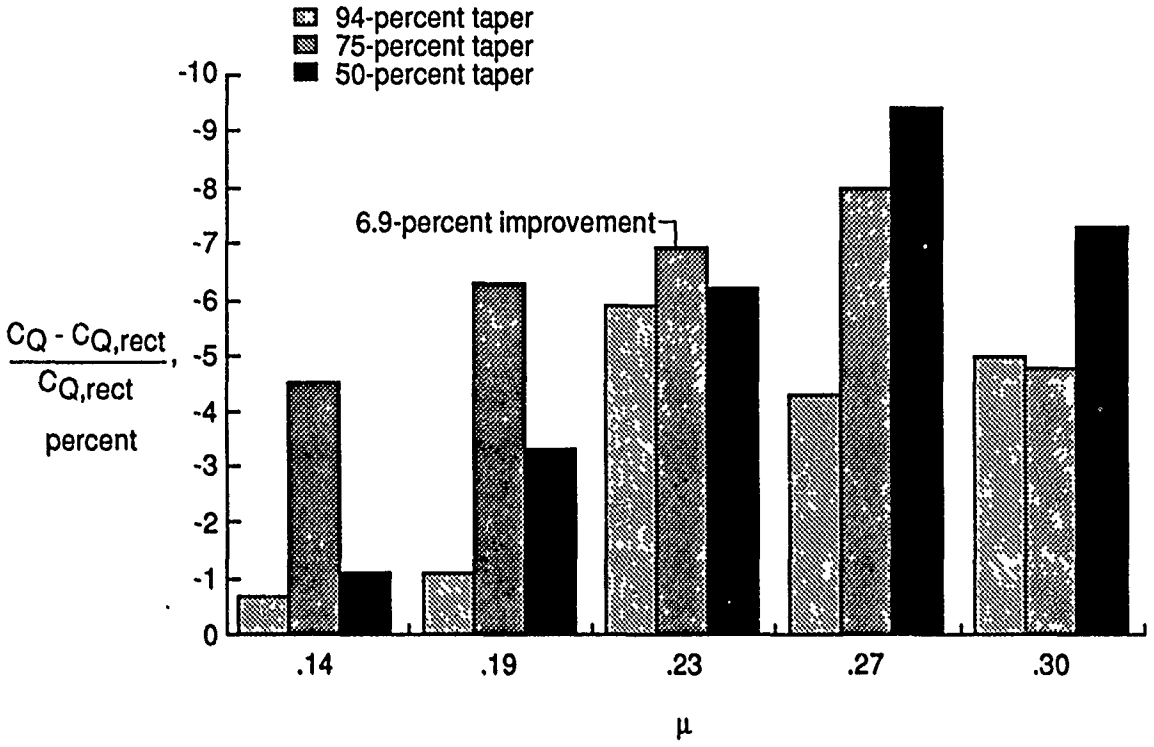

(b) $C_L = 0.006$.

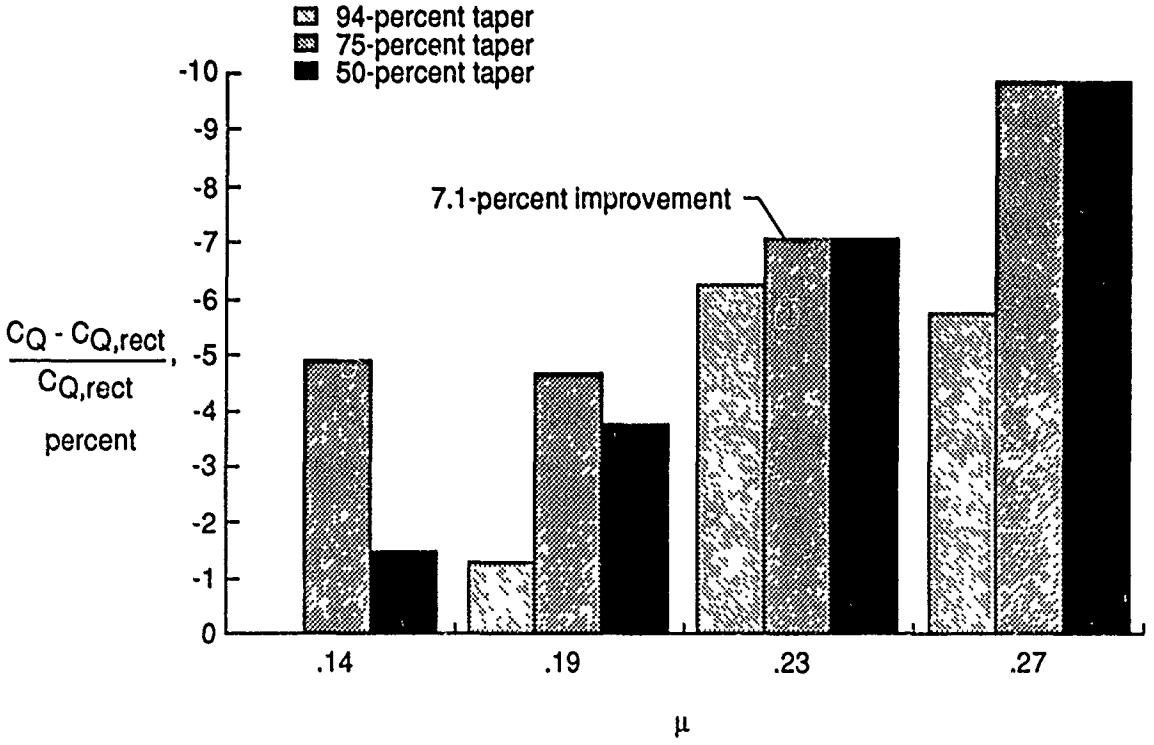

(c) $C_L = 0.007$.

Figure 43. Concluded.

Appendix

Data Repeatability

The repeatability of the performance data (basic characteristics) for the four blade sets is presented in figures A1 to A21, as shown in table A1. For a constant C_L, the maximum difference between two faired C_L versus C_D curves is about 0.000025 in C_D, and the maximum difference between two faired C_L versus C_Q curves is about 0.00001 in C_Q.

Table A1. Performance Data for Blade Sets

Parameter	μ	α_s, deg	Figures for rotor planform—			
			Rectangular	94-percent taper	75-percent taper	50-percent taper
C_L vs C_D	0.14	−2	A1	A4	A12	A17
and	.19	−2		A5		
C_L vs C_Q	.23	−2	A2		A13	A18
	.24	−4		A6		
	.27	−4		A7	A14	
	.30	−4				A19
	.30	−6			A15	
	.31	−4	A3	A8		
	.35	−6			A16	A20
	.35	−8			A16	
	.36	−6		A9		
	.40	−7				A21
	.40	−8		A10		
	.43	−7		A11		

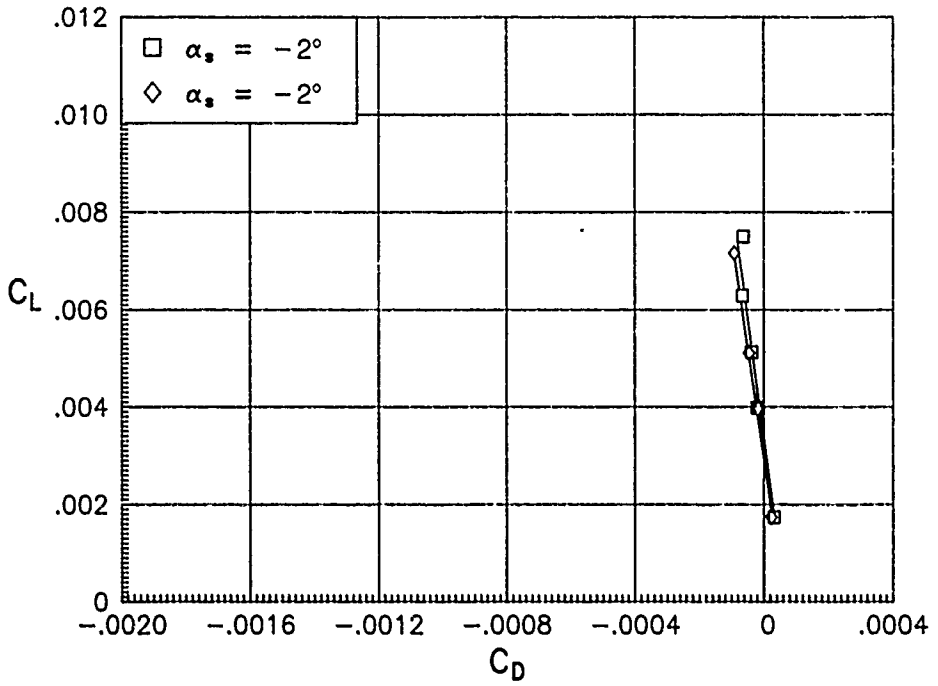

(a) C_L versus C_D.

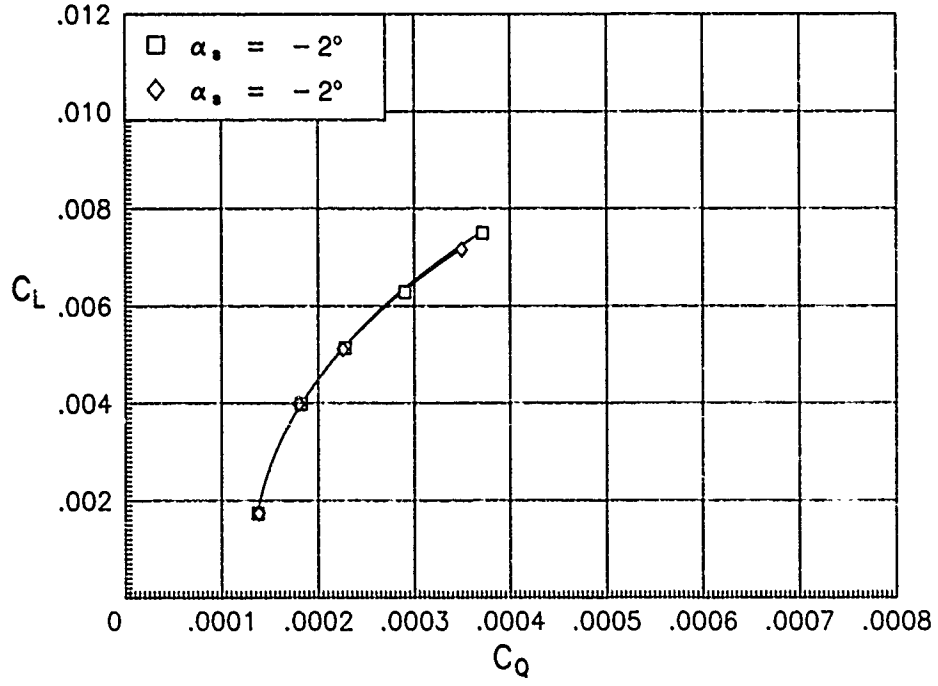

(b) C_L versus C_Q.

Figure A1. Repeatability of basic forward-flight characteristics of rectangular rotor for $\mu = 0.14$.

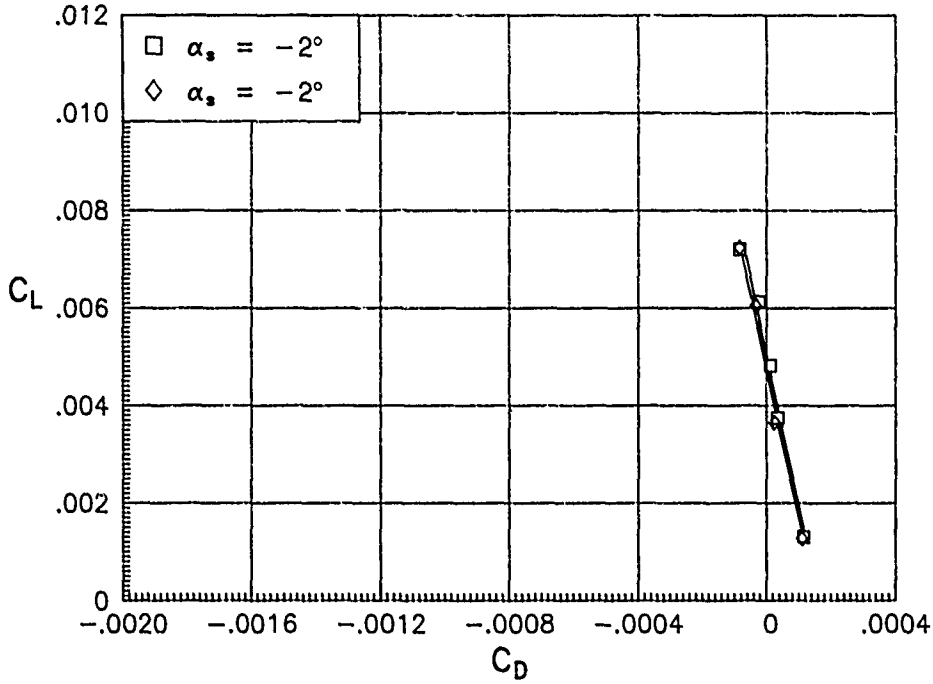

(a) C_L versus C_D.

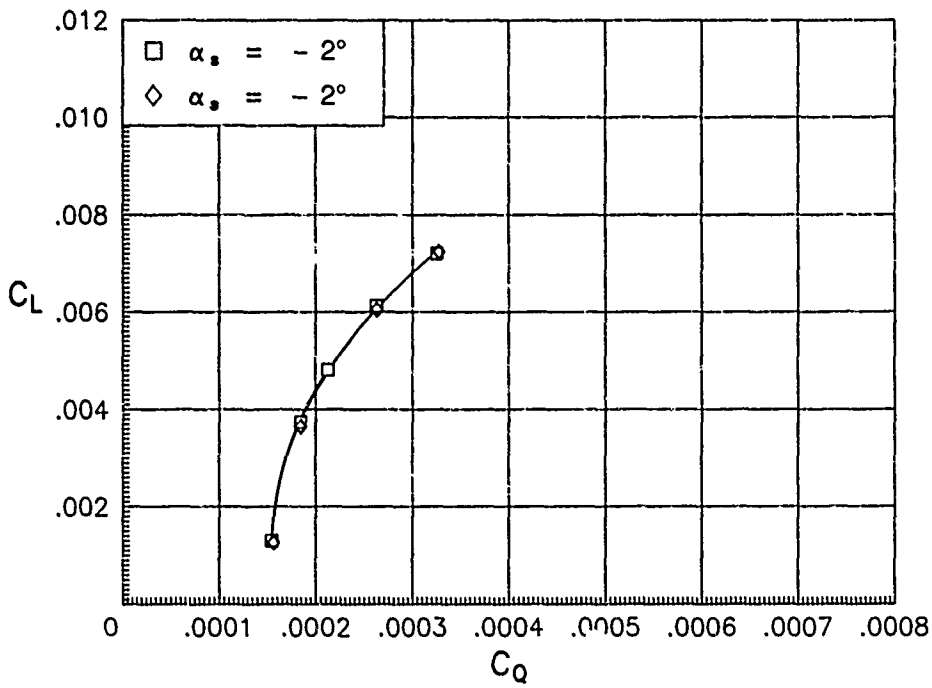

(b) C_L versus C_Q.

Figure A2. Repeatability of basic forward-flight characteristics of rectangular rotor for $\mu = 0.23$

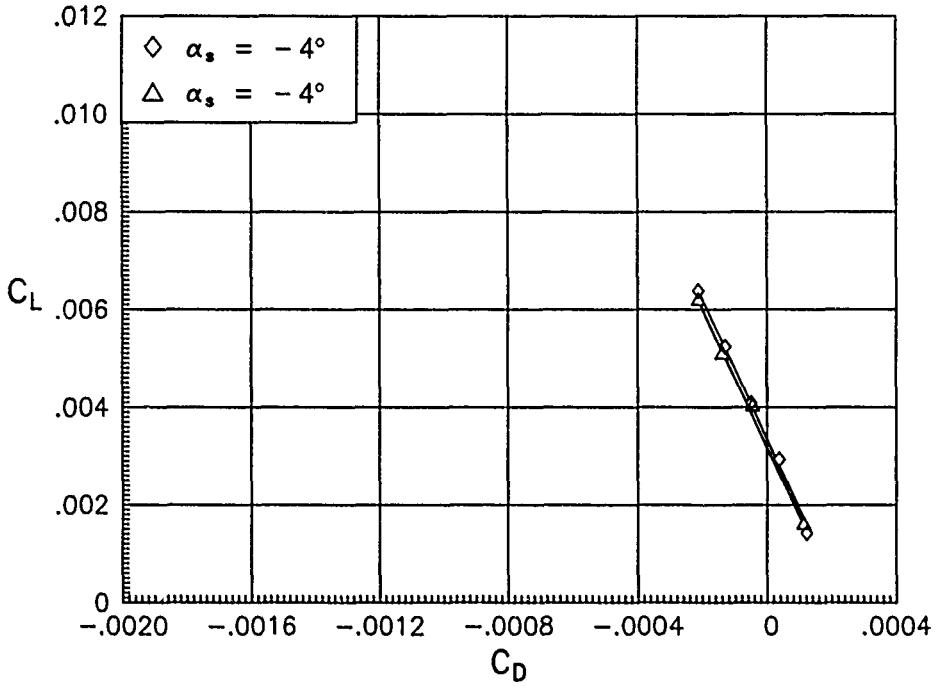

(a) C_L versus C_D.

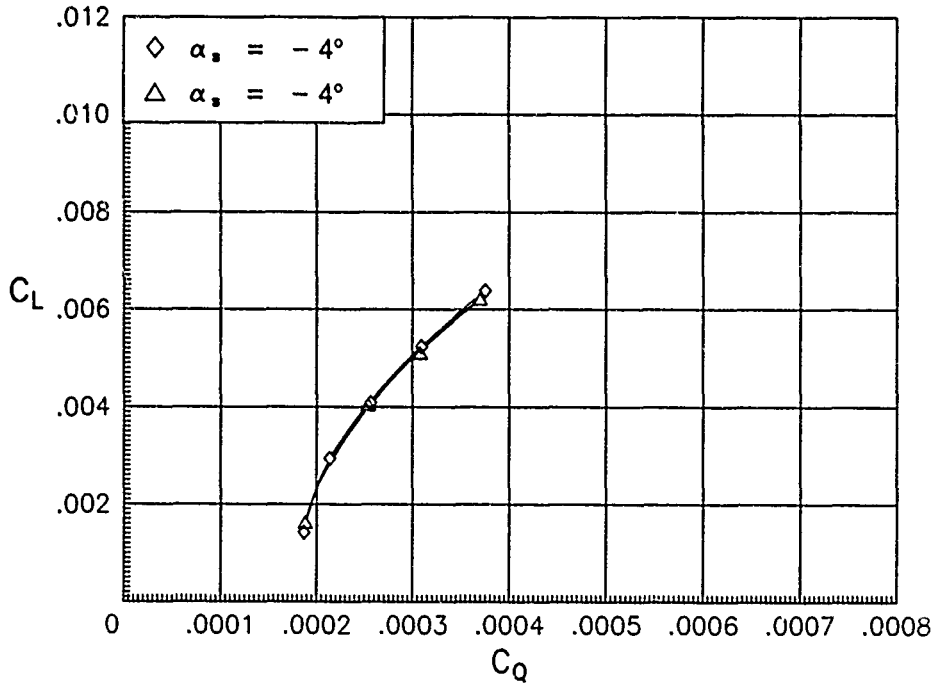

(b) C_L versus C_Q.

Figure A3. Repeatability of basic forward-flight characteristics of rectangular rotor for $\mu = 0.31$.

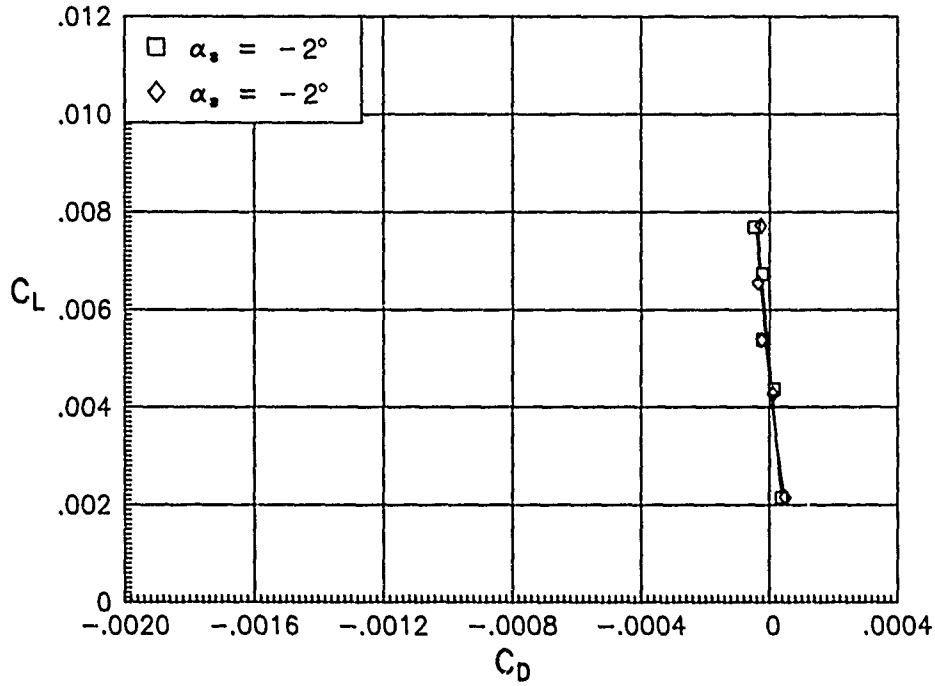

(a) C_L versus C_D.

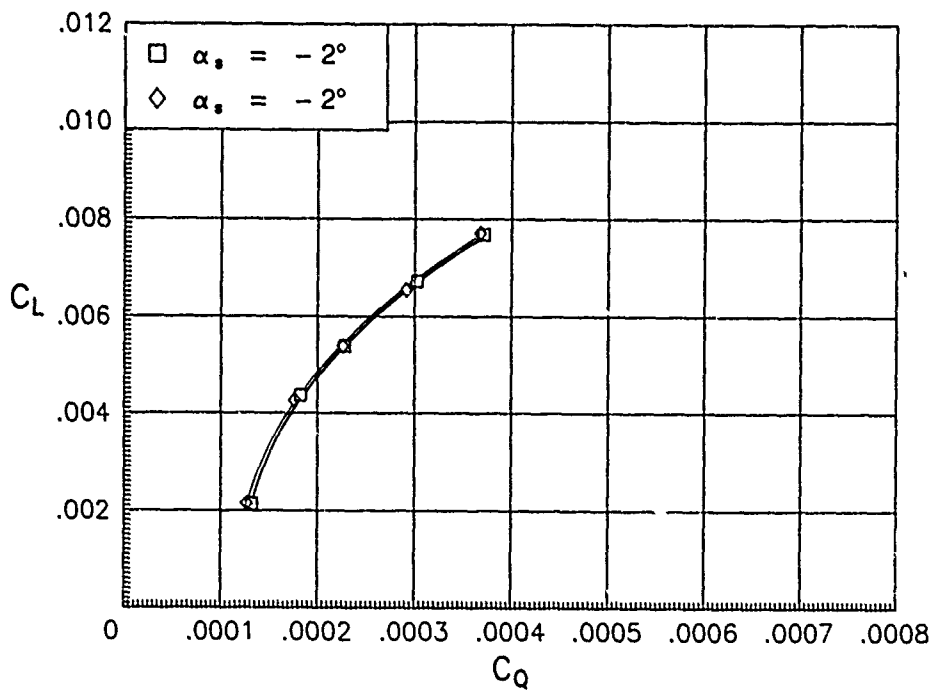

(b) C_L versus C_Q.

Figure A4. Repeatability of basic forward-flight characteristics of 94-percent tapered rotor for $\mu = 0.11$.

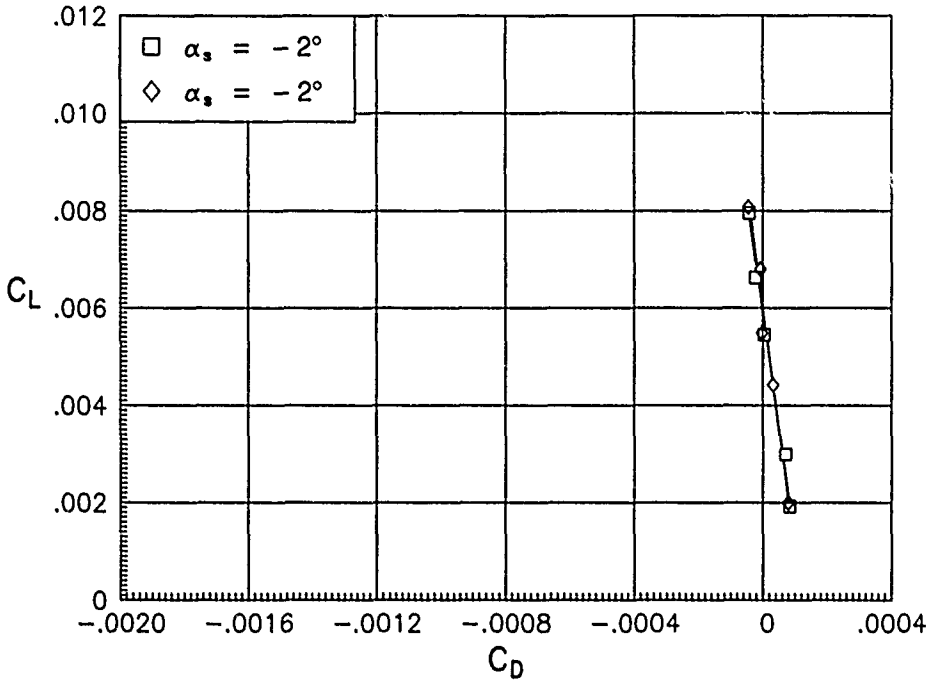

(a) C_L versus C_D.

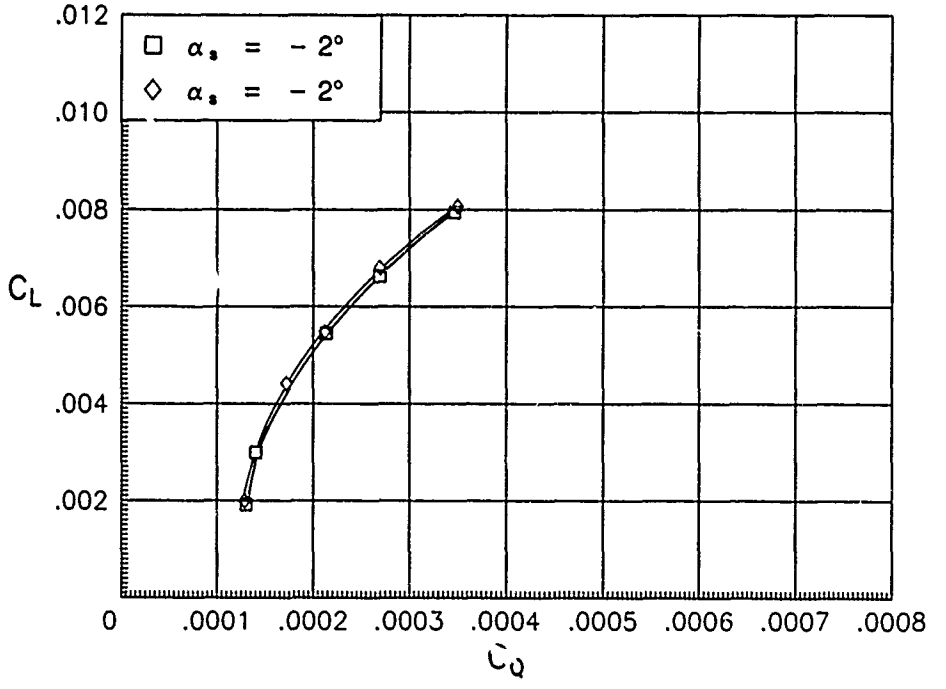

(b) C_L versus C_Q.

Figure A5. Repeatability of basic forward-flight characteristics of 94-percent tapered rotor for $\mu = 0.19$.

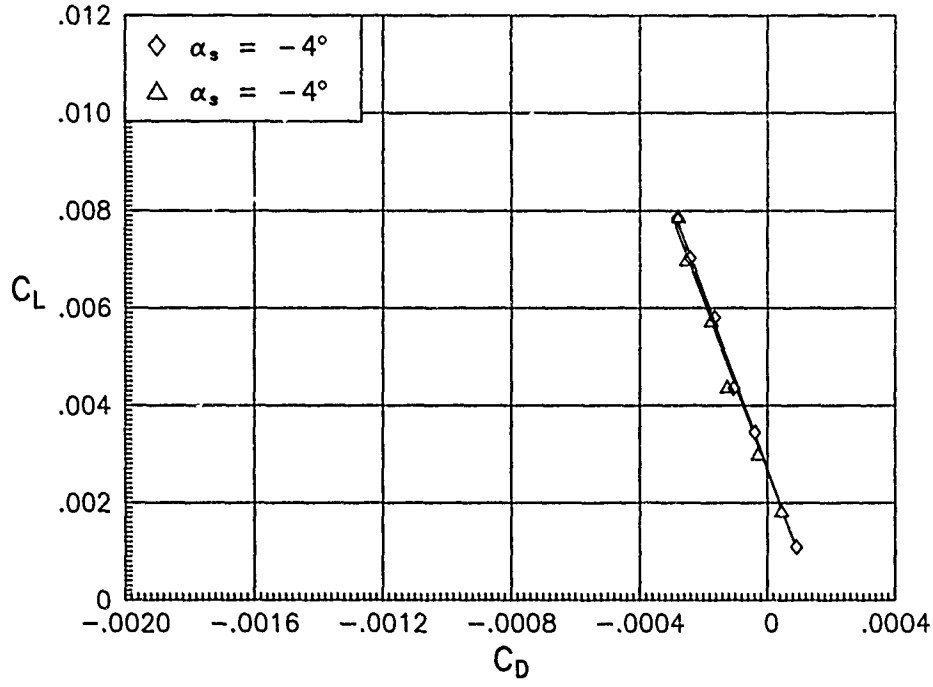

(a) C_L versus C_D.

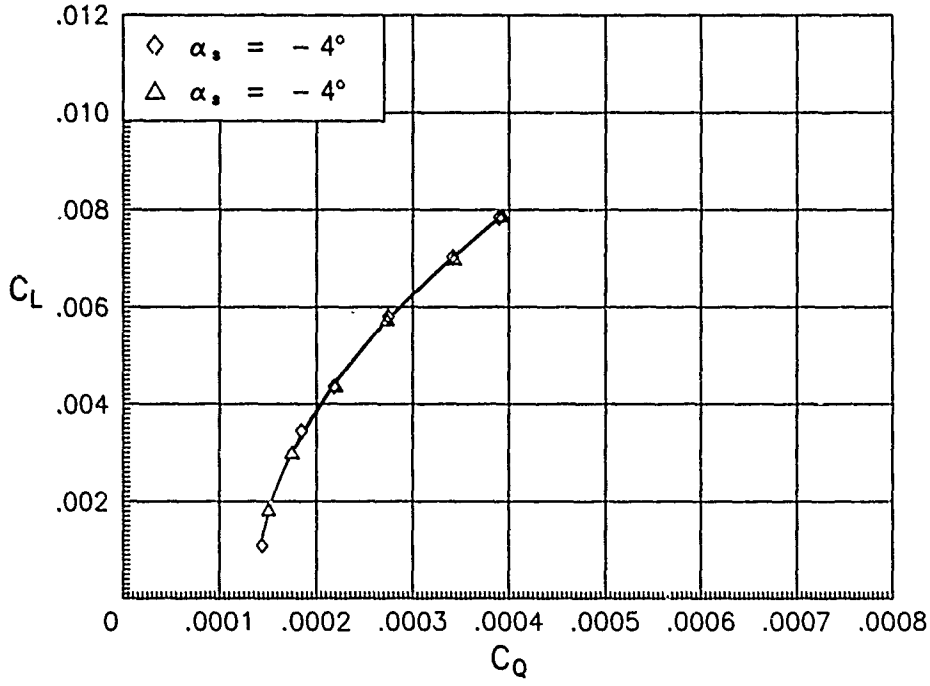

(b) C_L versus C_Q.

Figure A6. Repeatability of basic forward-flight characteristics of 94-percent tapered rotor for $\mu = 0.24$.

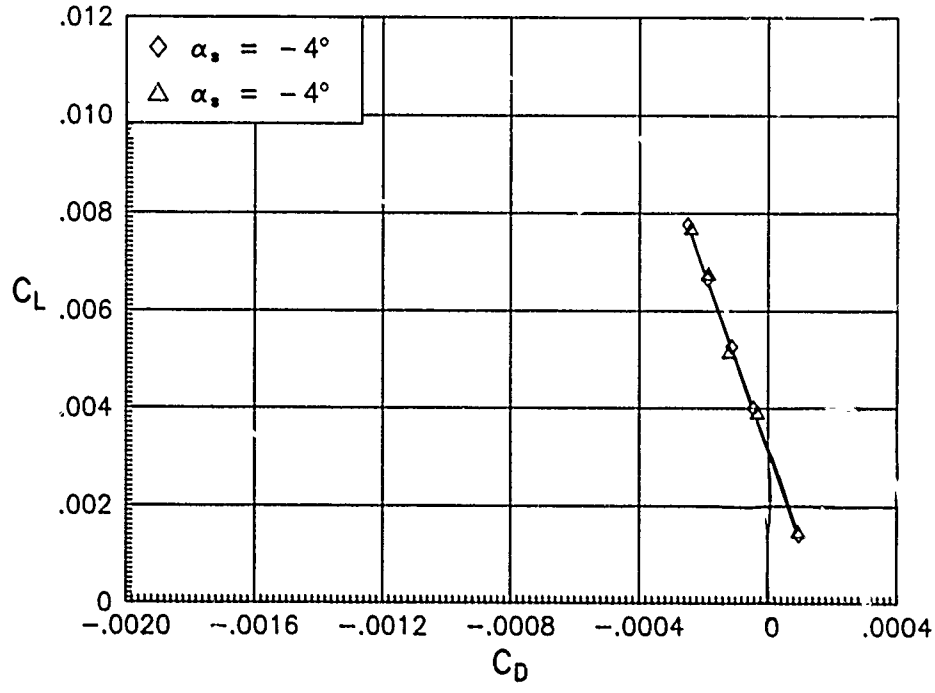

(a) C_L versus C_D.

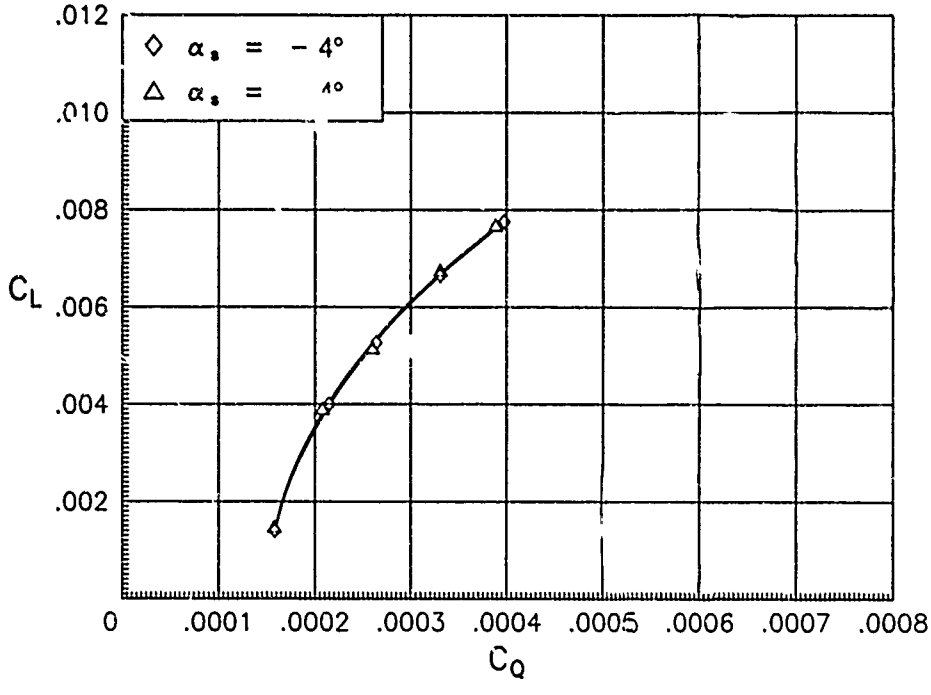

(b) C_L versus C_Q.

Figure A7. Repeatability of basic forward-flight characteristics of 91-percent tapered rotor for $\mu = 0.27$.

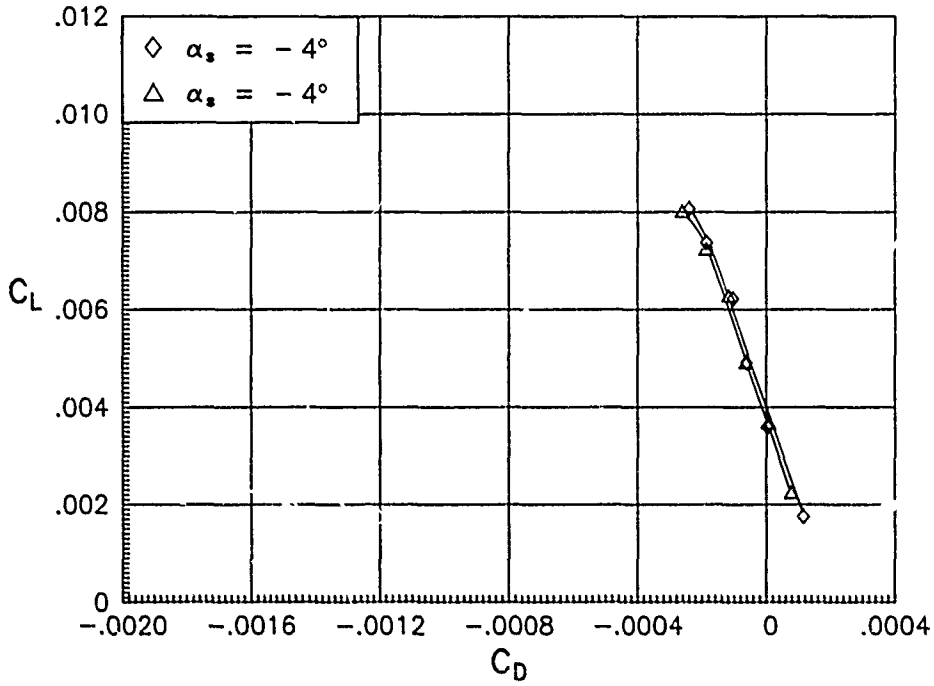

(a) C_L versus C_D.

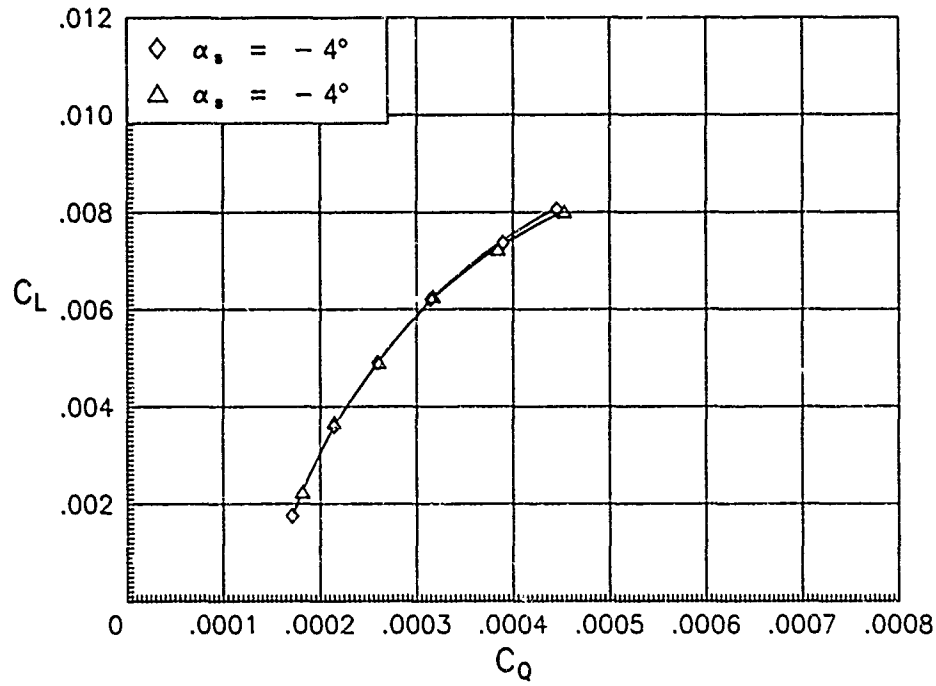

(b) C_L versus C_Q.

Figure A8. Repeatability of basic forward-flight characteristics of 94-percent tapered rotor for $\mu = 0.31$

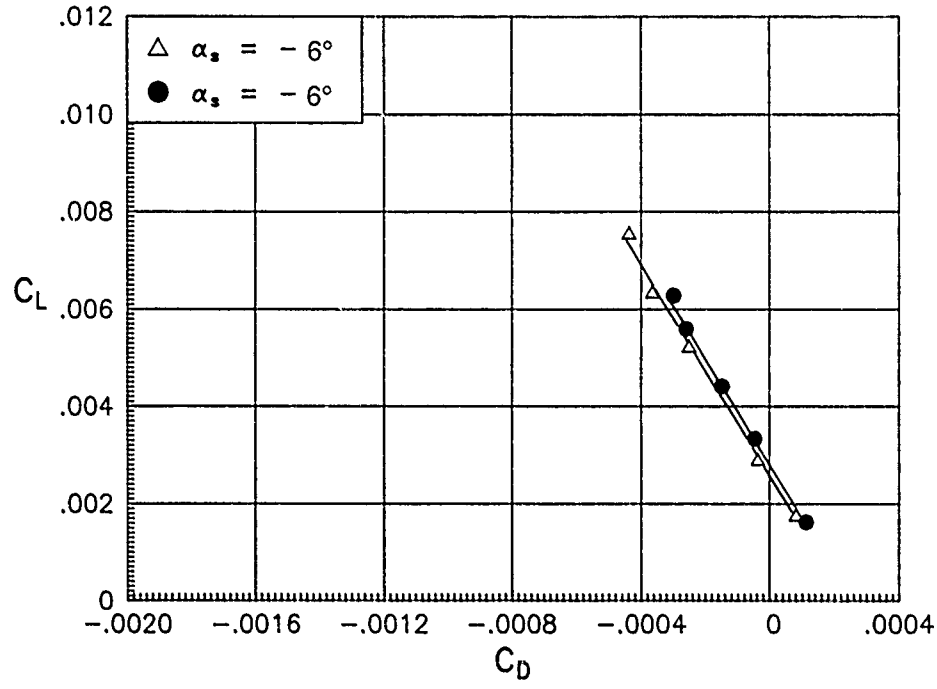

(a) C_L versus C_D.

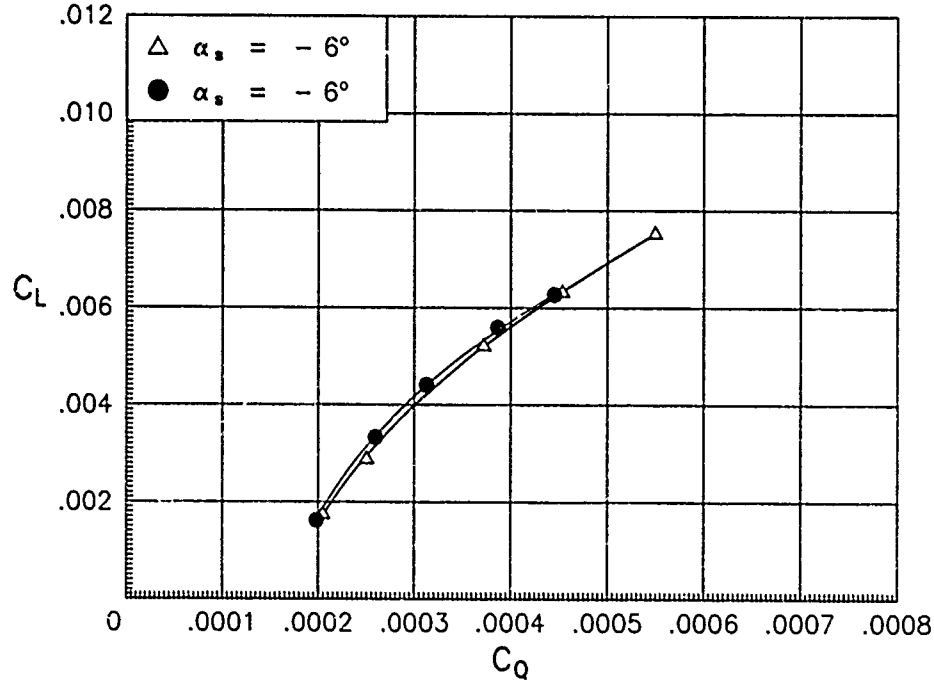

(b) C_L versus C_Q.

Figure 49 Repeatability of basic forward-flight characteristics of 94-percent tapered rotor for $\mu = 0.36$.

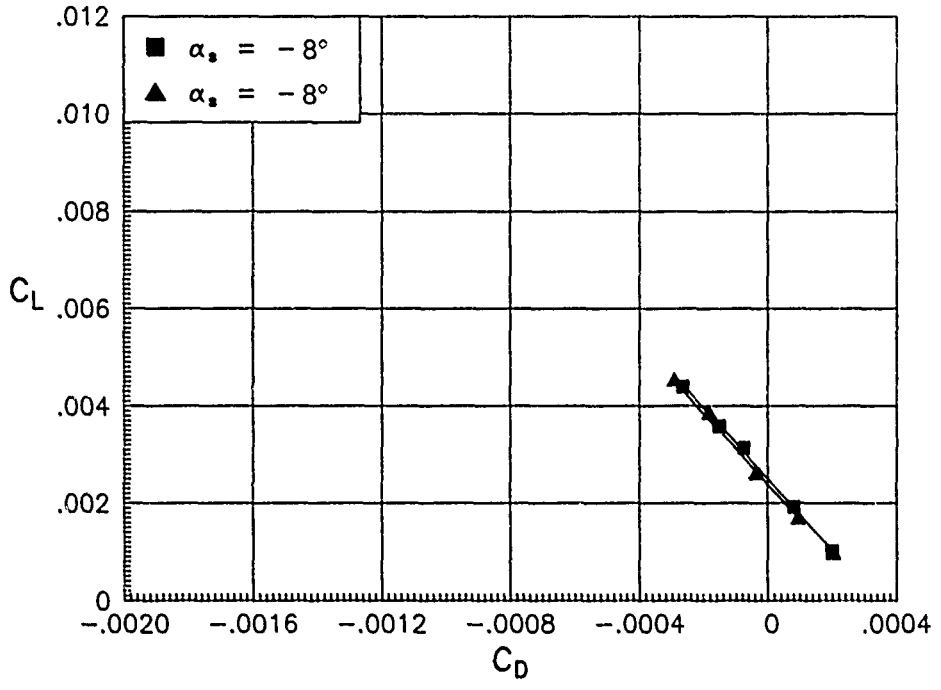

(a) C_L versus C_D.

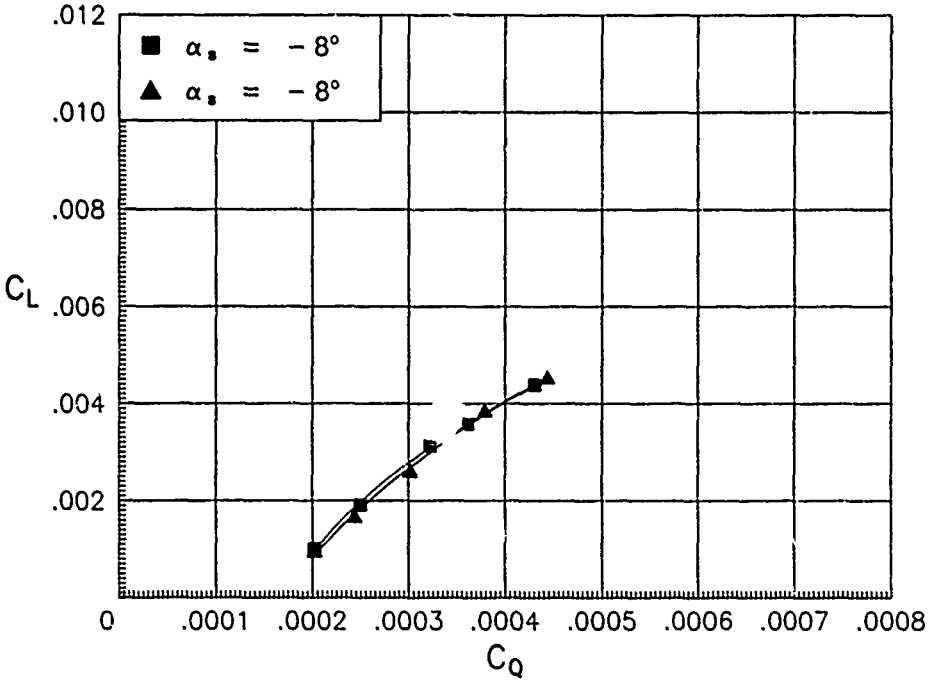

(b) C_L versus C_Q.

Figure A10. Repeatability of basic forward-flight characteristics of 94-percent tapered rotor for μ = 0.10

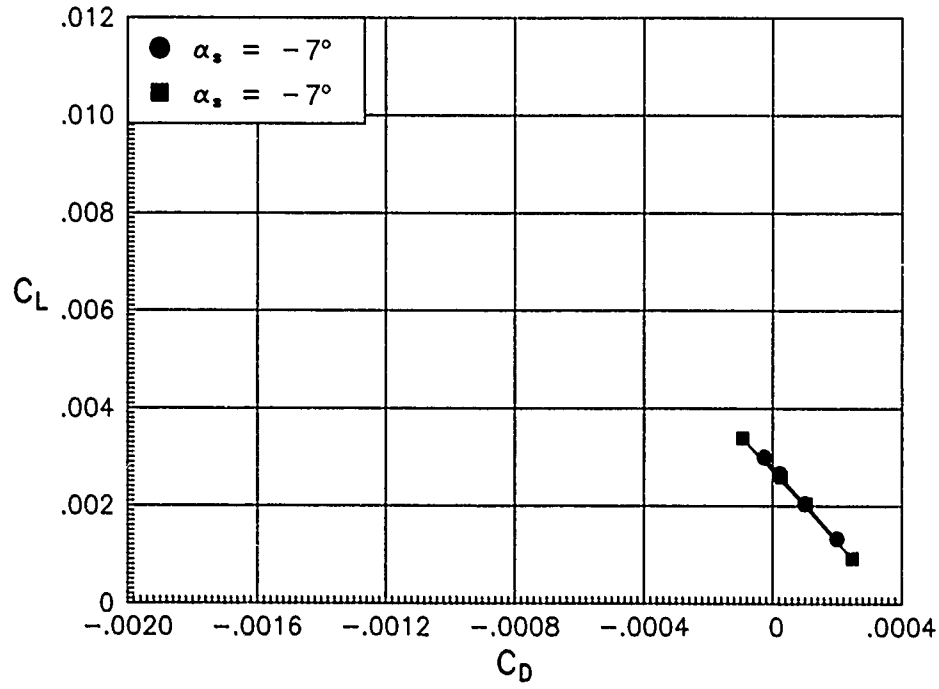

(a) C_L versus C_D.

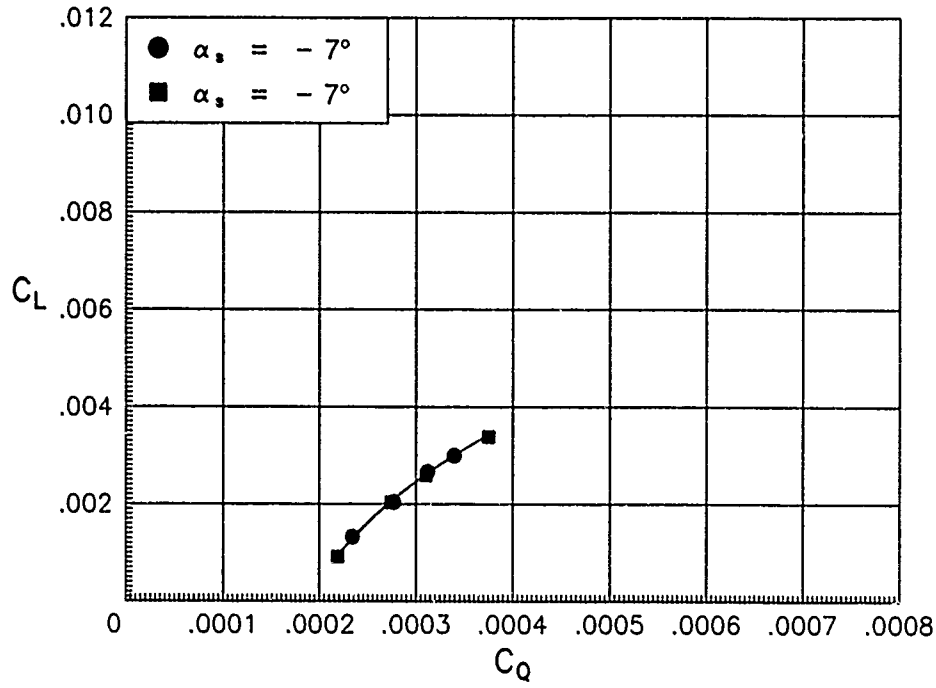

(b) C_L versus C_Q.

Figure A11. Repeatability of basic forward-flight characteristics of 94-percent tapered rotor for $\mu = 0.43$.

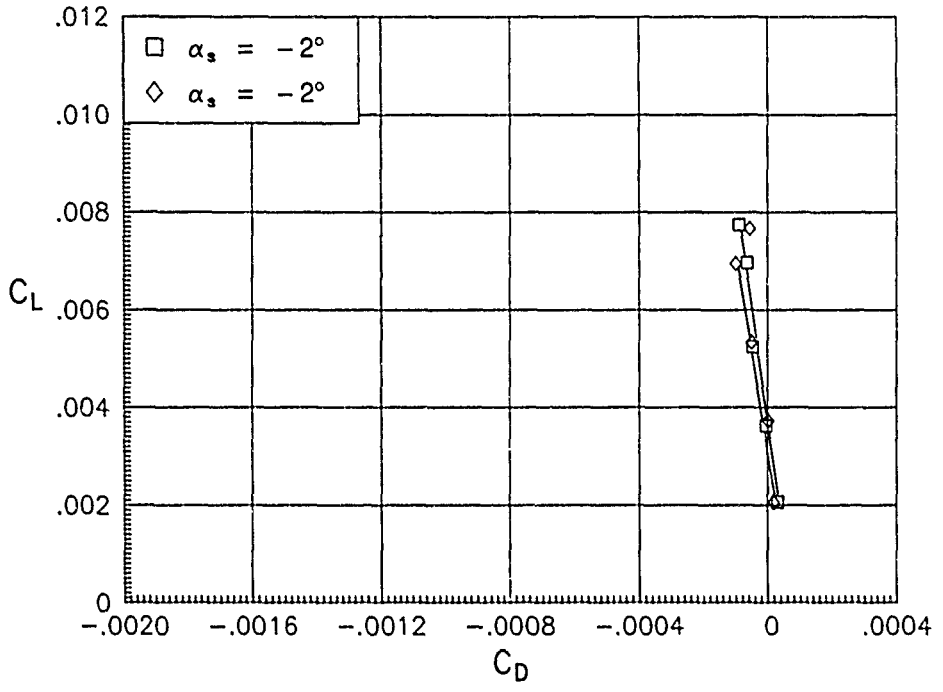

(a) C_L versus C_D.

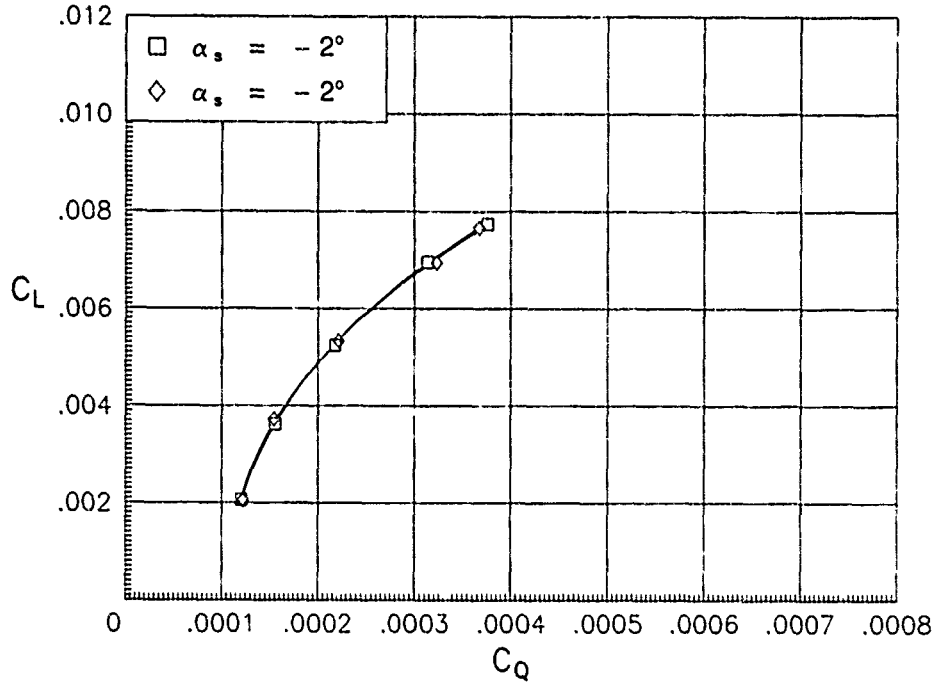

(b) C_L versus C_Q

Figure A12. Repeatability of basic forward-flight characteristics of 75-percent tapered rotor for $\mu = 0.11$

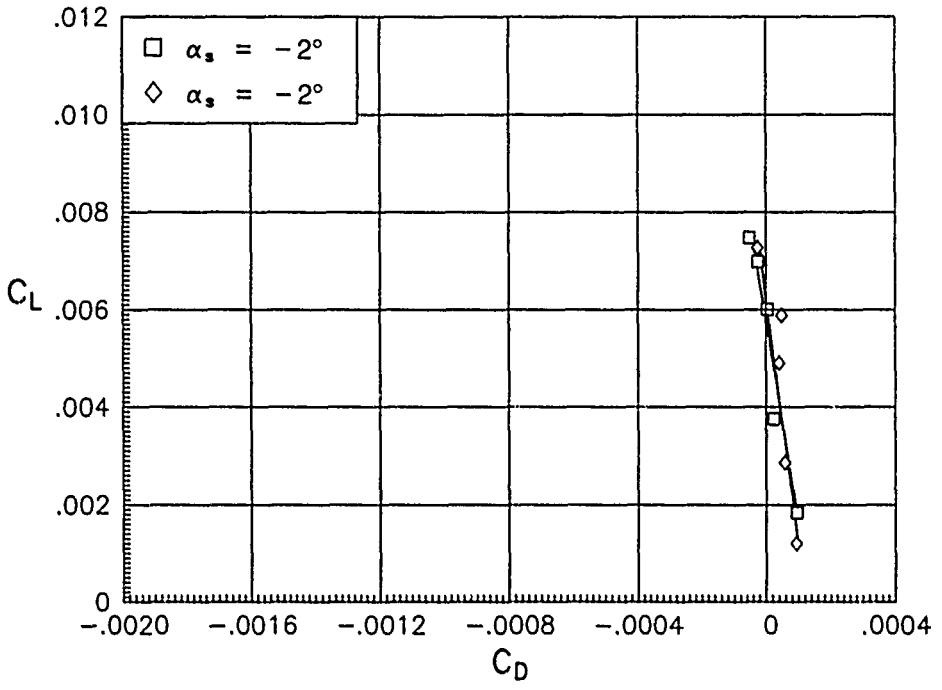

(a) C_L versus C_D.

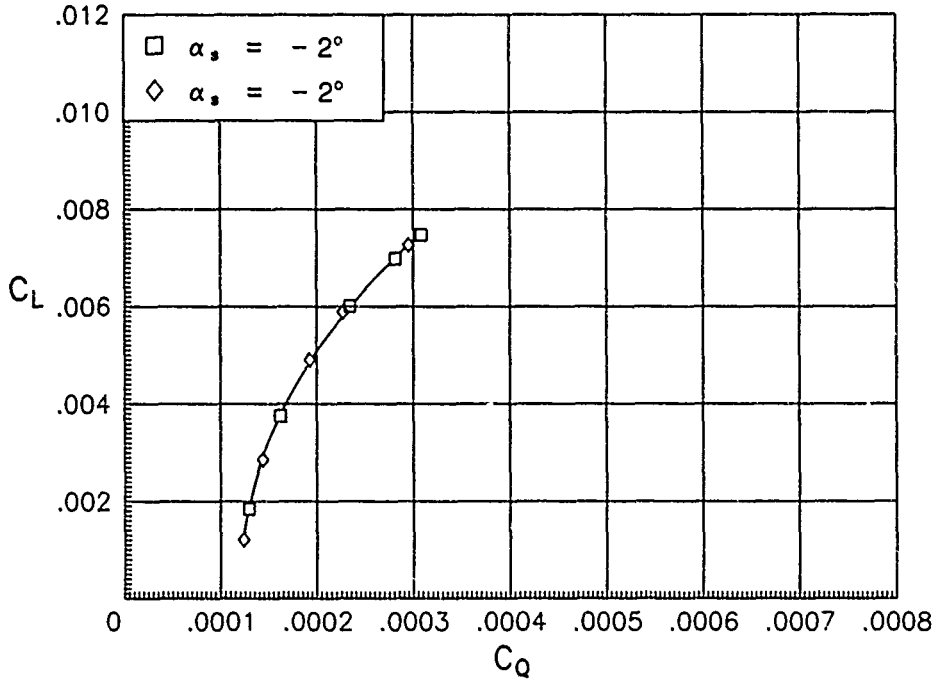

(b) C_L versus C_Q.

Figure A13 Repeatability of basic forward-flight characteristics of 75-percent tapered rotor for $\mu = 0.23$.

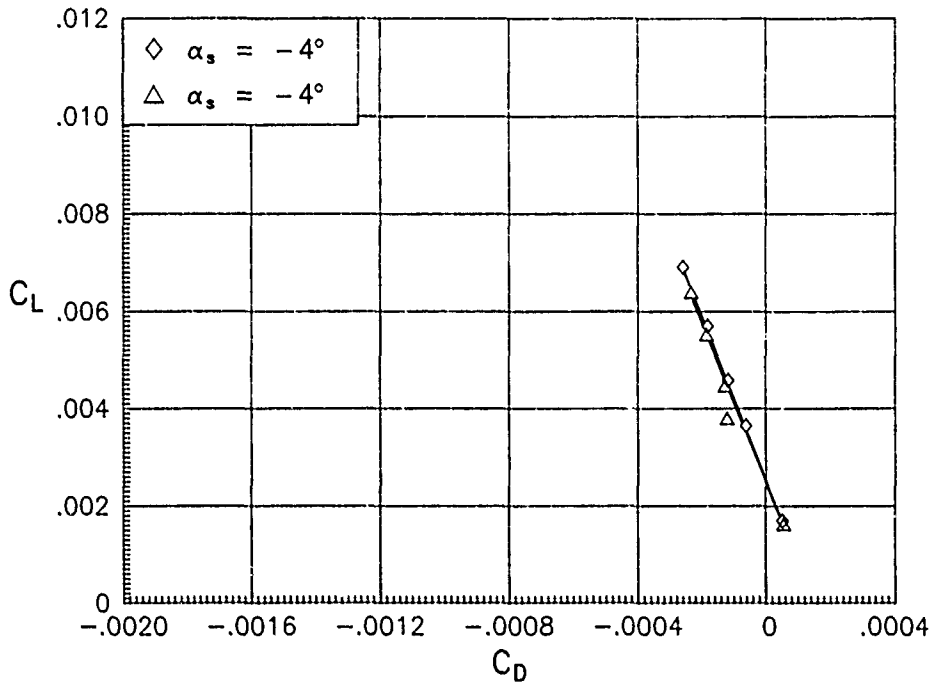

(a) C_L versus C_D.

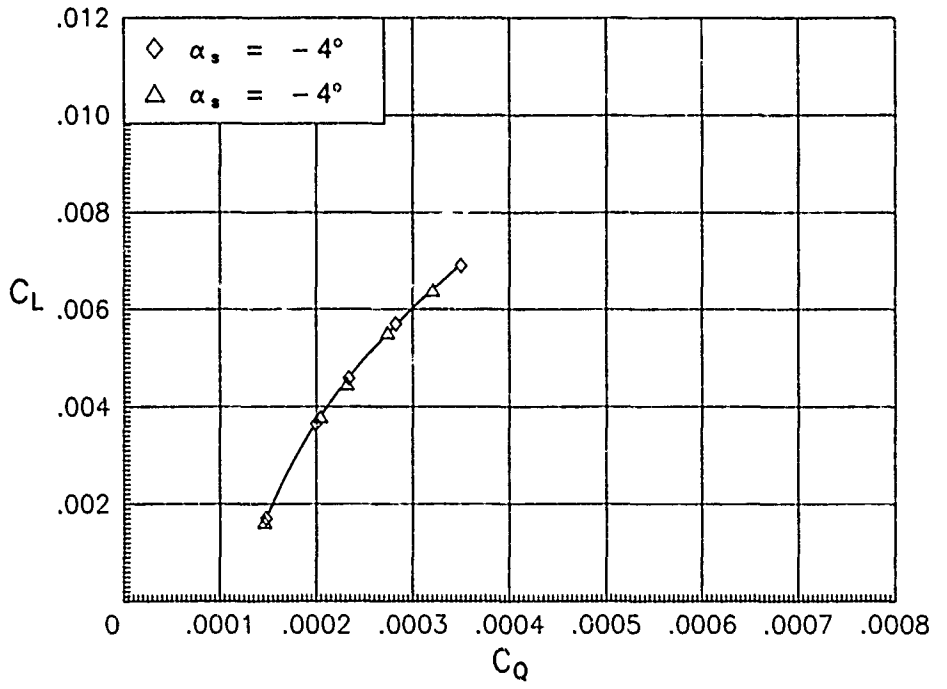

(b) C_L versus C_Q.

Figure A14. Repeatability of basic forward-flight characteristics of 75-percent tapered rotor for $\mu = 0.27$.

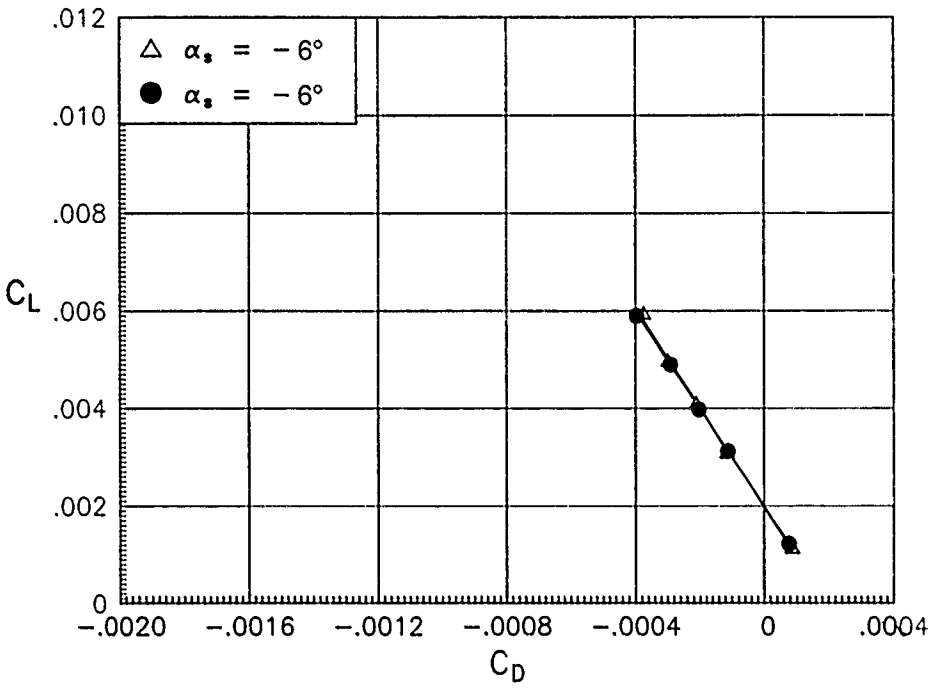

(a) C_L versus C_D.

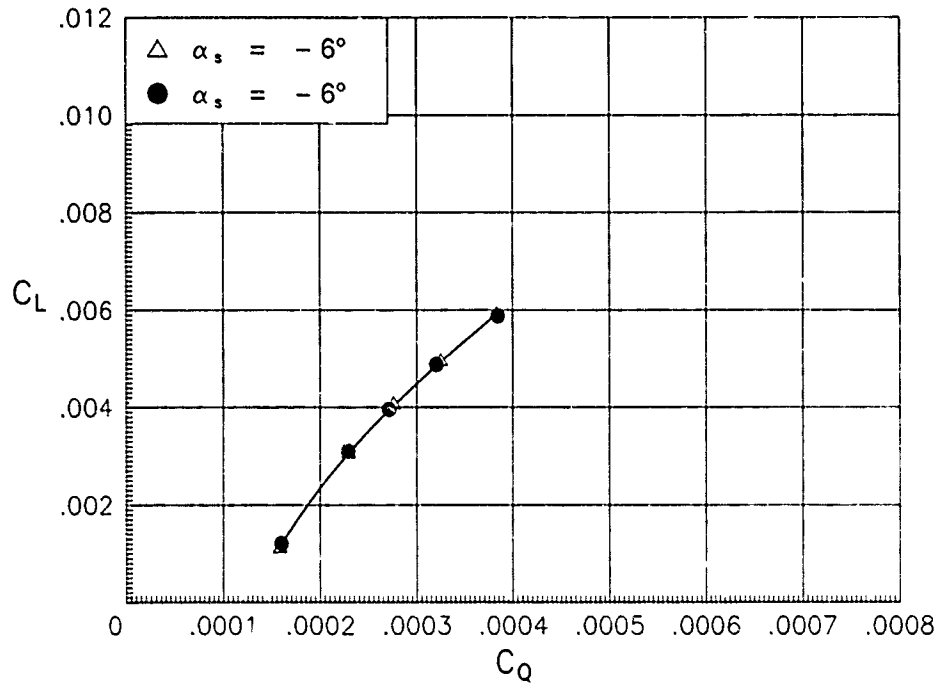

(b) C'_L versus C_Q.

Figure A15. Repeatability of basic forward-flight characteristics of 75-percent tapered rotor for $\mu = 0.30$.

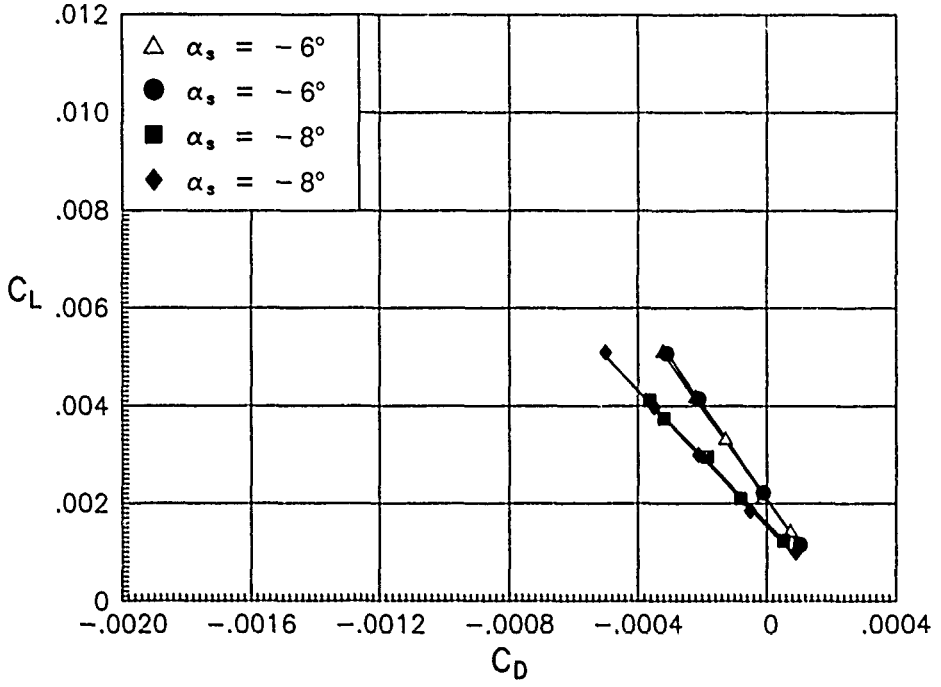

(a) C_L versus C_D.

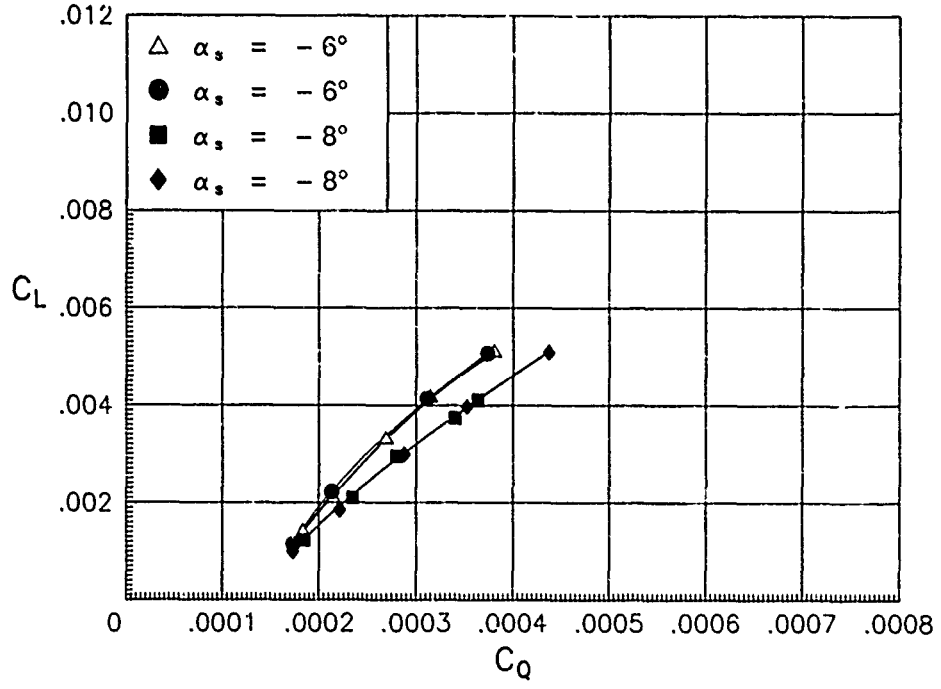

(b) C_L versus C_Q.

Figure A16. Repeatability of basic forward-flight characteristics of 75-percent tapered rotor for $\mu = 0.35$.

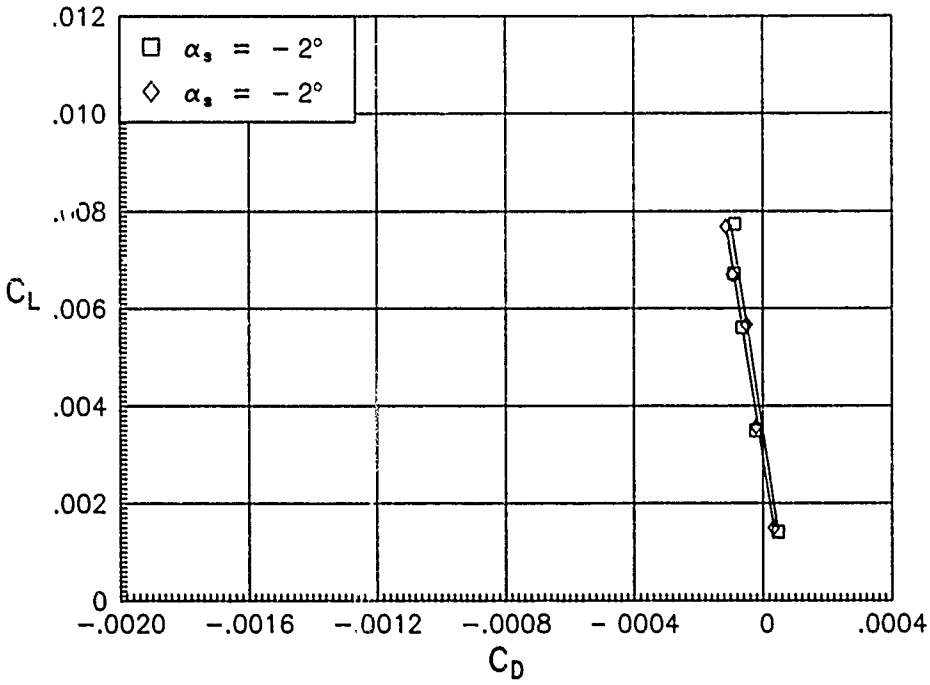

(a) C_L versus C_D.

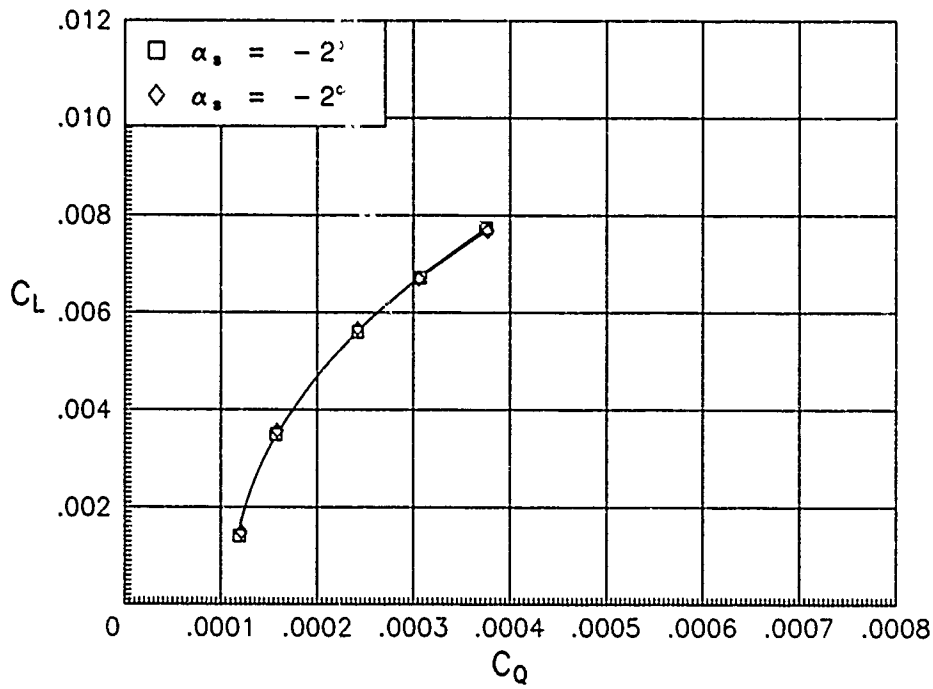

(b) C_L versus C_Q.

Figure A17. Repeatability of basic forward-flight characteristics of 50-percent tapered rotor for $\mu = 0.14$.

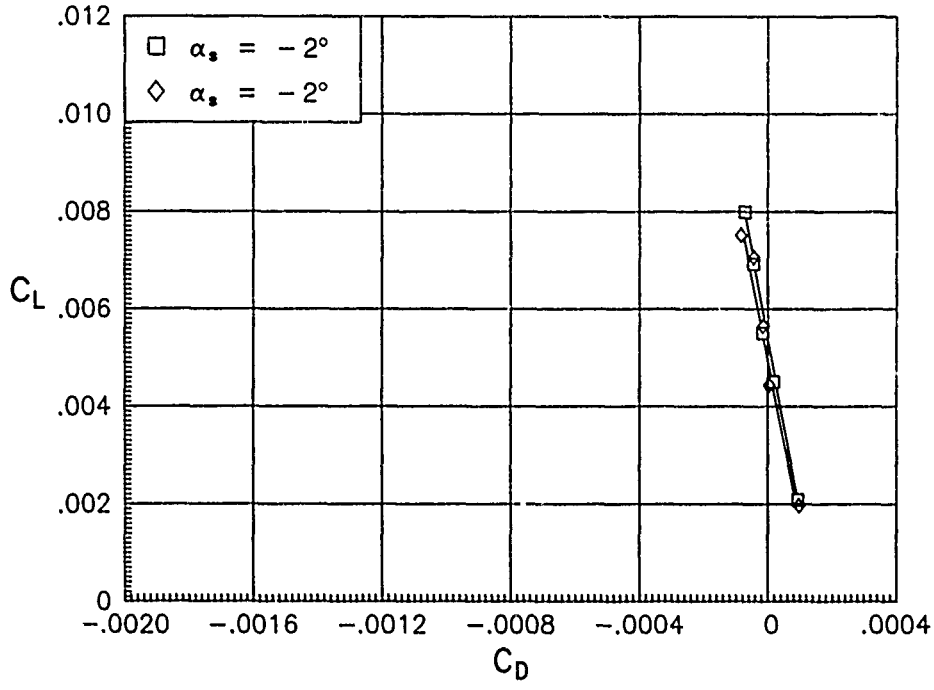

(a) C_L versus C_D.

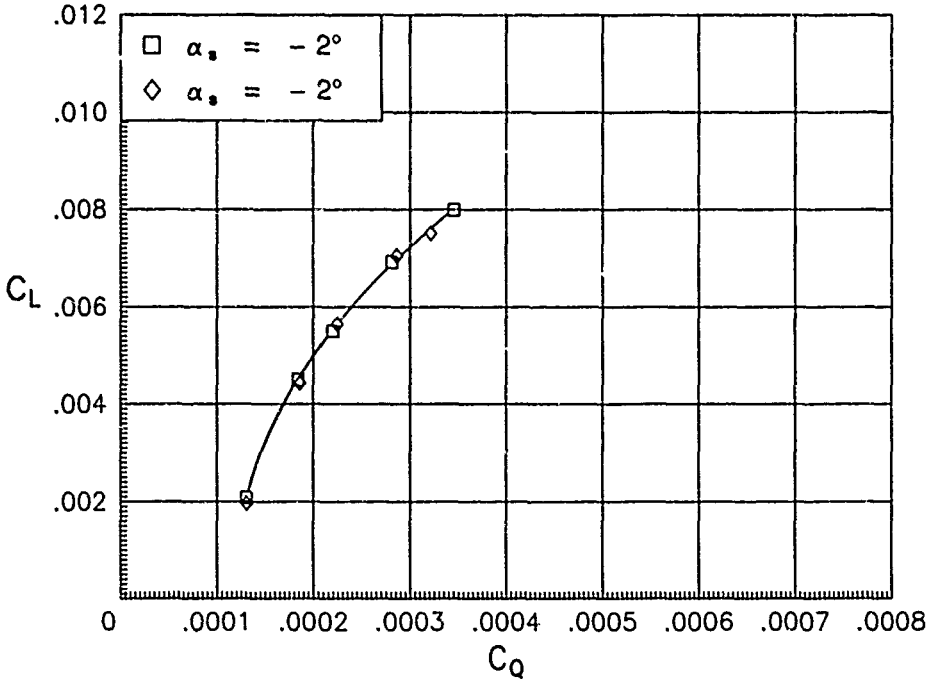

(b) C_L versus C_Q.

Figure A18. Repeatability of basic forward-flight characteristics of 50-percent tapered rotor for $\mu = 0.23$.

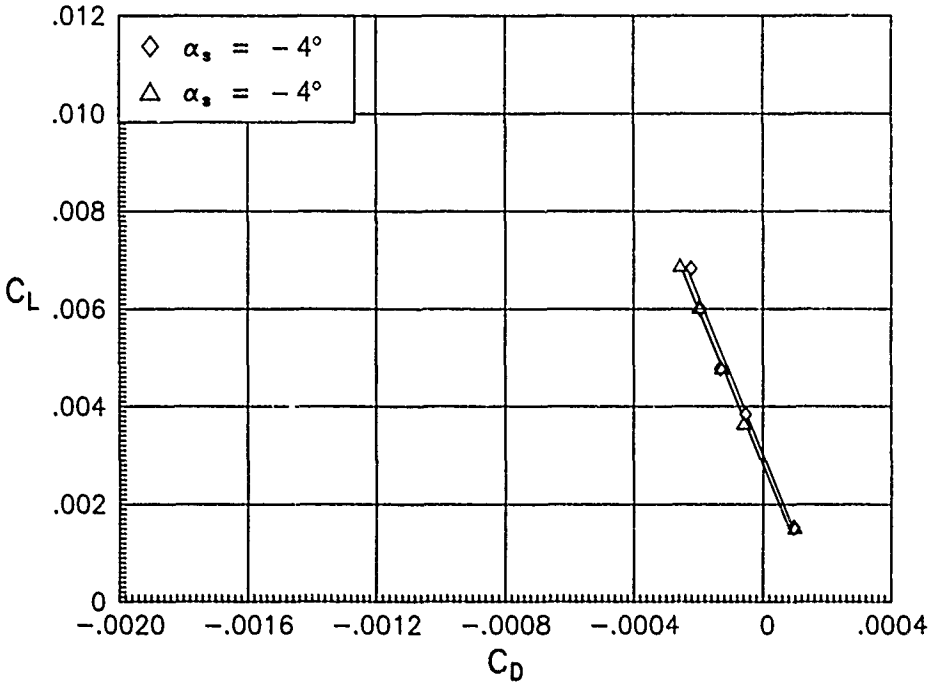

(a) C_L versus C_D.

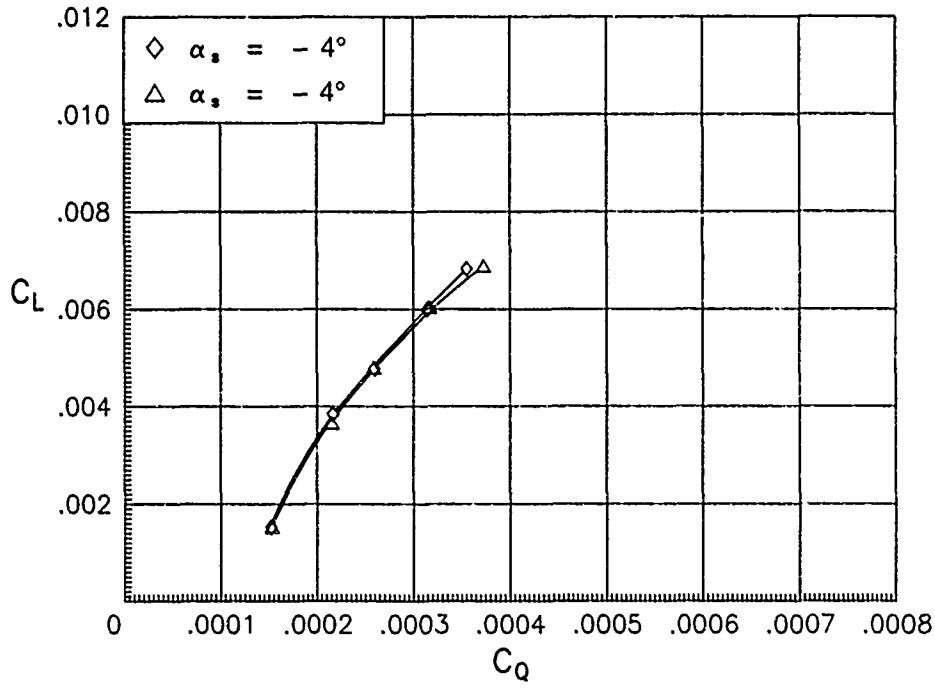

(b) C_L versus C_Q.

Figure A19. Repeatability of basic forward flight characteristics of 50-percent tapered rotor for $\mu = 0.30$.

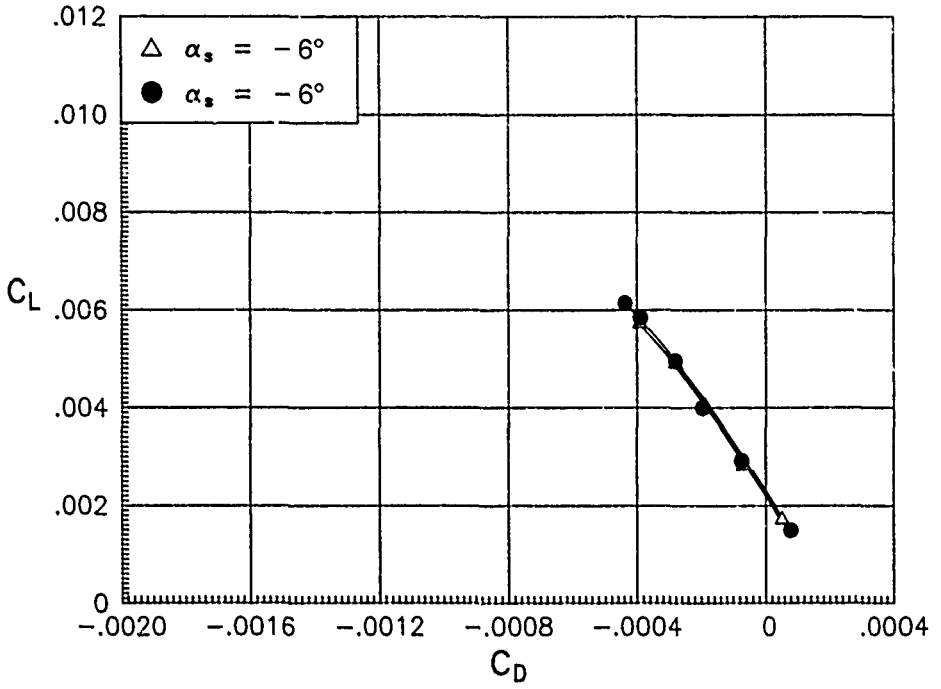

(a) C_L versus C_D.

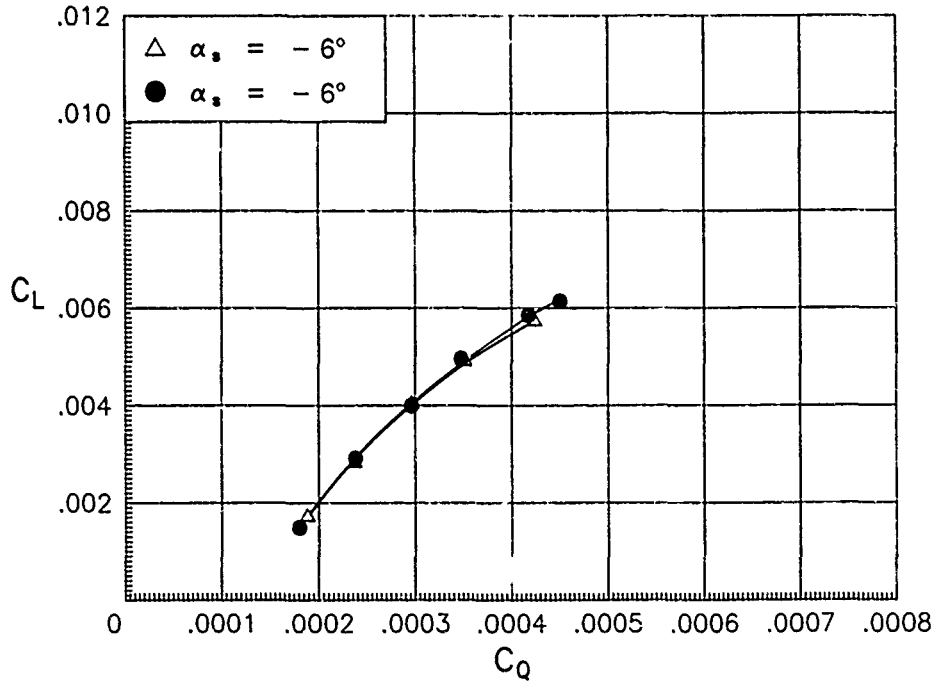

(b) C_L versus C_Q.

Figure A20. Repeatability of basic forward-flight characteristics of 50-percent tapered rotor for $\mu = 0.35$

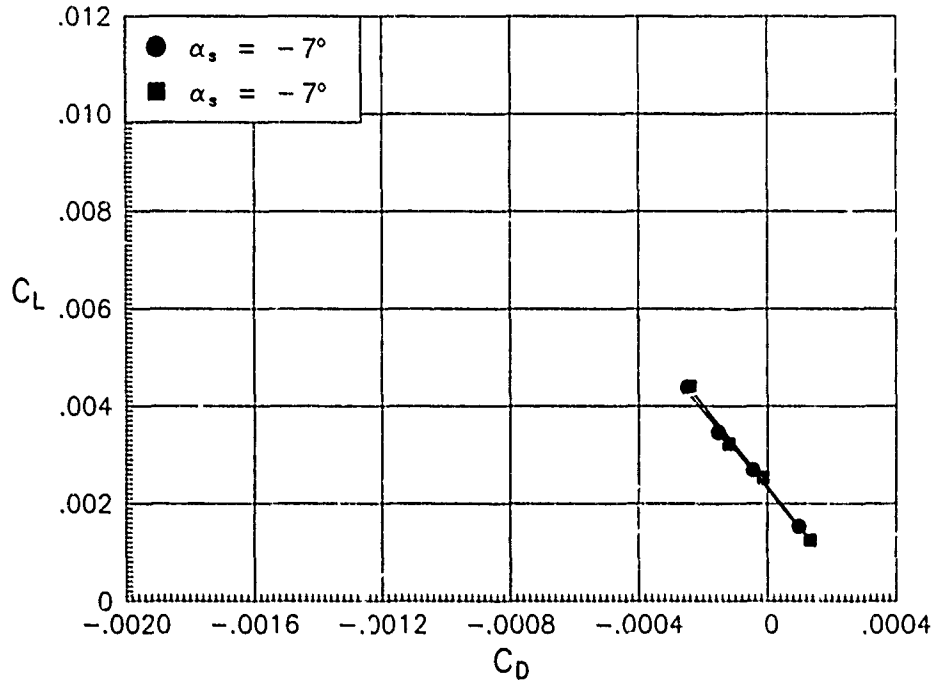

(a) C_L versus C_D.

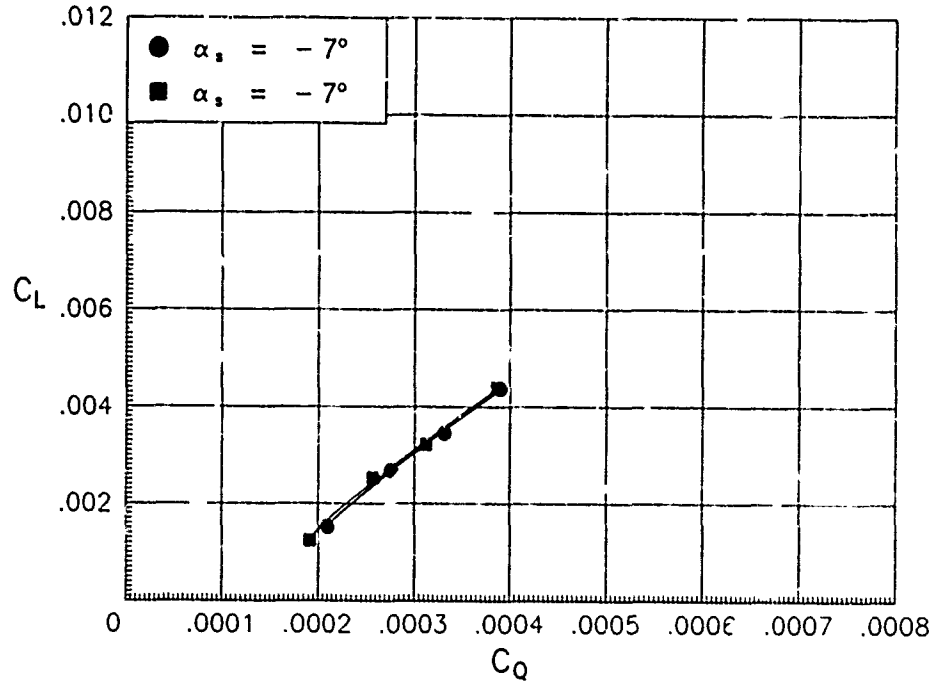

(b) C_L versus C_Q.

Figure A21. Repeatability of basic forward-flight characteristics of 50-percent tapered rotor for $\mu = 0.40$.

REPORT DOCUMENTATION PAGE

Form Approved
OMB No. 0704-0188

1. AGENCY USE ONLY *(Leave blank)*	2. REPORT DATE	3. REPORT TYPE AND DATES COVERED
	April 1992	Technical Memorandum

4. TITLE AND SUBTITLE
Effect of Blade Planform Variation on the Forward-Flight Performance of Small-Scale Rotors

5. FUNDING NUMBERS
PR 1L162211A47A
WU 505-59-87-54

6. AUTHOR(S)
Kevin W. Noonan, Susan L. Althoff, Dhananjay K. Samak, and Michael D. Green

7. PERFORMING ORGANIZATION NAME(S) AND ADDRESS(ES)
Aeroflightdynamics Directorate—AVSCOM
JRPO—Langley
Langley Research Center
Hampton, VA 23665-5225

8. PERFORMING ORGANIZATION REPORT NUMBER
L-16994

9. SPONSORING/MONITORING AGENCY NAME(S) AND ADDRESS(ES)
National Aeronautics and Space Administration
Washington, DC 20546-0001
and
U.S. Army Aviation Systems Command
St. Louis, MO 63120-1798

10. SPONSORING/MONITORING AGENCY REPORT NUMBER
NASA TM-4345
AVSCOM TR-92-B-005

11. SUPPLEMENTARY NOTES
Noonan and Althoff: Aeroflightdynamics Directorate—AVSCOM, JRPO—Langley, Hampton, VA; Samak and Green: University of Maryland, College Park, MD.

12a. DISTRIBUTION/AVAILABILITY STATEMENT
Unclassified–Unlimited

Subject Category 02

12b. DISTRIBUTION CODE

13. ABSTRACT *(Maximum 200 words)*

An investigation was conducted in the Glenn L. Martin Wind Tunnel to determine the effects of blade planform variation on the forward-flight performance of four small-scale rotors. The rotors were 5.417 ft in diameter and differed only in blade planform geometry. The four planforms were (1) rectangular, (2) 3:1 linear taper starting at 94 percent radius, (3) 3:1 linear taper starting at 75 percent radius, and (4) 3:1 linear taper starting at 50 percent radius. Each planform had a thrust-weighted solidity of 0.098. The investigation included forward-flight simulation at advance ratios from 0.14 to 0.43 for a range of rotor lift and drag coefficients. Among the four rotors, the rectangular rotor required the highest torque for the entire range of rotor drag coefficients attained at advance ratios greater than 0.14 for rotor lift coefficients C_L from 0.004 to 0.007. Among the rotors with tapered blades and for $C_L = 0.004$ to 0.007, either the 75-percent tapered rotor or the 50-percent tapered rotor required the least amount of torque for the full range of rotor drag coefficients attained at each advance ratio. The performance of the 94-percent tapered rotor was generally between that of the rectangular rotor and the 75- and 50-percent tapered rotors at each advance ratio for this range of rotor lift coefficients.

14. SUBJECT TERMS
Rotor performance; Helicopter rotor; Helicopter; Blade planform geometry

15. NUMBER OF PAGES
83

16. PRICE CODE
A05

17. SECURITY CLASSIFICATION OF REPORT	18. SECURITY CLASSIFICATION OF THIS PAGE	19. SECURITY CLASSIFICATION OF ABSTRACT	20. LIMITATION OF ABSTRACT
Unclassified	Unclassified		

NSN 7540-01-280-5500

Standard Form 298(Rev. 2-89)
Prescribed by ANSI Std. Z39-18
298-102

NASA-Langley, 1992